


3-22-2016

Cement Heat of Hydration and Thermal Control

Ahmadreza Sedaghat

Follow this and additional works at: <http://scholarcommons.usf.edu/etd>

 Part of the [Civil Engineering Commons](#), and the [Materials Science and Engineering Commons](#)

Scholar Commons Citation

Sedaghat, Ahmadreza, "Cement Heat of Hydration and Thermal Control" (2016). *Graduate Theses and Dissertations*.
<http://scholarcommons.usf.edu/etd/6142>

This Dissertation is brought to you for free and open access by the Graduate School at Scholar Commons. It has been accepted for inclusion in Graduate Theses and Dissertations by an authorized administrator of Scholar Commons. For more information, please contact scholarcommons@usf.edu.

Cement Heat of Hydration and Thermal Control

by

Ahmadreza Sedaghat

A dissertation submitted in partial fulfillment
of the requirements for the degree of
Doctor of Philosophy
Department of Civil and Environmental Engineering
College of Engineering
University of South Florida

Major Professor: A. Zayed, Ph.D.
Manoj K. Ram, Ph.D.
Mahmood H. Nachabe, Ph.D.
Ajit Mujumdar, Ph.D.
Abdul Malik, Ph.D.

Date of Approval:
January 29, 2016

Keywords: Portland Cement, Isothermal Calorimetry, Graphene Nanoplatelet, Statistical Analysis, Thermal Cracking

Copyright © 2016, Ahmadreza Sedaghat

DEDICATION

I would like to dedicate my dissertation to my parents (Aliasghar Sedaghat, Golnar J. Javidan), my beloved wife Rana, my brother Arsalan and my grandmother Ms. Koukab Sanakhan. A special feeling of gratitude to my parents whose words of encouragement and push for tenacity ring in my ears. My brother Arsalan who supported me emotionally and was a strong pier for my parents to lean on while I was far away from home pursuing my education. He is a true brother and I will owe him for the rest of my life. I dedicate this work to my beloved wife Rana Falahat whose unconditional encouragement and support made it possible for me to pursue my PhD degree.

ACKNOWLEDGMENTS

I am deeply indebted to my PhD adviser Dr. A. Zayed for her fundamental role in guiding and coordination of my PhD research study during these past five years. She has been motivating and encouraging and provided me with the fund to continue my PhD course of study. My gratitude is also extended to my PhD committee members Dr. Nachabe, Dr. Ram, Dr. Mujumdar and Dr. Malik. Also, I would like to thank Dr. Charles Ishee and Dr. Harvey Deford at the State Materials Office of the Florida Department of Transportation. They provided me with access, training and guide to conduct my experiments. I must acknowledge with tremendous and deep thanks to my uncle Hamid Javan Javidan and my aunt Maryam Zahir Emami who sponsored me financially and provided me with a path to pursue my PhD in U.S. Next I'd like to thank my friends, Osama Ali, Andre Bien-Aime, Dan Buidens, Thomas Meagher, Sina Izadi, Mehdi Khodayari, Natallya Shanahan, and Rajeev Kamal who supported me and provided me with assistance during my PhD course of study. Last but not the least I would like to thank Dr. Goswami for providing access to his lab and equipment for conducting the required experiments.

TABLE OF CONTENTS

LIST OF TABLES	iii
LIST OF FIGURES	v
ABSTRACT	vii
CHAPTER 1: INTRODUCTION	1
1.1 Initial Stage	2
1.2 Induction and Acceleration Stages.....	4
1.3 Deceleration and Steady State Stages	6
1.4 Statement of Objectives	14
1.5 References.....	15
CHAPTER 2: MEASUREMENT AND PREDICTION OF HEAT OF HYDRATION OF PORTLAND CEMENT USING ISOTHERMAL CONDUCTION CALORIMETRY	19
2.1 Introduction.....	19
2.2 Experimental	22
2.3 Results and Discussion	27
2.3.1 Signal to Maximum Baseline Deviation Ratio	27
2.3.2 Heat Flow and Heat of Hydration Data from Cement Samples.....	28
2.3.3 Extrapolation of Total Heat After 24 to 84 Hours of Hydration.....	29
2.4 Conclusions.....	36
2.5 References	37
CHAPTER 3: PREDICTION OF ONE, THREE AND SEVEN DAY HEAT OF HYDRATION OF PORTLAND CEMENT	39
3.1 Introduction.....	39
3.2 Experimental.....	44
3.3 Results and Discussion	47
3.3.1 X-ray Diffraction and Phase Quantification of Cements (1) Through (4)	47
3.3.2 Particle Size Distribution of As-received and Ground Cements (1) Through (4).....	50
3.3.3 Development of Proposed Heat of Hydration Equations	53
3.3.4 Validation of Proposed Heat of Hydration Equations	58
3.3.5 Evaluation of the Equations Predicting the Seven Day HOH Proposed by the Authors of This Paper and Also, Available in the Literature.....	60
3.4 Conclusions and Proposed Future Work	65
3.5 References	68

CHAPTER 4: INVESTIGATION OF PHYSICAL PROPERTIES OF GRAPHENE-CEMENT COMPOSITE FOR STRUCTURAL APPLICATIONS	72
4.1 Introduction.....	72
4.2 Experimental	75
4.2.1 As-received Materials	75
4.2.2 Composite Materials Preparation	75
4.2.3 Materials Characterization.....	75
4.3 Results and Discussion	78
4.3.1 Cement Characterization.....	78
4.3.2 X-ray Diffraction and Rietveld Analysis.....	80
4.3.3 Temperature Treatment of Hydrated Graphene- Cement Composites	81
4.3.4 Morphological Properties of Composite Materials in Hydration	83
4.3.5 Electrical Conductivity Properties of Composite Materials in Hydration	83
4.3.6 Thermal Diffusivity Properties of Composite Materials in Hydration	85
4.4 Conclusions.....	88
4.5 References	89
 CHAPTER 5: INVESTIGATION OF THE PHYSICAL PROPERTIES OF GRAPHENE NANOPLATELET CEMENT PASTE MATRIX IN CONCRETE ELEMENTS SUSCEPTIBLE TO CRACKING	92
5.1 Introduction.....	92
5.2 Material and Methods	96
5.3 Results and Discussion	100
5.3.1 Evaluation of Cracking Potential of Mortar Specimens under Restrained Shrinkage.....	100
5.3.2 Investigation of Hydration Mechanism of Graphene Cement Paste	108
5.3.3 Investigation of Compressive Strength of Graphene Cement Mortars	111
5.3.4 Determination of Hardness and Young's Modulus of Graphene Cement Samples	116
5.4 Conclusions.....	117
5.5 References	120
 CHAPTER 6: CONCLUSIONS AND RECOMMENDATIONS	124
 APPENDICES	126
Appendix A Copyright Permissions	127

LIST OF TABLES

Table 1.1 Abbreviations of oxide and chemical composition of Portland cement	1
Table 1.2 Comparison of precisions for isothermal conduction calorimetry and solution calorimetry (per ASTM C1702-09)	9
Table 1.3 Cements characterization, potential phase composition, H.I., Blaine fineness and heat of solution of 9 as-received Portland cements	11
Table 2.1 Comparison of precisions for isothermal conduction calorimetry and solution calorimetry (per ASTM C1702-09).....	21
Table 2.2(a) Chemical oxide composition of as-received cements	23
Table 2.2(b) Potential phase composition, Blaine fineness, measured and predicted 7 day heat of hydration of as received cements	24
Table 2.3 Experimental matrix, isothermal conduction calorimetry tests at 23 °C	24
Table 2.4 Measured and predicted 7 day heat of hydration by isothermal calorimeter	30
Table 2.5 S-shaped analytical function constants	32
Table 3.1 Major phase composition of cements (1) through (4).....	50
Table 3.2 Particle size distribution of as-received and ground cements (1) through (4)	52
Table 3.3 Measured Blaine fineness, mean particle size, one; three and seven day heat of hydration for as-received and ground cements (1) through (4)	55
Table 3.4 Coefficients of determination (R^2) for actual versus calculated intercepts and slopes for cements (1) through (4)	57
Table 3.5 Measured Blaine fineness, mean particle size, X-ray Rietveld phase quantification, one; three and seven day heat of hydration of as received cements A through H	58
Table 3.6 Statistical analysis on cements A through H for evaluation of proposed equations (3.6) through (3.8)	59

Table 3.7 Statistical analysis on cements A through H for evaluation of proposed equations (3.8) through (3.13).....	64
Table 4.1 Hydrated graphene-cement composite properties.....	87
Table 5.1 Quantification of crystal phase composition of cements G (1) through G (6)	96
Table 5.2 Blaine fineness, measured seven day heat of hydration and particle size analysis data for cements G (1) through G (6)	97
Table 5.3 Restrained shrinkage results of mortar specimens for cements G (1) through G (6).....	100
Table 5.4 Analysis of variance for compressive strength of graphene-cement mortars based on three factor model, full factorial design and analysis.....	112
Table 5.5 Analysis of variance for compressive strength of graphene cement mortar cubes	115

LIST OF FIGURES

Figure 1.1 Mechanism of heat of hydration of Portland cement	7
Figure 1.2 Heat of hydration of 38 as-received cements versus H.I.....	10
Figure 2.1 Admixer and vial for internal mixing (isothermal conduction calorimetry)	26
Figure 2.2 (a): Heat flow from sand sample, 0-7 days (b): Heat flow from sand sample compared to the heat flow from a 3.30 g Portland cement sample towards the end of the 7 days test period	29
Figure 2.3 (a) Heat of hydration of cement A (internal and external mixing) (b) - Heat flow of cement A (internal and external mixing)	30
Figure 2.4 (a&b) Heat of hydration for cement A, external vs. internal mixing	31
Figure 2.5 Measured and extrapolated 7 day heat of hydration of cement A	32
Figure 2.6 (a&b) - 7 Day heat of hydration difference “Predicted & Measured”	33
Figure 2.7 (a&b) Measured versus predicted 7 day heat of hydration of cements (Internal mixing)	34
Figure 3.1 Evaluation of the repeatability of the heat flow measurements	47
Figure 3.2 X-ray patterns and Rietveld refinement quantification of as received and ground cements, (a) cement (1), (b) cement (2), (c) cement (3), (d) cement (4).....	48
Figure 3.3 Particle size distribution of as received and ground cements, (a) cement (1), (b) cement (2), (c) cement (3), (d) cement (4)	51
Figure 3.4 Cement heat of hydration versus Blaine fineness, (a) cement (1), (b) cement (2), (c) cement (3), (d) cement (4)	54
Figure 3.5 Cement heat of hydration versus mean particle size, (a) cement (1), (b) cement (2), (c) cement (3), (d) cement (4)	56
Figure 3.6 Predicted and measured heat of hydration difference for as-received cements A through H, using equations (3.6) through (3.8)	59

Figure 3.7 Predicted and measured seven day heat of hydration difference for as-received cements A through H, using equations (3.8) through (3.13)	63
Figure 4.1 Schematic of hydrated graphene-cement composite and possible nanocomposite structure	77
Figure 4.2 Mineralogical analysis of as-received cement using XRD.....	78
Figure 4.3 Particle size distribution of as-received cement	79
Figure 4.4 Cement paste (a) total heat & (b) heat flow	80
Figure 4.5 XRD patterns of cement & graphene-cement composites (a) anhydrous & (b) hydrated.....	82
Figure 4.6 Temperature treatment of hydrated graphene-cement composites.....	84
Figure 4.7 Scanning electron microscopy image of hydrated graphene-cement composite.....	85
Figure 4.8 Electrical conductivity of hydrated graphene-cement composites.....	86
Figure 4.9 Thermal diffusivity of hydrated graphene-cement composites.....	87
Figure 5.1 Thermal diffusivity of graphene cement composite measured using Linseis (C) XFA500	93
Figure 5.2 Particle size distribution of the cements studied here, G (1) through G (6).....	98
Figure 5.3 Restrained shrinkage ring specimens	99
Figure 5.4 Restrained shrinkage results of mortar specimens for cements G (1) through G (6)	101
Figure 5.5 Heat and heat flow curves for cements G (1) through G (6).....	104
Figure 5.6 Calcium hydroxide determination for cements G (1) through G (6).....	107
Figure 5.7 G (6) graphene cement heat flow and heat flow curves	108
Figure 5.8 Surface roughness of G (6) graphene cement.....	119
Figure 5.9 G (6) graphene-cement hardness and Young modulus for different quantities of graphene	119

ABSTRACT

Heat of hydration is a property of Portland cement and a direct result of the chemical reaction between cement and water. The amount of heat released is dependent upon the cement mineralogical composition, curing temperature, water to cement ratio, and cement fineness. High temperature resulting from heat of hydration (thereon referred to as HOH) of cement can affect the hydration process, and consequently the kinetics of development of the mechanical properties of concrete. One of the main reasons triggering the interest in HOH of cement is its implication in thermal cracking of concrete. The high temperature gradient between the inner core and the outer surface of a concrete element is known to result in large tensile stresses that may exceed tensile strength, thus leading to early-age thermal cracking in mass concrete.

This dissertation initially addresses accurately predicting the heat of HOH of Portland cement at seven days based on the heat flow data collected from isothermal calorimetry for a time interval of 0-84 h. This approach drastically reduces the time required to identify the seven-day HOH of Portland cement.

The second part of this study focuses on cement fineness and its critical role on the heat generated by Portland cement during hydration. Using a matrix of four commercially available Portland cements, representing a wide range of mineralogical composition, and subjecting each of the as-received cements to several grinding increments, a linear relationship was established between cement fineness and heat of hydration. The effect of cement fineness and mineralogical composition on HOH of Portland cement was then related through a mathematical expression to predict the HOH of Portland cement based on its mineralogical composition and fineness. Three

expressions were proposed for the 1, 3 and 7 day HOH. The findings indicate that the equations developed, based on cement main phase composition and fineness, can be used to identify cements with high heat of HOH that may cause thermal cracking in mass concrete elements. Also, the equations can be used to correlate the HOH with the other properties of Portland cement for quality control and prediction of chemical and physical properties of manufactured Portland cement and concrete.

Restrained shrinkage experiments results on mortar specimens prepared with cements of variable phase composition and fineness indicate that interaction of C_3A and sulfate source is the prime phenomenon followed by cement fineness as the second main factor influencing concrete cracking. In order to minimize this effect, the third part of this study focused on studying alternatives that can lower the heat generated by concrete on hydration through the incorporation of nanomaterials; namely, graphene nanoparticles. The results indicate that incorporation of graphene as replacement for Portland cement improves thermal diffusivity and electrical conductivity of the cement paste. Consequently, the use of graphene can trigger improvement of the thermal conductivity of concrete elements thus reducing the cracking potential of concrete.

Measurements of HOH of graphene-cement paste, at $w/c=0.5$, using isothermal conduction calorimetry, indicate that incorporation of graphene up to 10% increases the length of the induction period while reduces the magnitude of the alite main hydration peak due to the filler effect. Furthermore, increasing the w/c ratio from 0.5 to 0.6 and graphene content from 1 % to 10% (as a partial replacement of cement) increases the 7 day HOH of Portland cement by 50 J/g. Isothermal conduction calorimetry heat flow curves show that incorporation of graphene particles up to 10% does not have significant effect on interaction of aluminates and sulfates

sources since the time of occurrence of the C_3A sulfate depletion peak is not affected by graphene substitution up to 10%.

Full factorial statistical design and analysis conducted on compressive strength data of mortar specimens prepared at two w/c ratios, using cements of different finenesses and graphene content indicates that the quantity of graphene and the physical interaction due to variable w/c, graphene and cement fineness, have the smallest P-value among all the samples, representing the most significant impact on compressive strength of mortar samples. It appears that in graphene-cement paste composites, addition of 1% graphene results in 21% reduction of Young's modulus. Increasing the graphene content from 1% to 5% and/or 10% does not show significant effect on Young's modulus. Similar trends can be observed in the hardness of graphene cement paste samples.

In conclusion, partial replacement of Portland cement with graphene nanoparticles in concrete mixtures is a good alternative to lower the cracking potential in mass concrete elements.

CHAPTER 1: INTRODUCTION

Heat of hydration is a property of Portland cement and a direct result of the chemical reactions between cement and water. The amount of heat released is dependent upon the cement composition, curing temperature, water to cement ratio, and cement fineness. The phases mainly responsible for heat generation are tricalcium silicate (C₃S), dicalcium silicate (C₂S), tricalcium aluminate (C₃A) and tetracalcium aluminoferrite (C₄AF) [1, 2]. Portland cement oxide and chemical composition abbreviations are outlined in Table 1.1 Bogue equations, as outlined in ASTM C150 [3], are used to estimate the potential compound composition of Portland cement.

Table 1.1 Abbreviations of oxide and chemical composition of Portland cement

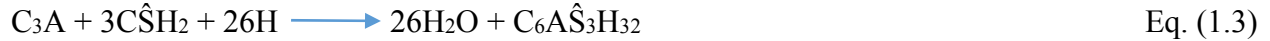
Oxide	Abbreviation	Compound	Abbreviation
CaO	C	3CaO.SiO ₂	C ₃ S
SiO ₂	S	2CaO.SiO ₂	C ₂ S
Al ₂ O ₃	A	3CaO.Al ₂ O ₃	C ₃ A
Fe ₂ O ₃	F	4CaO.Al ₂ O ₃ .Fe ₂ O ₃	C ₄ AF
MgO	M	4CaO.3Al ₂ O ₃ .SO ₃	C ₄ A ₃ Ŝ
SO ₃	Ŝ	3CaO.2SiO ₂ .3H ₂ O	C ₃ S ₂ H ₃
H ₂ O	H	CaSO ₄ .2H ₂ O	CŜH ₂

The main chemical reactions associated with C₃S and C₂S hydration are outlined in Equations (1.1) and (1.2). Both reactions are exothermic, which means they release heat to the surroundings. Calcium silicate hydrate is the compound of interest due to its critical role and contribution to concrete strength [4].



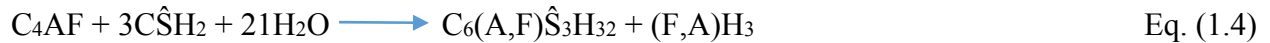
Another significant reaction in the hydration of Portland cement is the interaction of C₃A with

gypsum in the hydrating cement paste system. The reaction is summarized in Equation (1.3).



If the sulfates present are not adequate, a lower sulfate form of aluminate hydrate, namely; monosulfoaluminate, can also form.

C₄AF forms similar hydration products as C₃A. Gypsum retards C₄AF reaction even more drastically than C₃A. C₄AF hydration reaction is summarized in Equation (1.4):



Portland cement hydration stages are typically identified by five main stages outlined as follows [1]:

1.1 Initial Stage

Hydration of Portland cement consists of a series of reactions between cement minerals, calcium sulfates and water (See Figure 1.1). The initial heat release that occurs once water is added to cement relies on the rate of dissolution of the main cement phases and the available sulfates. Upon contact of water with cement, the alkali sulfates would dissolve rapidly and release K⁺, Na⁺ and SO₄²⁻ ions into solution. Calcium sulfates dissolve until saturation. Tricalcium silicate dissolves rapidly and C-S-H starts to precipitate on the surface of anhydrous cement particles. The hydration process is accompanied by the release of Ca²⁺ and OH⁻ in the liquid phase. Silicate ions also dissolve in liquid phase. The amount of tricalcium silicate dissolved in the initial stage is estimated to be between 2 to 10 percent [1]. It is understood that with the increase in the amount of C₃S dissolution and C-S-H formation, Ca(OH)₂ concentration would increase. An increase in Ca(OH)₂ retards C₃S hydration. One theory explains this effect that Ca(OH)₂ would not precipitate in the liquid phase even after reaching its saturation point due to the incorporation of silicate ions in its nuclei. As the Ca(OH)₂ concentration increases, it then can cope with the poisoning effect of

silicate and starts to precipitate and acts as a sink for Ca^{2+} ions. This process would result in an opportunity for C-S-H formation and a renewed increase in C_3S hydration [1]. From solubility standpoint, when the concentration of calcium hydroxide is between 0 and 36 mmol/L, which corresponds to the maximum amount of supersaturation in regards to calcium hydroxide (Portlandite), C_3S is more soluble than C-S-H so C_3S always hydrates [5]. It is evident from the chemical analysis of the solution phases that C_3S dissolves congruently and quite rapidly in the first minute on contact with water. C_3S would continue to dissolve up until reaching the equilibrium of silicate and calcium concentration in solution of several hundred mmol/L [6]. Tricalcium aluminate would also dissolve in water and reacts with the Ca^{2+} and SO_4^{2-} ions provided by the dissolution of calcium sulfate phases to yield ettringite (Aft) and subsequently precipitate on the surface of cement particles [1]. C_3A is estimated to hydrate between 5 to 25 percent during the initial stage of hydration. Gypsum has been used as a retarder to reduce the intense reaction of C_3A with water and to avoid flash set [7]. Ettringite is the main product of reaction of C_3A and Gypsum. Some researchers evaluated the effect of gypsum and hemihydrate at initial stage of hydration and concluded that the initial reaction of C_3A was much greater in presence of gypsum compared to hemihydrate [8, 9]. In contrast, some researchers show that at the beginning of heat evolution curve, the amount of gypsum does not have any effect on the heat of hydration [10]. Ferrite phase also reacts in the same manner as tricalcium aluminate and yield ettringite (Aft).

Only very small fraction of C_2S would react in the initial period releasing C-S-H phase and contributing to the Ca^{2+} and OH^- release in the liquid phase [1]. It is important to note that although C_3S and C_2S are more soluble than C-S-H in liquid phase; however, C_2S cannot dissolve as long as C_3S hydrates since the ionic concentration maintained during C_3S hydration are higher

than the solubility of C_2S [5]. Intense liberation of heat in the initial stage is mainly the result of C_3S and C_3A hydration. It is noteworthy that C_3S and C_3A hydration is also dependent on the dopant ions incorporated into their lattice structures [1].

1.2 Induction and Acceleration Stages

Fast reaction kinetics during the initial stage of hydration is followed by a dormant period as shown in Figure 1.1 Julliard et al. concluded from SEM work of Makars that during alite hydration in the induction period there is not enough evidence showing that there is a complete layer of hydration products forming around anhydrous particles to protect alite surface from continued rapid hydration. In fact, the reactive sites, noted at the edges, indicate the coverage by reaction products. Lack of reaction of the other parts of the grain is attributed to rapid ions concentration built up in solution in a way that there was insufficient undersaturation to overcome the free energy barrier to etch pitting [8, 11]. Some researchers including Stein indicated that the induction period is the effect of rapid formation of a metastable layer of a calcium silicate hydrate phase passivating the surface by limiting access to water or diffusion of detaching ions away from the surface of the cement grains. This metastable layer is interpreted to be permeable to calcium and water but not to silicates. For the metastable hypothesis to be correct a fairly dense layer must cover the great majority of C_3S surface; however, evidence of a continuous layer has not been found using different direct methods of surface examination [6]. Nonat et al. [12] has developed a mechanistic explanation for the slow reaction of C_3S during the induction period. He expressed that the superficially hydroxylated C_3S formed after the initial stage has much lower solubility compared to the one calculated for C_3S and that its dissolution decreases very rapidly while calcium hydroxide concentration increases. When C-S-H concentration exceeds maximum supersaturation, C-S-H shall nucleate rapidly on C_3S surface.

Based on some research on post thermal annealing treatment at 650 °C, surface defects control the rate of dissolution and consequently affect the length of induction period [6]. The rate of hydration in the acceleration period is based on the rate of formation of the hydration products, primarily C-S-H. It is perceived from the experiments that the rate controlling step of the reaction is due to heterogeneous nucleation and growth of C-S-H on alite surface and likely on other mineral surfaces. Thomas performed some experiments by seeding C₃S pastes with C-S-H at the time of mixing. The results indicated that the induction period was almost eliminated and the hydration process progressed immediately and at higher rate compared to unseeded C₃S pastes [13].

The findings indicate that the start of the acceleration stage depends on the existence of growing regions of C-S-H to give considerable hydration rate. Without the seeding process, more time is required to facilitate natural nucleation and growth processes to provide sufficient C-S-H surface area to revive the hydration rate during the acceleration stage [6]. Gartner listed four mechanisms for shifting from induction to acceleration periods. Two of his proposed mechanism models including metastable barrier hypothesis and slow dissolution step hypothesis support this theory that the rate of C₃S dissolution is controlled by the rate of C-S-H nucleation and growth [6, 14]. Juilland et al. [11] realized that small addition of free lime to alite would prolong the induction period while higher amounts may shorten it. It can be perceived that rapid dissolution of free lime increases the amount of calcium ions in solution. This phenomenon may restrict the dissolution of alite and etch pit formation and increases the induction period as a consequence. At higher addition of free lime, the free lime may act as a nucleation site for the precipitation of the hydration products and consequently decreases the duration of the induction period. Tricalcium aluminate would harden fast when in contact with water. To delay the time of setting, a calcium sulfate source can be added to the cement to control the chemical reaction between water and aluminate and to

delay the initial and final time of setting. In presence of calcium sulfate, the pattern of reaction between water and aluminate would change.

Bullard et al. [6] mentioned that Scrivener and Pratt discovered a disorganized layer covering C_3A . They consider this gel like layer to be accountable for the slow reaction period of C_3A . Minard et al. [10] showed by scanning electron micrograph that at the initial C_3A hydration in presence of gypsum, the grain would be covered with two types of hydrates with diverse morphologies, sheets of AFm phase and ettringite needles. He thought adsorption of calcium and/or sulfate ions on the surface of C_3A particles block the dissolution sites of C_3A and results in retardation of C_3A hydration. Rapid hydration reaction of C_3A , after depletion of sulfate source, is a strong evidence to prove this theory [10].

1.3 Deceleration and Steady State Stages

Deceleration and steady state stages of hydration starts with formation and thickening of hydration products primarily C-S-H around anhydrous phases. As hydration progresses, the layer gets thicker and the hydration process moves toward ionic diffusion through the thickening layer. It is noteworthy that an increase in this layer thickness diminishes the amount of ions passing through and as a result decreases the rate of heat flow. Costoya [15] work showed that the hydration product C-S-H forms thicker diffusion controlled layer around smaller anhydrous C_3S particles.

The interest in heat of hydration (thereon referred to as HOH) of cement is due to its effect on inducing thermal cracking in concrete elements. The high temperature gradient between the inner core and the outer surface of the concrete element is known to result in large tensile stresses that may exceed the tensile strength of concrete, thus leading to early-age thermal cracking in massive concrete elements [16]. The thermal cracking can result in degradation of the concrete

structure including problems in serviceability, loss of water tightness, reduction in durability of structures and increase in probability of corrosion or carbonation of contained steel in concrete [17-21].

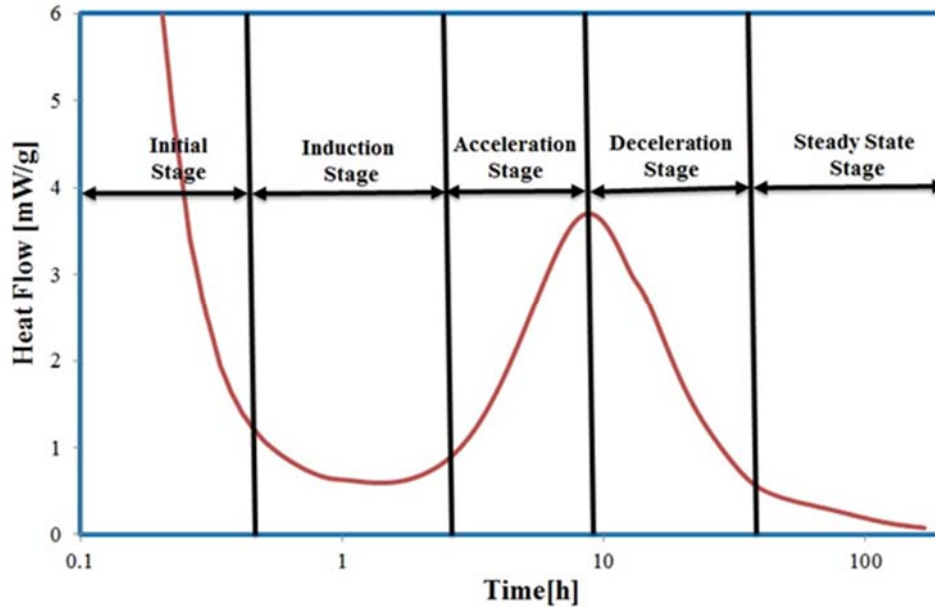


Figure 1.1 Mechanism of heat of hydration of Portland cement

The high temperature resulting from the heat generated by cement on hydration can also affect the hydration process, and consequently the kinetics of the development of the mechanical properties of concrete [22]. Higher hydration temperature can be beneficial in cold weather concrete placement due to its accelerating effect on the hydration process [23]. Cement fineness is a critical component affecting the HOH of Portland cement. The primary reason for contractors to resort to finer cement is its higher early strength and consequently faster construction operations [24]. Higher fineness provides higher surface area for cement to react with water, therefore resulting in an increase in rate of heat liberation at early ages and higher early internal temperature in concrete elements [25].

ASTM C1702 (isothermal conduction calorimetry) [26] and ASTM C186 (heat of solution calorimetry) [27] are the two available ASTM standard methods for HOH measurements of

hydraulic Portland cements. Heat of solution calorimetry measures the temperature rise of the acidic solution resulting from the decomposition of the anhydrous and partially hydrated cement separately. The difference between the heat of solution of the anhydrous and partially hydrated cement can be calculated as the heat evolved during the hydration period. Considering the experimental procedure, this method is labor intensive and requires the use of hazardous acidic substances [28].

Isothermal conduction calorimetry has the advantage of measuring the HOH instantly from the time of mixing of cement with water. It is a useful technique in studying the effects of admixtures on cement hydration. This method can be executed with low labor input and with better precision as compared to the heat of solution method [29]. Isothermal conduction calorimetry can typically operate at a wide range of temperature and using different water to cement ratios. The major advantage of isothermal conduction calorimetry is that it not only measures the total heat but also records the thermal power or “heat flow” at different ages. The calorimeter provides the user the ability to study the hydration stages from the recorded heat flow curve at the desired hydration age. Sample preparation and operation of the instrument are fairly easy, though its use requires some basic training. The cumulative heat, at any age, can be calculated by the integration of the area under the heat flow curve versus time [30-32]. Isothermal calorimetry performs well with blended cements while the solution calorimetry is less suited [33]. Isothermal calorimetry shows improved precision if compared with the heat of solution method as shown in Table 1.2 [34]. Additionally, the former offers simplicity in procedure and the availability of commercial equipment to conduct the test. Long term studies by Wadso [35] indicate that the calibration coefficients are remarkably stable over time as long as there is no hardware or bath temperature change. It is noteworthy that ASTM C1702 method is not dependent on the knowledge of

compound composition, which makes it much more useful for the analysis of non-Portland cements.

Table 1.2 Comparison of precisions for isothermal conduction calorimetry and solution calorimetry (per ASTM C1702-09)

Standard Deviation	ASTM C186	ASTMC1702 (Wadso et al.'s Data) [35-37]	ASTM C1702 (VDZ 2006) [38]
Within lab	14.8 KJ/Kg (7 days)	Not available	4.6 KJ/Kg (7 days)
Between lab	16.9 KJ/Kg (7 days)	10.5 KJ/Kg (3 days)	13.6 KJ/Kg (7 days)

To control the HOH of Types II (MH) and Type II (MH)A portland cements, ASTM C150-12 defines a heat index parameter (HI), per its standard chemical composition requirements, as the sum of $C_3S + 4.75C_3A$. An HI limit of 100 and a Blaine fineness limit of 2600-4300 cm^2/g are assigned to the Types II (MH) and II (MH)A portland cements to control the seven day HOH under 335 J/g [80 Cal/g] as measured conforming to ASTM C186. ASTM C150 specifies that the Blaine fineness limit of 2,600-4,300 cm^2/g does not apply to the Types II (MH) and II (MH)A cements if the HI limit is maintained below 90. It is therefore implied that the effect of cement fineness on HOH of Portland cements with HI of 90 or less is not significant. This criterion shall permit cements with HI of less than 90 to be used or categorized as a Type II (MH) Portland cement regardless of their fineness. This criterion may not be very accurate as Portland cement fineness has significant effect on HOH. The proposed HI limit was originally developed from the statistical analysis conducted by Toy Poole on the seven day HOH of hydraulic Portland cements [39]. The HOH data were obtained from the CCRL samples and U.S. army corps of engineers research and development center. The HOH data were collected using ASTM C186 (heat of solution calorimetry) method. The potential phase composition of the cements were calculated using Bogue

formulas. The Blaine fineness of the cements used in this study ranged from 2,640 to 4,360 cm^2/g . Based on Poole's analysis, Figure 1.2, it was shown that the measured HOH of 80 Cal/g on the trend line corresponds to HI of 100.

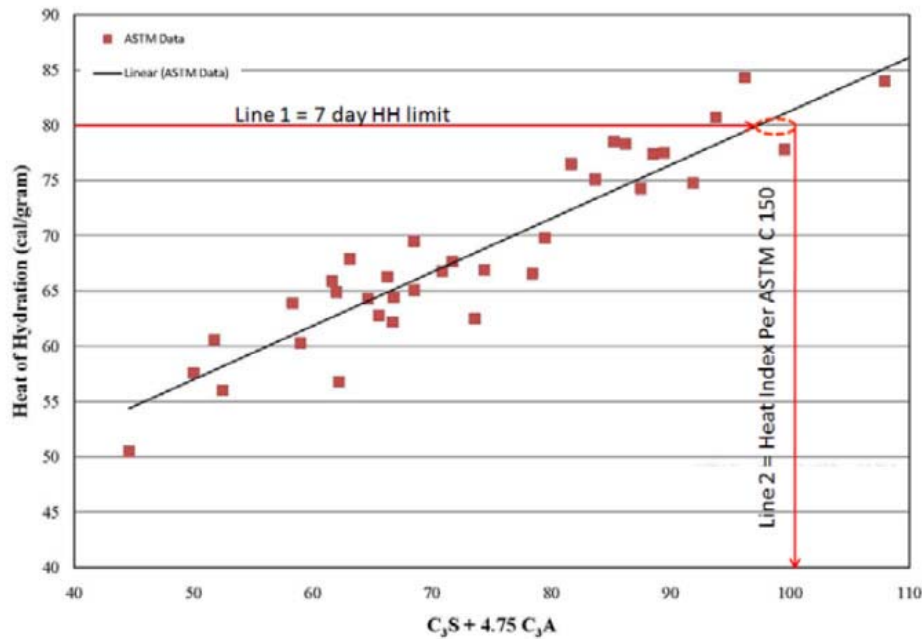


Figure 1.2 Heat of hydration of 38 as-received cements versus H.I. [40]
(No copyright permission required as the image obtained from the public domain)

To evaluate the efficiency of the HI in predicting and controlling the HOH, nine Portland cements were selected. The potential phase composition, HI, Blaine fineness and 7-day HOH (using ASTM C186) were determined as outlined in Table 1.3. As shown in Table 1.3, Cements 2, 3, 6, 7 and 8 have a HI of less than 90 while their seven day HOH exceeds 335 J/g. Specifically, cements 3, 6 and 8 with high finesses also have high HOH (366-370 J/g). It is well perceived that cement fineness has significant effect on HOH and dismissing the placement of limit on the fineness of cements with $\text{HI} < 90$ cannot provide an appropriate means to control the HOH of Portland cements.

Based on HI definition, cements (1) through (8) can be classified as Type II (MH) Portland cements. However, with the exception of cement 1, all the other seven cements have the seven day

HOH exceeding 335 J/g indicating the deficiency of the HI to be used as an appropriate control or identifier for the potential of a given cement to generate heat, which is basically the main purpose of including HI in the specifications. There are two major factors that may contribute to the deficiency of the HI to appropriately mark or control the HOH of Portland cements. Firstly, the Blaine fineness for all the cements used to establish the HI (38 cements obtained from the CCRL sample results and U.S. army corps of engineers research and development center) were in a narrow range of 2,640 to 4,360 cm²/g thus resulting in limiting its use to investigate the effect of cement fineness on HOH of portland cement and effectively incorporating the cement fineness into the HI expression while not specifying a limit on cement fineness in the event that the heat index is less than 90. Secondly, the quantification of the major cement phases (C₃S, C₃A, C₂S, and C₄AF), as used in establishing the HI, was done through the calculation of the potential phases composition. Additionally, it is well established that the Bogue equations may cause erroneous results when quantifying the major phases in Portland cements [41-42]. It is therefore proposed that direct quantification methods; namely, quantitative X-ray diffraction (QXRD) and microscopy which are better tools in quantifying the phase composition of Portland cements, be included in any expressions used to identify the potential of a portland cement to generate heat.

Table 1.3 Cements characterization, potential phase composition, H.I., Blaine fineness and heat of solution of 9 as-received Portland cements

Property	1	2	3	4	5	6	7	8	9
C ₃ S (w/o)	61	63	59	65	57	53	56	52	47
C ₂ S (w/o)	14	12	15	7	14	17	17	20	18
C ₃ A (w/o)	5	5	5	6	7	8	7	7	11
C ₄ AF (w/o)	13	12	12	9	12	12	11	11	8
C ₃ S+4.75C ₃ A	85	87	83	95	91	89	88	85	99
Blaine fineness (cm ² /g)	3250	4140	5750	4260	4170	6120	4020	5900	4050
ASTM C186-7 day HOH (J/g)	312	340	366	362	349	370	337	367	361

Several researchers attempted to formulate the HOH of cements. Woods et al. [43] developed equations predicting the HOH of cements at the ages of 3, 7, 28, 90 and 180 days based on the measured HOH of 13 cements using solution calorimetry. The proposed HOH equations were based on linear regression analysis of the heat generated by the major cement phases; namely, C_3S , C_3A , C_2S , and C_4AF . The fineness of cements used in calibration were within the range of 1,390 to 1,670 cm^2/g as determined by a sedimentation device. It was concluded that the fineness of cements, within the studied range, does not have substantial effect on the generated heat. Good linear correlations were indicated between the HOH at the ages of 3 days, 180 days, and 1 year ages and $C_3S+2.1C_3A$ [43-44]. Comparison of measured and predicted (based on equations developed in terms of cement oxide composition) HOH for four commercial cements indicates that the equations can overestimate the HOH by 11 Cal/g at the ages of 3, 7 and 28 days and by 5 Cal/g at the age of 180 days [43]. Lerch, et al.'s [45] work on HOH shows a significant effect of cement fineness on HOH at the ages of one, three and seven days while it is less drastic at the ages of 28 days and up.

Verbeck et al. [46] established relationships between the HOH of cements and their composition at several ages ranging from three days up to 6.5 years. The least squares method was implemented in fitting the experimental data while assuming linear and independent relationship between the hydration reaction of C_3S , C_3A , C_2S , C_4AF , and SO_3 . Significant discrepancy between measured and the predicted heat could be observed for Types III and IIIA cements at ages of three and seven days. Although the relationships were established based on the main cement phases at various ages, fineness was not incorporated into the equations as a significant factor affecting the HOH. Fineness of the cements range from 1,630 -2,795 cm^2/g measured in conforming to ASTM C115 (determination of cement fineness using turbidimeter).

Poole [39] developed several equations based on the values of HOH of the individual compounds as outlined in Lea's chemistry of cement, and using the data provided by CCRL, US army corps of engineers, and Verbeck and Foster research study. Seven relationships were examined and analyzed. Five of the relationships incorporated cement potential phase composition, with two of the five expressions incorporating fineness. The last two expressions, analyzed in this work, were based on mortar cube strength at three and seven days with the former showing better random error and no apparent bias. The three developed equations that were established based on the potential phase composition and Blaine fineness are as follows:

Equation (1.5) is assembled based on the HOH of the individual compounds. The phases are expressed on a weight percent basis:

$$7 \text{ Day HOH} = 15.55C_3A + 2.21C_3S + 0.42C_2S + 5.82C_4AF \quad \text{Eq. (1.5)}$$

Equation (1.6) was developed by Poole using stepwise linear regression on the data provided by CCRL and US army corps of engineers (data on 38 cements). The Blaine fineness for those cements ranged from 2,640- 4,360 cm²/g :

$$7 \text{ Day HOH} = 133.9 + 9.36(C_3A) + 2.13(C_3S) \quad \text{Eq. (1.6)}$$

Equation (1.7) is a linear regression equation assembled by Poole based on the data taken from Verbeck and Foster. Blaine fineness of the cements used in this study ranged from 2,850-4,900 cm²/g. As it is evident from the formula, cement fineness has significant effect on the 7 day HOH. However, the formula does not take into account the effect of C₂S and C₄AF on HOH.

$$7 \text{ Day HOH} = 1.98 + 11.44(C_3A) + 1.53(C_3S) + 0.04(\text{Blaine (cm}^2/\text{g)}) \quad \text{Eq. (1.7)}$$

There are several ways to control the cracking potential of concrete; one way is to identify the cements generating high HOH (whether through experimental work or equations predicting the HOH) as explained above and limit their use or partially replace them with supplementary

cementitious materials. Another approach in alleviating the problem is to reduce the temperature gradient in concrete elements, which is primarily due to the high HOH of Portland cements. It is plausible to use nanomaterials to improve concrete thermal conductivity thus reducing the temperature gradient. Graphene was selected as a nanomaterial due to its excellent thermal properties. Graphene is a nanomaterial that has the potential of improving the thermal conductivity of cementitious materials. Graphene, a 2-D π -conjugation, has several extraordinary physical properties such as high thermal conductivity, high electrical conductivity, high surface area (2,630 m²/g), high elastic modulus and amphi-polar electric field effect [47-49].

1.4 Statement of Objectives

Based on the thorough literature review and in absence of accurate methods of predicting the heat generated by Portland cements on hydration, the following are the main objectives of this study:

1. Accurately predicting the HOH generated by Portland cements at seven days through:
 - 1.1 Minimizing data collection time
 - 1.2 Minimizing additional tests to determine HOH and assess the potential use of tests that are commonly conducted in characterizing Portland cement to predict HOH.
2. Explore the use of nanomaterials, specifically graphene nanoparticles, in minimizing the cracking potential of concrete elements through improving concrete thermal conductivity and heat dissipation properties.
3. Assess the effects of incorporating graphene nanoparticles on the physical, electrical and chemical properties of cementitious mixtures.

1.5 References

- [1] Odler, Ivan. "Hydration, setting and hardening of Portland cement." *Lea's Chemistry of Cement and Concrete* 4 (1998): 241-297.
- [2] Zayed, A., Ahmadreza Sedaghat, and Paul Sandberg. "Measurement and prediction of heat of hydration of portland cement using isothermal conduction calorimetry." *Journal of Testing and Evaluation* 41.6 (2013): 1-8.
- [3] ASTM Standard C150/C150M, "Standard Specification for hydrated hydraulic lime for structural purposes," Annual book of ASTM Standards, Vol.04.01, ASTM International, West Conshohocken, PA, (2009).
- [4] Mindess, Sidney, J. Francis Young, and David Darwin. *Concrete*. (2003).
- [5] Scrivener, Karen L., and André Nonat. "Hydration of cementitious materials, present and future." *Cement and concrete research* 41.7 (2011): 651-665.
- [6] Bullard, Jeffrey W., et al. "Mechanisms of cement hydration." *Cement and Concrete Research* 41.12 (2011): 1208-1223.
- [7] Soroka, I., and M. Abayneh. "Effect of gypsum on properties and internal structure of PC paste." *Cement and Concrete Research* 16.4 (1986): 495-504.
- [8] Cheung, J., et al. "Impact of admixtures on the hydration kinetics of Portland cement." *Cement and Concrete Research* 41.12 (2011): 1289-1309.
- [9] Pourchet, Sylvie, et al. "Early C₃A hydration in the presence of different kinds of calcium sulfate." *Cement and Concrete Research* 39.11 (2009): 989-996.
- [10] Minard, Hélène, et al. "Mechanisms and parameters controlling the tricalcium aluminate reactivity in the presence of gypsum." *Cement and Concrete Research* 37.10 (2007): 1418-1426.
- [11] Juilland, Patrick, et al. "Dissolution theory applied to the induction period in alite hydration." *Cement and Concrete Research* 40.6 (2010): 831-844.
- [12] Garrault, Sandrine, and André Nonat. "Hydrated layer formation on tricalcium and dicalcium silicate surfaces: experimental study and numerical simulations." *Langmuir* 17.26 (2001): 8131-8138.
- [13] Thomas, Jeffrey J., Hamlin M. Jennings, and Jeffrey J. Chen. "Influence of nucleation seeding on the hydration mechanisms of tricalcium silicate and cement." *The Journal of Physical Chemistry C* 113.11 (2009): 4327-4334.

- [14] Gartner, E. M., et al. "Hydration of Portland cement." *Structure and Performance of Cements* 13 (2002): 57-113.
- [15] Costoya Fernández, Maria Mercedes. "Effect of particle size on the hydration kinetics and microstructural development of tricalcium silicate." (2008).
- [16] Schindler, Anton Karel. "Concrete hydration, temperature development, and setting at early-ages." (2011).
- [17] Amin, Muhammad Nasir, et al. "Simulation of the thermal stress in mass concrete using a thermal stress measuring device." *Cement and Concrete Research* 39.3 (2009): 154-164.
- [18] Kim, Jang-Ho Jay, Sang-Eun Jeon, and Jin-Keun Kim. "Development of new device for measuring thermal stresses." *Cement and concrete research* 32.10 (2002): 1645-1651.
- [19] Azenha, Miguel, and Rui Faria. "Temperatures and stresses due to cement hydration on the R/C foundation of a wind tower-A case study." *Engineering Structures* 30.9 (2008): 2392-2400.
- [20] Faria, Rui, Miguel Azenha, and Joaquim A. Figueiras. "Modelling of concrete at early ages: Application to an externally restrained slab." *Cement and Concrete Composites* 28.6 (2006): 572-585.
- [21] Zreiki, J., F. Bouchelaghem, and M. Chaouche. "Early-age behavior of concrete in massive structures, experimentation and modelling." *Nuclear Engineering and Design* 240.10 (2010): 2643-2654.
- [22] Kaszyńska, Maria. "Early age properties of high-strength/high-performance concrete." *Cement and Concrete Composites* 24.2 (2002): 253-261.
- [23] Stutzman, Paul, Stefan Leigh, and Kendall Dolly. "Heat of hydration for cement: statistical modeling." *Transportation research record: Journal of the Transportation Research Board* 2240 (2011): 1-8.
- [24] Bentz, Dale P., Gaurav Sant, and Jason Weiss. "Early-age properties of cement-based materials. I: Influence of cement fineness." *Journal of Materials in Civil Engineering* 20.7 (2008): 502-508.
- [25] Portland Cement Association. "Portland cement, concrete, and heat of hydration." *Concrete Technology Today* 18.2 (1997): 1-4.
- [26] ASTM Standard C1702-09a, Standard test method for measurement of heat of hydration of hydraulic cementitious materials using isothermal conduction calorimetry, Annual Book of ASTM Standards, Vol. 04.01, ASTM International, West Conshohocken, PA (2010).

- [27] ASTM Standard C186-05, Standard test method for heat of hydration of hydraulic cement, Annual book of ASTM Standards, Vol. 04.01, ASTM International, West Conshohocken, PA, (2010).
- [28] Poole, Toy. Revision of test methods and specifications for controlling heat of hydration in hydraulic cement. No. PCA R&D Serial No. 2007. Portland Cement Association, (2007).
- [29] Qi, Chengqing, et al. "Use of isothermal conduction calorimetric method for measuring the heat of hydration of cement." *Journal of ASTM International* 6.10 (2009): 1-9.
- [30] Wadsö, Ingemar. "Isothermal microcalorimetry near ambient temperature: an overview and discussion." *Thermochimica Acta* 294.1 (1997): 1-11.
- [31] Kumar, Mukesh, Sanjay K. Singh, and N. P. Singh. "Heat evolution during the hydration of Portland cement in the presence of fly ash, calcium hydroxide and super plasticizer." *Thermochimica Acta* 548 (2012): 27-32.
- [32] Xu, Qinwu, et al. "Modeling hydration properties and temperature developments of early-age concrete pavement using calorimetry tests." *Thermochimica Acta* 512.1 (2011): 76-85.
- [33] Wadsö, Lars. "Applications of an eight-channel isothermal conduction calorimeter for cement hydration studies." *Cement International* 5 (2005): 94-101.
- [34] ASTM Standard C1702-09a, "Standard test method for measurement of heat of hydration of hydraulic cementitious materials using isothermal conduction calorimetry," Annual Book of ASTM Standards, Vol. 04.01, ASTM International, West Conshohocken, PA (2009).
- [35] Wadsö, Lars. "Operational issues in isothermal calorimetry." *Cement and Concrete Research* 40.7 (2010): 1129-1137.
- [36] Wadsö, Ingemar, and Robert N. Goldberg. "Standards in isothermal microcalorimetry (IUPAC technical report)." *Pure and Applied Chemistry* 73.10 (2001): 1625-1639.
- [37] Wadsö, Lars. "Temperature changes within samples in heat conduction calorimeters." *Thermochimica Acta* 366.2 (2001): 121-127.
- [38] VDZ, "Round Robin heat of hydration 2006," Research Institute of the German Cement Industry, Cement Chemistry Department, Dusseldorf, Germany, (2006).
- [39] Poole, Toy S. "Predicting seven-day heat of hydration of hydraulic cement from standard test properties." *Journal of ASTM International* 6.6 (2009): 1-10.
- [40] Ferraro, C. C., C. A. Ishee, and M. Bergin. Report of changes to cement specifications AASHTO M 85 and ASTM C150 subsequent to harmonization. FL/DOT/SMO/10-536). Tallahassee, FL: Florida Department of Transportation, (2010).

- [41] Stutzman, Paul E. Guide for X-ray powder diffraction analysis of Portland cement and clinker. US Department of Commerce, Technology Administration, National Institute of Standards and Technology, Office of Applied Economics, Building and Fire Research Laboratory, (1996).
- [42] Taylor, Harry FW. *Cement Chemistry*. Thomas Telford, (1997).
- [43] Woods, Hubert, Harold H. Steinour, and Howard R. Starke. "Effect of composition of Portland cement on heat evolved during hardening." *Industrial & Engineering Chemistry* 24.11 (1932): 1207-1214.
- [44] Woods, H., H. H. Steinour, and H. R. Starke. "Heat evolved by cement in relation to strength." *Engineering News-Record* (1933): 431-433.
- [45] Lerch, Wm, and Robert Herman Bogue. *The heat of hydration of Portland cement pastes*. Portland Cement Association Fellowship, (1934).
- [46] Verbeck, George J., and Cecil W. Foster. "Long-time study of cement performance in concrete: chapter 6. The heat of hydration of the cements." *Proceeding of American Society of Testing Materials* Vol. 50. (1950).
- [47] Wei, Weili, and Xiaogang Qu. "Extraordinary physical properties of functionalized graphene." *Small* 8.14 (2012): 2138-2151.
- [48] Shahil, Khan MF, and Alexander A. Balandin. "Thermal properties of graphene and multilayer graphene: Applications in thermal interface materials." *Solid State Communications* 152.15 (2012): 1331-1340.
- [49] Eletsii, Aleksandr Valentinovich, et al. "Graphene: fabrication methods and thermophysical properties." *Physics-Uspokhi* 54.3 (2011): 227-258.

CHAPTER 2¹: MEASUREMENT AND PREDICTION OF HEAT OF HYDRATION OF PORTLAND CEMENT USING ISOTHERMAL CONDUCTION CALORIMETRY

2.1 Introduction

Heat of hydration measurement is important for assessing the cement hydration rate as well as assessing the potential temperature rise/fall in concrete elements. Temperature rise that occurs due to mixing of cement with water is caused by the exothermic nature of the interaction of anhydrous cement with water [1]. The interest in cement heat of hydration is primarily due to its contribution to massive concrete elements cracking [2]. It is well established that there is a large temperature rise that occurs within a few days of concrete placement, typically within first 24 to 72 hours. In structural elements, temperature rise and the subsequent cooling results in shrinkage strains that have been implicated in concrete cracking. The resulting tensile stress is partly a function of the temperature rise experienced by the concrete element [2]. The latter is a strong function of the heat of hydration of Portland cement, which is primarily affected by the mineralogy and fineness of the cement.

Experimental measurements and calculations for the heat of hydration (thereon referred to as HOH) of different types of Portland cement have been extensively published in the literature. For several decades, Portland cement specifications adopted ASTM C186 [3] for HOH measurements, which is the heat of solution method. Although the ASTM C186 method has been

¹ Note. "Measurement and Prediction of Heat of Hydration of Portland Cement Using Isothermal Conduction Calorimetry," A. Sedaghat, A. Zayed and P. Sandberg, 2013, Journal of Testing and Evaluation, Vol. 41, No. 6, Copyright © 2013 by ASTM International. Reprinted with permission.

reported to cause difficulties during implementation, [3, 4, 5] but it has the advantage of not requiring the instrument to be occupied for the whole period of experiment. In fact, several tests can be run on overlapping schedules using only one instrument. The test can be used for long test ages as it measures the HOH indirectly instead of adding up the heat for a long period of time [5].

Recently, a new standard method for HOH determination was adopted by ASTM under test method C1702-09 [6]. The method, isothermal conduction calorimetry, indicates two possible mixing routines, namely, internal and external mixing. However, the use of this method has not been incorporated into cement specification ASTM C150 [7]. For Type II (MH) and Type IV, a maximum HOH is indicated for seven days, also, for Type IV, for 28 days in accordance with optional physical requirements of ASTM C150/C150M-09. Besides, ASTM C595 [8] and C1157 [9] have set limits for HOH in accordance with physical requirements while ASTM C1600 [10] has set limits per optional physical requirements. The ASTM specification identifies ASTM C186 for HOH measurements in spite of the availability of ASTM C1702-09.

The isothermal conduction calorimetry has the advantage of measuring the HOH instantly from the time of mixing of water with cement. It is therefore a useful instrument in analyzing the effects of admixtures on cement hydration. This method can be executed with low labor input and with better precision as compared to the heat of solution method [11]. Isothermal conduction calorimetries typically operate at a range of temperatures and with different water to cement ratios. The major advantage of the isothermal conduction calorimetry is that it not only measures the total heat but also records the thermal power “heat flow” at different times. This instrument can perform well with blended cements while the solution calorimetry is less suited [12]. The isothermal conduction calorimetry shows improved precision if compared with the heat of solution method as shown in Table 2.1 [6]. Additionally, the isothermal conduction calorimetry offers simplicity in

the procedure and availability of commercial equipment to conduct the test. Long term studies by Wadso [13] indicate that the calibration coefficients are remarkably stable over time as long as there is no hardware or bath temperature change. It is noteworthy that the ASTM C1702 method is not dependent on knowledge of compound composition, which makes it much more useful for analysis of non-Portland cement.

Table 2.1 Comparison of precisions for isothermal conduction calorimetry and solution calorimetry (per ASTM C1702-09) [6]

Standard Deviation	ASTM C186	ASTMC1702 (Wadso et al.'s Data) [22,23]	ASTM C1702 (VDZ 2006) [24]
Within lab	14.8 KJ/Kg (7 days)	Not available	4.6 KJ/Kg (7 days)
Between lab	16.9 KJ/Kg (7 days)	10.5 KJ/Kg (3 days)	13.6 KJ/Kg (7 days)

The prediction of Portland cement HOH had been proposed earlier using several relationships. Poole [4] has summarized the different approaches that were proposed in the literature. Primarily, the relationships rely on other standard test properties of Portland cement known to relate to HOH. Seven relationships were analyzed for Portland cement, with five of them incorporating cement potential phase composition; two of the five expressions incorporated fineness. The other two expressions analyzed in this work were based on mortar cube strength at three and seven days with the former showing better random error and no apparent bias, a finding that has been confirmed by others [11]. Based on this work [4], ASTM C150 has adopted a heat index expression that would ensure a seven day HOH for Type II MH of 80 cal/g or less. Ferraro, et al.'s [14] analysis indicates that the expression needs to be modified in order to ensure appropriate prediction of HOH using the heat index concept. A concern about the heat index is the fact that it relies on the potential phase composition of Portland cement, namely, tricalcium

silicate and tricalcium aluminate. Previous research has indicated that the potential compound composition for those two phases can be considerably different from direct quantification techniques such as petrography or X-ray diffraction techniques [15].

An alternative method, as described in this research, proposes an empirical relationship by which 84 hours HOH can be used to predict accurately the seven days value. The proposed empirical S-shaped function is given in Equation (2.1). The general exponential function has been used previously by Schindler [16] to quantify the degree of hydration development based on the equivalent age concept. It has also been used by Freiesleben Hansen and Pederson to model strength development [17]. Initially, an effort was made to model HOH data from the time cement was mixed with water up to seven days; however, using a single exponential function to fit all different stages of hydration did not seem to work very well. It is well established in the literature that the hydration process is primarily diffusion controlled once the hydration process is well into the steady state stage [18]. Implementing the proposed S-function to the HOH data between 24 and 84 hours was therefore considered, where the HOH profile can be used successfully to predict HOH at seven days.

$$-\left[\left(\frac{\tau_1 - t_1}{t_1}\right)^{\beta_1}\right]$$

$$H_t = C_1 \cdot e \tag{Eq. (2.1)}$$

[24 < t₁ (hour) ≤ 72 or 84]

H_t = Total heat at given age, J/g

C₁ = Constant, J/g

t₁ = Time from mixing cement with water, Hours

τ₁ and β₁ = Constants defined by the curve shape

2.2 Experimental

Table 2.2 (a&b) depicts the oxide chemical composition and potential phase composition of as received cements (labeled A-J) used in this study as determined by X-ray fluorescence

spectrometry. The ten cements studied are typical industrial Portland cements with Blaine fineness in the range of 325- 612 m²/kg, while C₃S and C₃A are in the range of 52- 65% and 5-11%, respectively. Each cement sample was tested in duplicate runs for HOH for up to seven days in accordance with ASTM C1702 (Method A, internal mixing) [6] using a TAMAIR isothermal conduction calorimetry manufactured by TA instruments. Cement A was also tested in accordance with ASTM C1702 (Method B, external mixing) using the same instrument. The experimental matrix is summarized in Table 2.3.

Table 2.2(a) Chemical oxide composition of as-received cements

Analyte	A	B	C	D	E	F	G	H	I	J
% (SiO ₂)	20.01	20.02	20.51	20.85	20.83	20.74	20.86	18.67	19.01	19.67
% (Al ₂ O ₃)	5.15	5.32	4.91	4.9	4.61	4.45	4.42	5.7	5.66	4.17
% (Fe ₂ O ₃)	3.86	3.88	3.70	3.62	4.2	4.07	3.86	2.63	2.55	2.89
% (CaO)	63.52	63.43	63.54	63.5	64.33	64.83	64.02	60.15	60.89	62.94
% (MgO)	0.92	0.93	0.63	0.64	0.83	0.92	1.12	2.92	2.76	2.58
% (SO ₃)	3.18	3.99	3.03	3.33	2.06	2.58	2.82	4.83	4.6	3.23
%(Na ₂ O)	0.12	0.12	0.09	0.09	0.07	0.07	0.11	0.41	0.37	0.25
%(K ₂ O)	0.42	0.43	0.45	0.45	0.29	0.28	0.28	1.1	1.02	1.07
%(TiO ₂)	0.26	0.27	0.31	0.29	0.29	0.28	0.26	0.25	0.26	0.22
%(P ₂ O ₅)	0.13	0.13	0.12	0.11	0.11	0.1	0.1	0.26	0.25	0.05
%(Mn ₂ O ₃)	0.01	0.01	0.04	0.03	0.08	0.08	0.08	0.07	0.08	0.05
%(SRO)	0.06	0.06	0.06	0.06	0.04	0.04	0.04	0.28	0.28	0.04
%(CR ₂ O ₃)	0.01	0.01	0.01	0.01	0.01	0.01	0.01	<0.01	<0.01	0.01
%(ZnO)	0.01	<0.01	0.05	0.05	0.05	0.05	0.05	0.06	0.07	0.03
% LOI	2.4	1.68	2.7	2.3	1.36	1.22	1.44	2.58	2.54	2.77

Table 2.2(b) Potential phase composition, Blaine fineness, measured and predicted 7 day heat of hydration of as received cements

Potential Phase Compositions	A	B	C	D	E	F	G	H	I	J
%(C ₃ S)	57	53	56	52	61	63	59	47	49	65
%(C ₂ S)	14	17	17	20	14	12	15	18	18	7
%(C ₃ A)	7	8	7	7	5	5	5	11	11	6
%(C ₄ AF)	12	12	11	11	13	12	12	8	8	9
C ₃ S + 4.75*C ₃ A	91	89	88	85	85	87	83	99	101	94
C ₄ AF+2*C ₃ A	26	28	25	25	23	22	22	30	30	21
Fineness (Blaine)m ² /kg	417	612	402	590	325	414	575	405	530	426
Measured 7-day HOH, J/g (cal/g) ASTM C1702 Isothermal conduction calorimetry (Internal mixing)	348 (83)	387 (93)	332 (79)	356 (85)	296 (71)	322 (77)	371 (89)	386 (92)	406 (97)	344 (82)
Predicted 7-day HOH, J/g (cal/g) based on Equation (2.1)& 24-72h data fitted	340 (81)	390 (93)	326 (78)	354 (85)	283 (68)	307 (73)	384 (92)	401 (96)	408 (98)	347 (83)
Predicted 7 -day HOH, J/g (cal/g) based on Equation (2.1) & 24-84h data fitted	347 (83)	389 (93)	330 (79)	356 (85)	291 (70)	314 (75)	382 (91)	394 (94)	406 (97)	344 (82)
Measured 7day HOH, J/g (cal/g) ASTM C186 Heat of Solution	349 (83)	370 (88)	337 (80)	367 (88)	312 (75)	340 (81)	366 (87)	361 (86)	391 (93)	362 (86)

Table 2.3 Experimental matrix, isothermal conduction calorimetry tests at 23 °C

Cement ID	Cement A, B, C, D, E, F, G, H, I, J	Cement A	
		External Mixing 1	External Mixing 2
ASTM C 1702	Internal Mixing	External Mixing 1	External Mixing 2
Cement, g	3.30	9.81	3.38
Water, g	1.65	4.90	1.69
Sand reference, g	12.33	37.37	12.61
Test duration, h	168	168	168

The admixer and 20 ml glass vial, as shown in Figure 2.1, were used for the internal mixing procedure. Internal mixing was conducted by preconditioning the cement and distilled water at $23\pm 0.2^{\circ}\text{C}$. The specified mass of cement was weighed in the glass vial and later was attached to the bottom of the admixer. The admixer syringe was filled with the required mass of water and a small amount of vacuum grease was placed at the tip of the needle to avoid evaporation of water and reaction with cement in the vial. It is noteworthy that a small amount of air between the tip of the needle and the water in the syringe can successfully avoid the evaporation of water and undesired reaction with the cement. The prepared admixer was inserted into the calorimetry cell for 90 minutes to achieve baseline stabilization of $\pm 2 \mu\text{W}$. Afterwards, the TAMAIR Assistant software was set to record the heat flow at 10 second intervals, and the water was injected into the vial over the period of 10 seconds before 60 seconds of manual internal mixing.

The external mixing procedure was conducted by preconditioning the cement and distilled water at $23\pm 0.2^{\circ}\text{C}$. The specified mass of cement and distilled water were weighed in two separate glass vials. At the time of mixing, the distilled water was added to the cement and manual mixing over the period of 45 seconds with a toothpick inside the vial followed. Afterwards, the toothpick was left in the vial, and the vial was immediately sealed and placed into the calorimetry cell. The data logging was initiated one minute before placing the vial into the calorimetry. The baseline stabilized at $\pm 2 \mu\text{W}$ before logging. This method of external mixing has the advantage of taking less than one minute and has minimal thermal effect due to mixing and handling. It appeared that external mixing corrections, as outlined in ASTM C1702, can be avoided for both mixing & handling and lost HOH data at early ages.

The isothermal conduction calorimetry used in this study has eight twin channels that partially share the same heat-sink; therefore, there is a possibility that thermal power in one channel

might affect the power in neighboring channels (crosstalk). This case may occur when two adjacent channels have a significant difference in thermal power or if a sample, with significantly different temperature than the calorimetry, is inserted into the calorimetry [13].



Figure 2.1 Admixer and vial for internal mixing (isothermal conduction calorimetry)

To minimize noise due to cross talk, only two out of the eight channels were simultaneously used, with the two active cells positioned diagonally to each other and all other sample cells charged with Ottawa sand. The w/c ratio was fixed at 0.5 for all samples. The sand reference mass had heat capacity matching the cement paste. The isothermal temperature used was 23 °C. Performance calibration was conducted in accordance with the manufacturer specifications [19]. The highest overall heat flow measured from the cells charged with sand in the period of seven days was used as a measure of the baseline level during the HOH test. The baseline level was used to assess the signal to baseline ratio at different measurement times. The baseline noise level was examined for conformance to the instrument stability criteria, as specified in ASTM C1702, for all the cells used for HOH measurements [16].

2.3 Results and Discussion

2.3.1 Signal to Maximum Baseline Deviation Ratio

Figure 2.2(a) shows the heat flow measured from the sample cell charged with sand that displayed the highest overall heat flow. This was taken as a measure of baseline deviation for the purpose of this study. Figure 2.2(b) also compares the signal from a 3.30 g cement sample relative to the signal from the sand sample (baseline deviation), plotted from four days (96 h) and onwards. The data displayed in Figure 2.2(a) indicate that, for a measurement age of up to seven days, the maximum baseline deviation was at 0.023 mW while the heat flow signal from the cement paste was an order of magnitude higher. This indicates that, for the current system, the signal strength is significantly higher than the maximum baseline deviation even at seven days of hydration. However, for longer hydration times, such as 28 days, that might not necessarily be the case. It is plausible that, rather than specifying the baseline noise level and drift as defined in ASTM C1702, it would be intuitive and practical to define a minimum signal to maximum baseline deviation ratio

of five in addition to specifying the baseline deviation limit of $\pm 20 \mu\text{W}$ to define the criteria for valid HOH measurement for a given system or instrument. A convenient way to define the baseline deviation would be to measure the signal for the period of seven days from an inert reference sample such as sand with the mass matching the heat capacity of the targeted sample and establish the maximum baseline deviation.

2.3.2 Heat Flow and Heat of Hydration Data from Cement Samples

Figures 2.3 & 2.4 present the HOH or the cumulative heat and heat flow over a period of seven days for the Cement A using internal and external mixing methods. The results indicate that the method of mixing (internal versus external) has an effect on the amount of heat measured by isothermal conduction calorimetry; however, differences might not be that significant, as seen in Figure 2.3 & 2.4. The internal mixing method registers the cement and water interaction instantly while external mixing, depending on the time of mixing, might result in missing the dissolution stage and most of the dormant stage of hydration. Internal mixing is expected to yield a more accurate measurement of the heat evolution initially (Figure 2.4(a)), since some heat is either lost or gained from the environment during the external mixing procedure. Furthermore, non-isothermal disturbances are expected to occur during external mixing, which in turn would result in a longer time to reach isothermal condition in the sample and calorimetry. However, the external mixing procedure generates a higher total heat compared to internal mixing, supporting a concern that internal mixing may not result in as efficient mixing as is easily achieved with external mixing. The higher heat values captured for external mixing methods might also reflect differences in the mixing methodology and might not necessarily duplicate the actual concrete mixing methodology.

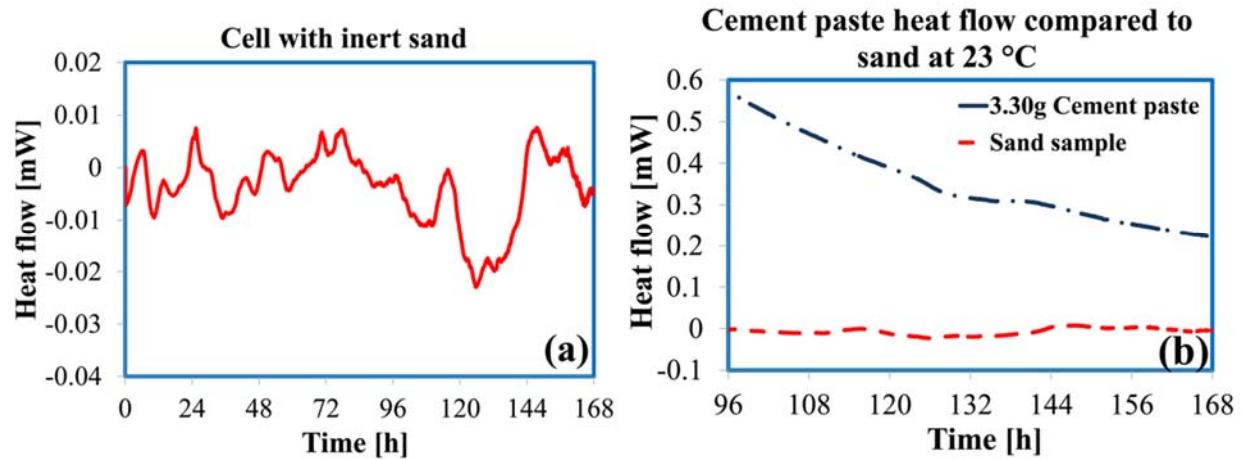


Figure 2.2 (a) Heat flow from sand sample, 0-7 days (b) Heat flow from sand sample compared to the heat flow from a 3.30 g Portland cement sample towards the end of the 7 days test period.

2.3.3 Extrapolation of Total Heat After 24 to 84 Hours of Hydration

All experimental HOH data measurements (isothermal conduction calorimetry) from 24 hours up to 72 or 84 hours of hydration were fitted to the S-shaped analytical function presented in Equation (2.1). Fitting parameters for Equation (2.1) were obtained by using the Solver command, executable in Excel (2010) software. The Microsoft Office Excel Solver tool uses the Generalized Reduced Gradient (GRG2) nonlinear optimization code [20]. The total heat was then extrapolated for up to seven days and was compared to the seven day HOH, experimentally measured by isothermal conduction calorimetry as shown in Figure 2.5, for Cement A. Table 2.4 shows the measured and predicted seven day HOH of Cements A and C based on the internal mixing method (isothermal conduction calorimetry) in addition to HOH prediction results based on the external mixing method (isothermal conduction calorimetry) for cement A. The results indicate that the proposed equation could predict the seven day HOH of cement accurately for both internal and external mixing methods. It is further indicated that fitting the 24-84 hours experimental HOH data to the proposed equation can more accurately predict the seven day HOH than 24-72 hours data fitting.

Table 2.4 Measured and predicted 7 day heat of hydration by isothermal calorimeter

Cement ID	cement A internal mixing	cement A external mixing	cement C internal mixing
Time at maximum heat flow, h	8.8	8.8	8.9
Measured heat after 7 days, J/g	348	360	332
Measured heat after 7 days, J/g	352	358	329
Average	350	359	331
Stdev (measured duplicate runs)	2.83	1.41	2.12
Extrapolated from 24 h to 72 h	340	355	326
Error, J/g	-10	-4	-5
Error, %	-2.8	-1.1	-1.5
Extrapolated from 24 h to 84 h	347	362	330
Error, J/g	-3	3	-1
Error, %	-0.8	0.8	-0.1

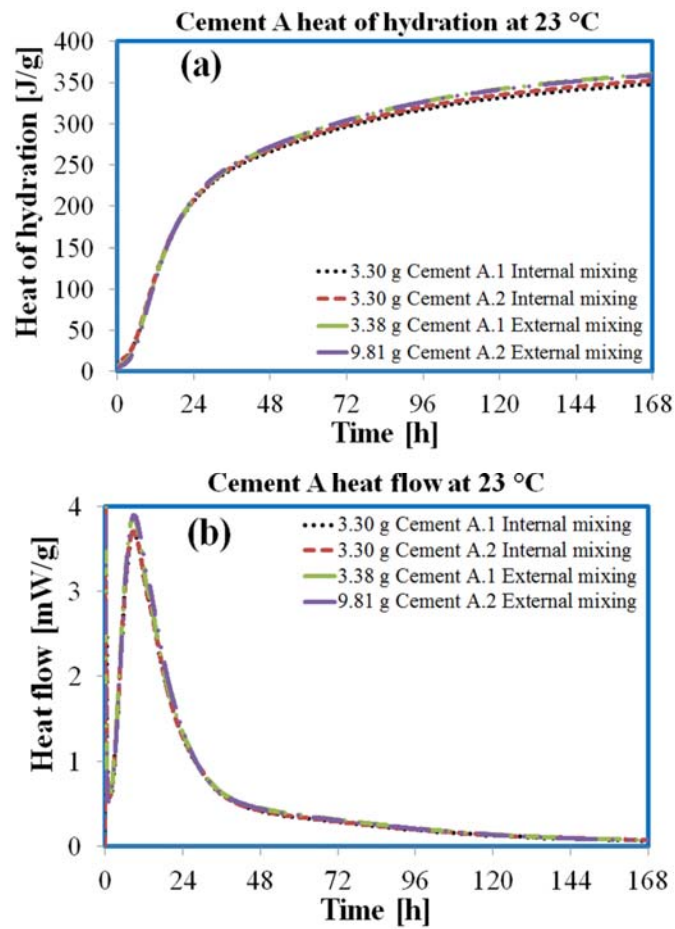


Figure 2.3 (a) Heat of hydration of cement A (internal and external mixing),
(b) - Heat flow of cement A (internal and external mixing)

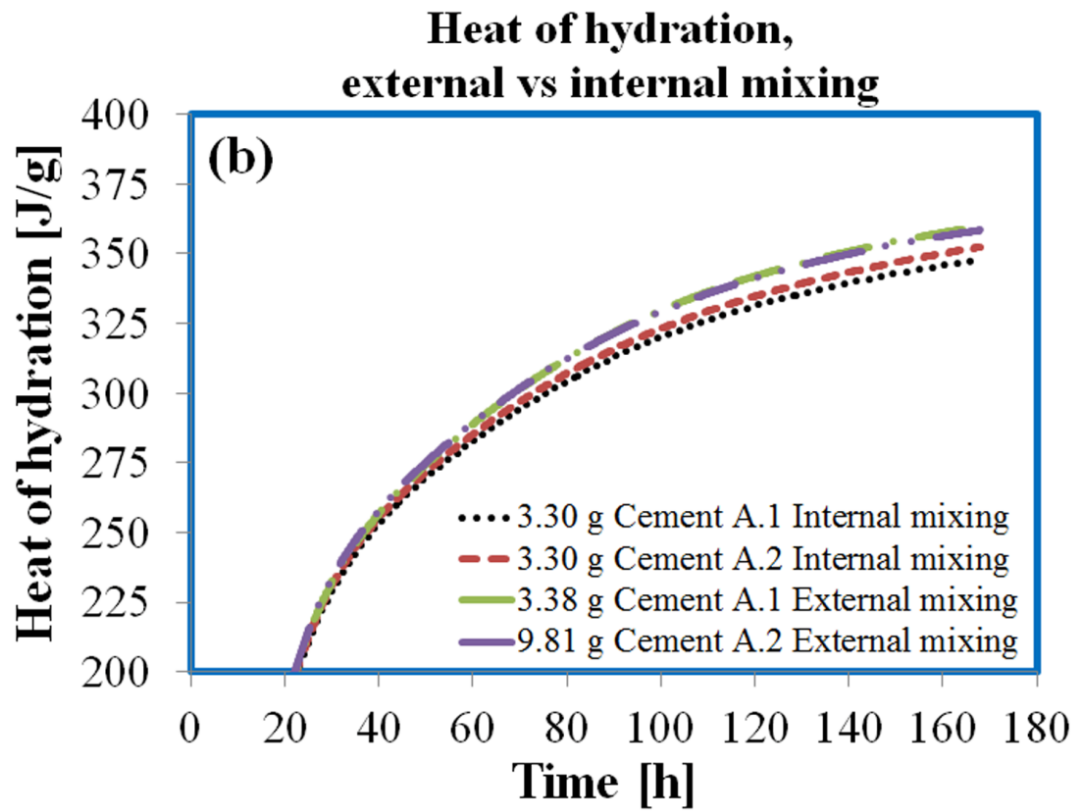
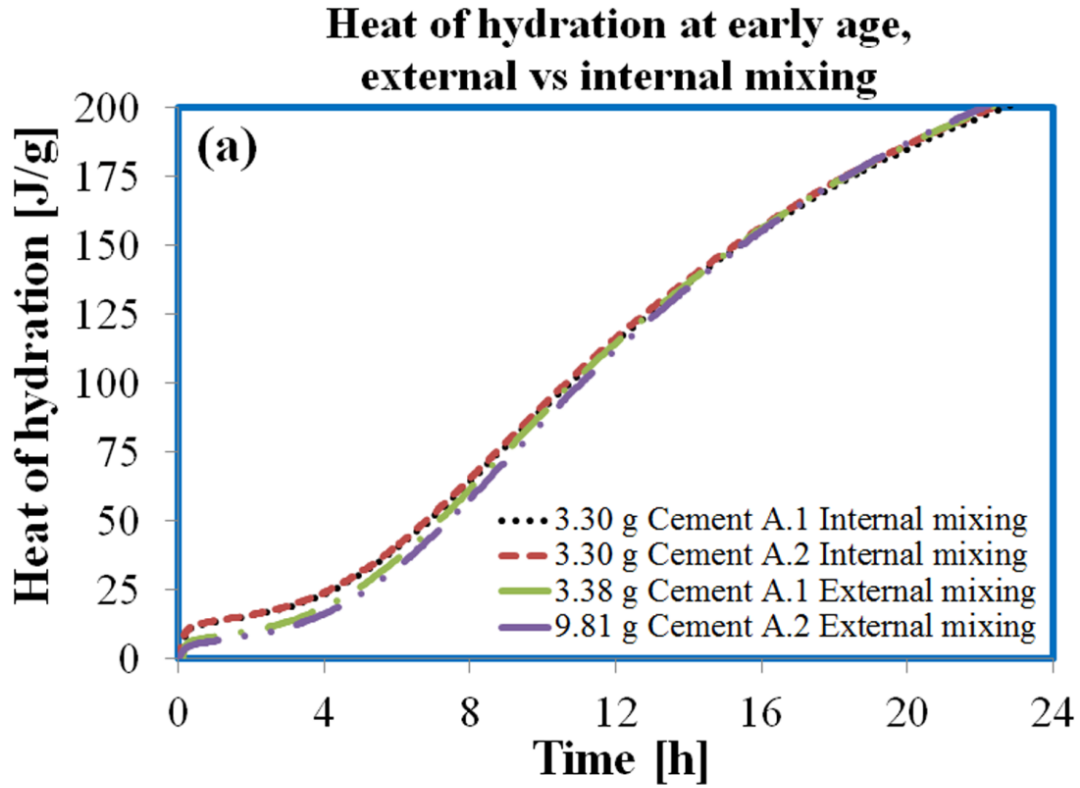


Figure 2.4 (a&b) Heat of hydration for cement A, external vs. internal mixing

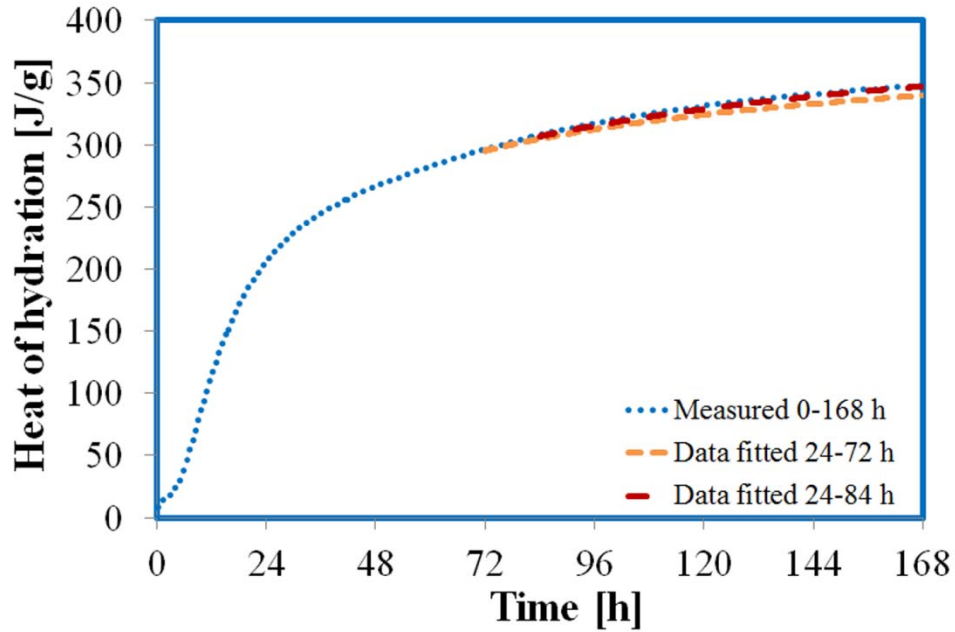


Figure 2.5 Measured and extrapolated 7 day heat of hydration of cement A

To evaluate the hypothesis, eight industrial Portland cements (Labeled B&D-K) were selected and their HOH was measured using the internal mixing method (isothermal conduction calorimetry) as tabulated in Table 2.2(b). The measured and predicted (using Equation (2.1)) seven day HOH were compared to each other to determine the suitability of Equation (2.1) to predict the seven day HOH. Fitting parameters for Equation (2.1) (based on isothermal conduction calorimetry method measurements) for all the cements (A-J) are tabulated in Table 2.5.

Table 2.5 S-shaped analytical function constants

Cement ID	Constants for data fitting 24-72 h			Constants for data fitting 24-84 h		
	C_1	τ_1	β_1	C_1	τ_1	β_1
Cement A (Internal mixing)	409.0	13.3	0.66	454.1	15.0	0.54
Cement A (External mixing)	457.2	15.3	0.57	519.4	19.0	0.47
Cement B (Internal mixing)	485.1	11.4	0.56	478.9	11.2	0.58
Cement C (Internal mixing)	390.7	11.9	0.64	414.9	12.6	0.57
Cement D (Internal mixing)	457.1	10.3	0.49	470.1	10.8	0.47
Cement E (Internal mixing)	452.9	21.9	0.37	732.3	117.8	0.23
Cement F (Internal mixing)	377.1	9.8	0.55	441.1	12.4	0.41
Cement G (Internal mixing)	625.5	17.5	0.32	594.4	15.1	0.34
Cement H (Internal mixing)	440.4	17.9	1.06	423.1	17.7	1.17
Cement I (Internal mixing)	421.1	11.7	1.30	416.7	11.9	1.37
Cement J (Internal mixing)	376.5	12.5	0.96	369.1	12.6	1.02

Figure 2.6 shows the difference between the measured HOH (internal mixing, isothermal conduction calorimetry) and the predicted HOH (Equation (2.1)) at seven days. The mean and standard deviation of errors were calculated as -0.8 and 10J/g (24-72 hours data fitted) and 0.5 and 5.6J/g (24-84 hours data fitted), respectively.

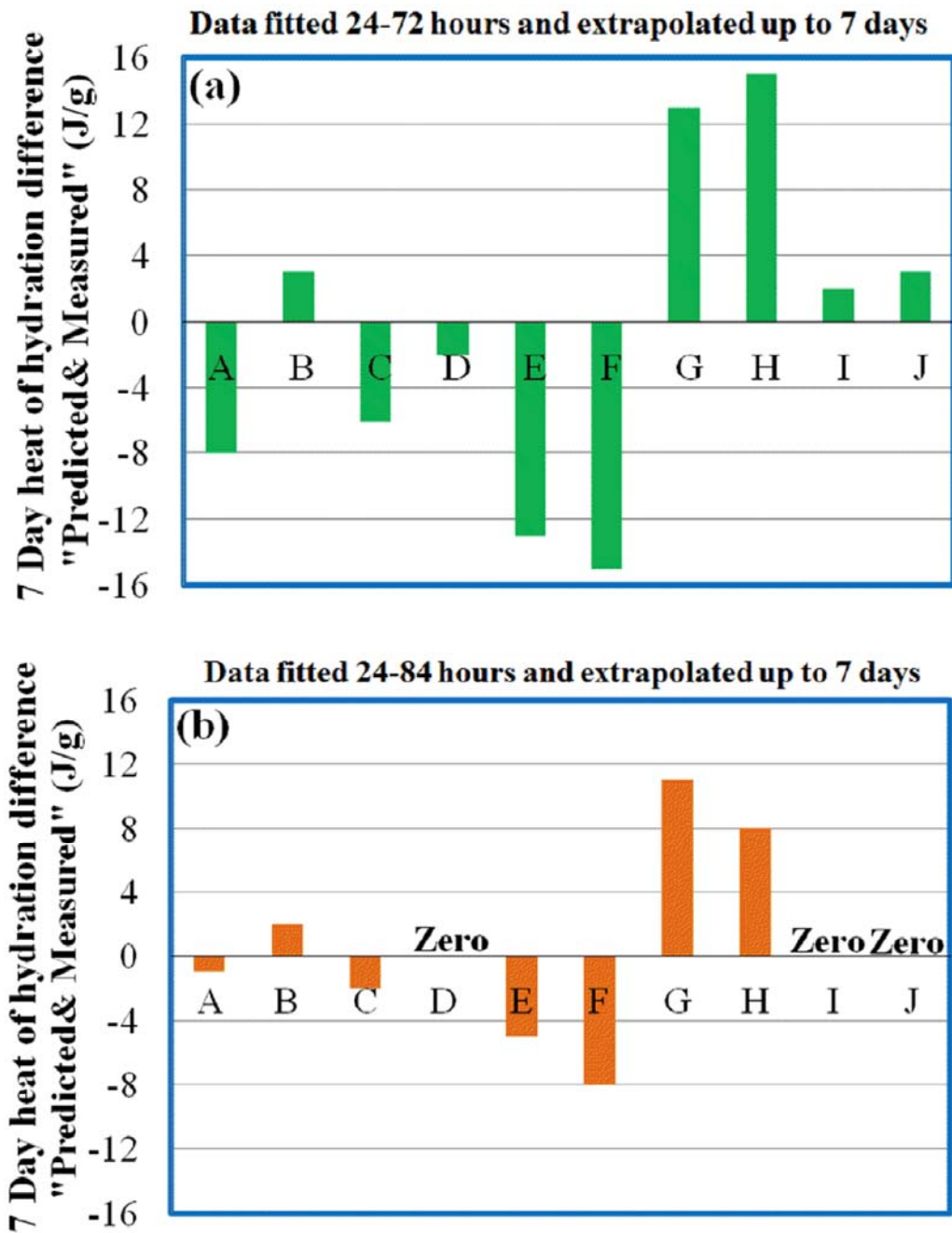


Figure 2.6 (a&b) - 7 Day heat of hydration difference "Predicted & Measured"

The results indicate that fitting 24-84 hours of experimental data measurements generates less difference between the predicted and actual HOH measurements for seven days. The difference between the predicted and measured seven day HOH ranges from -8 J/g to about 11 J/g resulting from the 24-84 hours experimental data fitted. To better analyze the data, the measured seven day HOH was plotted versus the predicted at seven days as shown in Figure 2.7.

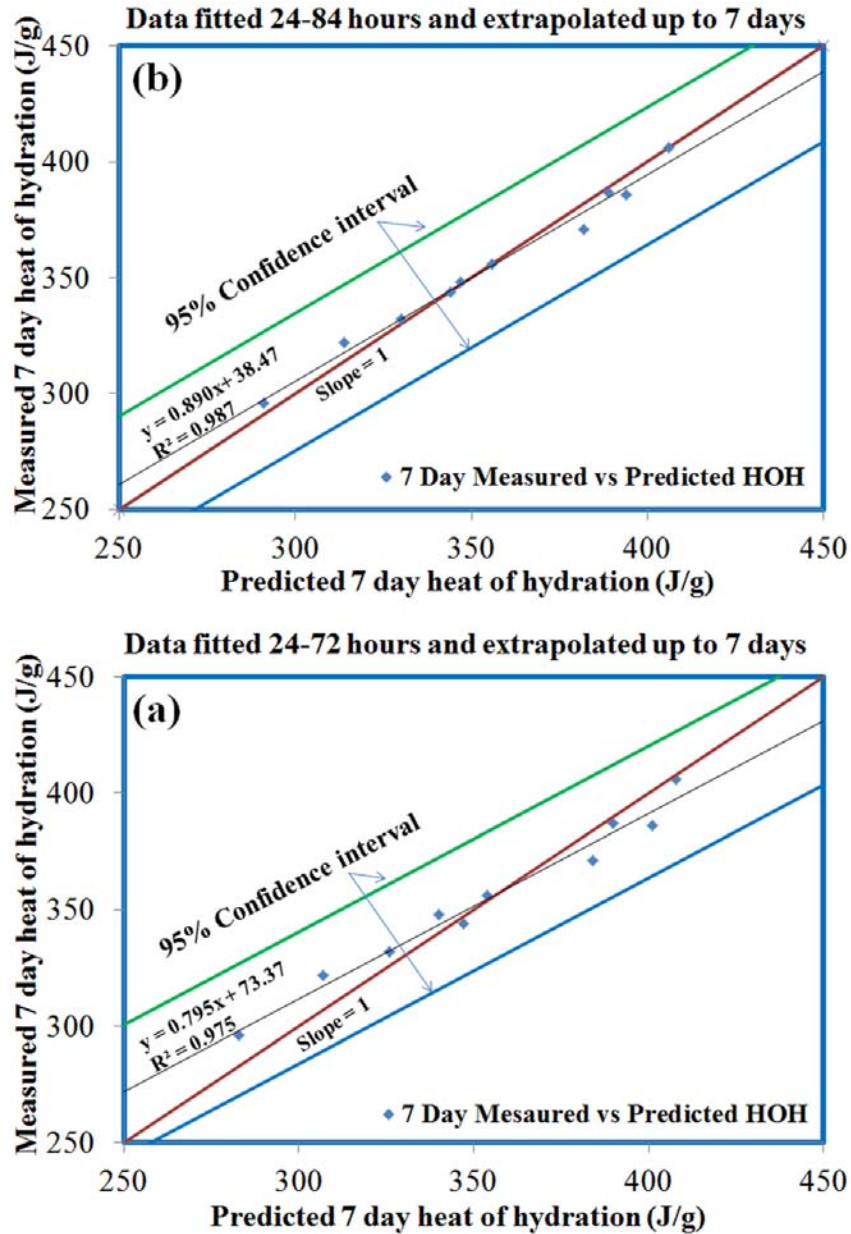


Figure 2.7 (a&b) Measured versus predicted 7 day heat of hydration of cements (Internal mixing)

The results indicate that the relationship is linear with a high coefficient of determination (R^2), exceeding 0.97 for both cases of 24-72 and 24-84 hours experimental data fitted. Comparing this value to values reported earlier in the literature, it appears that the proposed equation shows less random error than Bogue dependent relationships for the seven day HOH predictions. The line of equivalency indicates minimal bias especially for the predicted seven day HOH resulted from fitting the 24-84 hours experimental data.

The confidence interval based on two sample t-test hypothesis are also calculated and shown in Figure 2.7. In general, the 95% confidence interval is dependent on the sample size incorporated into the calculation of means and standard deviations [21]. It is recognized that two data sets with the same means and standard deviations but different sample sizes shall create different confidence intervals. As a simple example, a data set with 10 pairs of determination sample size (measured and predicted seven day HOH) has a confidence interval about three times larger than a data set with 30 pairs of determination even if both data sets have similar means and standard deviations [21]. In this study, the confidence intervals on seven day HOH were calculated as ± 36 J/g (24-72 hours experimental data fitted) and ± 34 J/g (24-84 hours experimental data fitted). It is believed that the confidence intervals (Figure 2.7) are large as a result of small sample size (10 pairs of determination for each data set).

Statistically, a smaller sample size shall result in a larger confidence interval. This measure cannot accurately evaluate the proposed equation due to the small sample size but can be used as a suitable means in future works where data sets with larger sample size is implemented to validate the model. It is understood that the comparison of different models can be obtained by determining the confidence interval for each model with the same sample size as used for all the models; then, the model with the smallest confidence interval is the most suitable for prediction purposes.

Considering the mean and standard deviation of errors for the predicted seven day HOH resulted from fitting the 24-72 and 24-84 hours measured HOH data, and smaller confidence interval of ± 34 J/g (24-84 hours data fitted) compared to ± 36 J/g (24-72 hours data fitted), seven day HOH can be predicted with better accuracy if 24-84 hours experimental data is fitted to Equation (2.1).

Due to the low systematic bias and random error observed on working with 10 cements, it is proposed that a larger matrix of cements be examined to further verify the usefulness of the proposed method for specification consideration. It is expected that if the sample size is increased to 30 cements, with the same means and standard deviations as the sample size of 10 cements, the confidence limits of approximately ± 12 J/g resulted from 24-72 hours fitted data and ± 11 for 24-84 hours fitted data can be observed for seven day HOH.

2.4 Conclusions

A careful study on the HOH of Portland cement using isothermal conduction calorimetry indicates that the total heat generated at seven days can be predicted based on heat measurements for only 84 hours and using an S-curve function, with acceptable accuracy when compared to the heat measured using isothermal conduction calorimetry (ASTM C1702). The authors suggest that a wider sample matrix (larger sample size) be examined to validate the proposed function as an alternative method of predicting the HOH of Portland cement at seven days. It is also suggested that the proposed function be examined for its suitability in predicting the 28 day HOH of Portland cement.

2.5 References

- [1] Odler, Ivan. "Hydration, setting and hardening of Portland cement." *Lea's Chemistry of Cement and Concrete* 4 (1998): 241-297.
- [2] Mehta, P. K., and Monteiro, P. J. M.. "Microstructure and properties of hardened concrete." *Concrete: Microstructure, properties and materials* (2006): 41-80.
- [3] ASTM Standard C186, "Standard test method for heat of hydration of hydraulic cement," Annual book of ASTM Standards, Vol. 04.01, ASTM International, West Conshohocken, PA, (2005).
- [4] Poole, Toy S. "Predicting seven-day heat of hydration of hydraulic cement from standard test properties." *Journal of ASTM International* 6.6 (2009): 1-10.
- [5] Poole, Toy. Revision of test methods and specifications for controlling heat of hydration in hydraulic cement. No. PCA R&D Serial No. 2007. Portland Cement Association, (2007).
- [6] ASTM Standard C1702 -09a, "Standard test method for measurement of heat of hydration of hydraulic cementitious materials using isothermal conduction calorimetry," Annual Book of ASTM Standards, Vol. 04.01, ASTM International, West Conshohocken, PA, (2009).
- [7] ASTM Standard C150/C150M, "Standard specification for hydrated hydraulic lime for structural purposes," Annual book of ASTM Standards, Vol.04.01, ASTM International, West Conshohocken, PA, (2009).
- [8] ASTM Standard C595/C595M-10, "Standard specification for blended hydraulic cements," Annual book of ASTM Standards, Vol. 04.01, ASTM International, West Conshohocken, PA, (2010).
- [9] ASTM Standard C1157/C1157-10, "Standard performance specification for hydraulic cement," Annual book of ASTM Standards, Vol. 04.01, ASTM International, West Conshohocken, PA, (2010).
- [10] ASTM Standard C1600/C1600M-08, "Standard specification for rapid hardening hydraulic cement," Annual book of ASTM Standards, Vol. 04.01, ASTM International, West Conshohocken, PA, (2008).
- [11] Qi, Chengqing, et al. "Use of isothermal conduction calorimetric method for measuring the heat of hydration of cement." *Journal of ASTM International* 6.10 (2009): 1-9.
- [12] Wadsö, Lars. "Applications of an eight-channel isothermal conduction calorimeter for cement hydration studies." *Cement International* 5 (2005): 94-101.

- [13] Wadsö, Lars. "Operational issues in isothermal calorimetry." *Cement and Concrete Research* 40.7 (2010): 1129-1137.
- [14] Ferraro, C. C., C. A. Ishee, and M. Bergin. Report of changes to cement specifications AASHTO M 85 and ASTM C150 subsequent to harmonization. FL/DOT/SMO/10-536). Tallahassee, FL: Florida Department of Transportation, (2010).
- [15] Lawrence, C. David. "The constitution and specification of Portland cements." *Leas's Chemistry of Cement and Concrete*, 4th ed. Edited by PC Hewlett. Butterworth-Heinemann, UK (1998): 131-193.
- [16] Schindler, Anton K., and Kevin J. Folliard. "Heat of hydration models for cementitious materials." *ACI Materials Journal* 102.1 (2005): 24-33.
- [17] Nicholas, J. Carino. "The maturity method: theory and application." *Cement, Concrete and Aggregates* 6.2 (1984): 61-73.
- [18] Scrivener, Karen L., and André Nonat. "Hydration of cementitious materials, present and future." *Cement and Concrete Research* 41.7 (2011): 651-665.
- [19] TAM AIR Calorimeter Operator's Manual. Revision C, TA Instrument, New Castle, Jan (2008): pp. 1-64.
- [20] Retrieved from: <http://office.microsoft.com/en-us/excel-help/define-and-solve-a-problem-by-using-solver-HP010072691.aspx?CTT=1>: On Jan 17th (2013).
- [21] Montgomery, Douglas C. *Design and analysis of experiments*. John Wiley & Sons, 2008.
- [22] Wadsö, Ingemar, and Robert N. Goldberg. "Standards in isothermal microcalorimetry (IUPAC technical report)." *Pure and Applied Chemistry* 73.10 (2001): 1625-1639.
- [23] Wadsö, Lars. "Temperature changes within samples in heat conduction calorimeters." *Thermochimica Acta* 366.2 (2001): 121-127.
- [24] VDZ, "Round Robin Heat of Hydration 2006," Research Institute of the German Cement Industry, Cement Chemistry Department, Dussel-dorf, Germany, (2006).

CHAPTER 3² : PREDICTION OF ONE, THREE AND SEVEN DAY HEAT OF HYDRATION OF PORTLAND CEMENT

3.1 Introduction

Heat of hydration is a property of Portland cement and a direct result of chemical reactions between cement and water. The amount of heat released is dependent upon the cement composition, curing temperature, water to cement ratio, and cement fineness. The phases mainly responsible for heat generation are tricalcium silicate (C₃S), dicalcium silicate (C₂S), tricalcium aluminate (C₃A) and tetracalcium aluminoferrite [1-4].

High temperature resulting from heat of hydration (thereon referred to as HOH) of cement can affect the hydration process, and consequently the kinetics of development of the mechanical properties of concrete [5]. While the current research correlates the heat of hydration with the cement fineness and mineralogical composition, others related the same property to the strength development in cement paste. Kumar et al. correlated the HOH with the compressive strength of the cement paste and developed a linear relationship for the strength prediction based on the heat release [6]. One of the main reasons triggering the interest in HOH of cement is its implication in thermal cracking in concrete. The high temperature gradient between the inner core and the outer surface of a concrete element is known to result in large tensile stresses that may exceed tensile strength, thus leading to early-age thermal cracking in mass concrete [7]. Cement fineness is a

² Note. "Prediction of One, Three & Seven Day Heat of Hydration of Portland Cement," A. Sedaghat, N. Shanahan and A. Zayed, 2014, Journal of Materials in Civil Engineering, p. 04014257, Copyright © 2014 by ASCE copyright Clearance Centre. Inc. Reprinted with permission.

critical component affecting the HOH of Portland cement; the primary reason for contractors to resort to finer cement is its high early strength and faster construction operations [8]. Higher cement fineness provides higher surface area for cement to react with water, therefore resulting in an increase in rate of heat liberation at early ages and higher internal temperature in the concrete elements [9]. Additionally, small particles can serve as nucleation sites for precipitation of hydration products. This effect has also been illustrated with the addition of mineral admixtures, such as fine limestone, to Portland cements. Chemical composition and interfacial properties of the mineral admixture may determine its tendency to serve as an efficient nucleant and/or participation of its dissociated ions in chemical reaction with the calcium silicate hydrate product [10]. Kumar et al. noted that smaller particles have higher nucleation rates possibly due to experiencing higher grinding action and consequent highly damaged surface [11]. Adjustment of cement or mineral fineness interground or blended together may provide a solution to maintain the early age properties similar to Portland cement while providing the desired strength and reducing the clinker factor of Portland cements [12].

ASTM C1702, Isothermal conduction calorimetry, [13] and ASTM 186, heat of solution calorimetry, [14] are two available methods under ASTM standard specifications to measure the HOH of cements. Heat of solution calorimetry measures the temperature rise of the acidic solution resulting from the decomposition of the anhydrous and partially hydrated cement separately. The difference between the heat of solution of anhydrous and partially hydrated cement can be calculated as the heat evolved during the hydration period. Considering the experimental circumstances, this method is labor intensive and requires application of hazardous acidic substances [15].

Isothermal conduction calorimetry has the ability to record the heat flow resulting from the cement hydration, immediately from the initiation of reaction of water with cement. The calorimetry provides the user the ability to study the hydration stages from the recorded heat flow curve at the desired hydration age. Isothermal conduction calorimetry maintains the bath temperature constant, therefore, avoiding the effect of temperature change on HOH development mechanism, contrary to the systems in adiabatic conditions in which the temperature change due to cement hydration process may affect the HOH development mechanism. Sample preparation and operation of the instrument are fairly easy, though it requires some basic training. The cumulative heat at any age can be calculated by the integration of the area under the heat flow curve versus time [16-19].

Effect of cement phase composition on HOH has been extensively studied by several researchers. Woods, et al. [20] developed equations predicting the HOH of cements at the ages of 3, 7, 28, 90 and 180 days based on the measured HOH of 13 cements using solution calorimetry. The HOH equations were defined as a linear regression of major phases of C_3S , C_3A , C_2S , and C_4AF . The fineness of cements used to calibrate the equations falls within the range of 1390 to 1670 cm^2/g determined by a sedimentation device. The study concluded that fineness of cement does not have substantial effect on the generated heat. Good linear correlations were indicated between the HOH at 3 days, 180 days, and 1 year ages and the amount of $C_3S+2.1C_3A$, separately [21]. Comparison of measured and predicted HOH in terms of oxide composition for four commercial cements indicates that the equations can overestimate the HOH by 11 Cal/g at the ages of 3, 7 and 28 days and by 5 Cal/g at the age of 180 days [20].

Lerch et al.'s [22] work on HOH shows a significant effect of cement fineness on HOH at the ages of one, three, and seven days while it is less drastic at the ages of 28 days and up.

Verbeck, et al. [23] established relationships between the HOH of cements and their composition at several ages ranging from three days up to 6.5 years. The least squares method was implemented to fit the experimental data to the proposed equations assuming linear and independent relationship between cement phases of C_3S , C_3A , C_2S , C_4AF , SO_3 and HOH. Significant discrepancy between measured and predicted heat by his methods can be observed for type III and type IIIA cements at ages of three and seven days. Although the relationships were established based on the main phases of cements affecting the heat at varied ages, the fineness was not incorporated into the proposed equations as a significant factor affecting the HOH.

Poole [24] developed several equations based on the values of HOH of individual compounds as outlined in the Lea's chemistry of cement [1], data provided by CCRL and US Army corps of engineers, and the data taken from the Verbeck and Foster's [23] research study. One of the equations predicting the seven day HOH was developed as a linear function of C_3S , C_3A , C_2S , C_4AF and Blaine fineness based on the data taken from the Verbeck and Foster's research study. It should be noted that these cements have variable phase compositions with the Blaine fineness in the range of 285 to 490 m^2/kg . Poole's analysis indicates approximately 0.4 J/g increase/decrease in seven day HOH per unit m^2/kg change (increase/decrease) of Blaine fineness. Poole concluded that Blaine fineness has an effect on seven day HOH, but a relatively large change in cement fineness is required to make a change in the seven day HOH of cements. Bentz [25] studied the change in seven day HOH of a cement with three finenesses of 302, 387 and 613 m^2/kg . He reported 0.46 J/g of change in HOH when the Blaine fineness changed from 302 to 387 m^2/kg , however this change was 0.07 J/g when the Blaine fineness changed from 387 to 613 m^2/kg . The change in seven day HOH, on average, occurred as 0.18 J/g when the Blaine fineness changed from 302 to 613 m^2/kg . It is understood from these research studies that the effect of Blaine

fineness on seven day HOH is strongly dependent on the phase composition of the cements studied as well as the range of the Blaine fineness in which the cements HOH are examined.

Bentz et al. [26] conducted several HOH experiments on type I/II Portland cement using isothermal conduction calorimetry at w/c' s of 0.325, 0.35, 0.4 and 0.45. It can be observed that the pastes prepared at w/c of 0.35, 0.4 and 0.425 show similar HOH at one day while this heat is 10% less for the mix prepared at w/c of 0.325. HOH of cement pastes prepared at w/c of 0.4 shows 1.7% and 2.9 % slightly less HOH, respectively at three and seven days, relative to the pastes prepared at w/c of 0.425. The HOH of pastes prepared at w/c of 0.35 and 0.325 relative to the paste prepared at w/c of 0.425 shows respectively, 3.4% and 16.9% less HOH at three days and respectively 7.4% and 23.5% less HOH at seven days. As it is evident from the findings, HOH of cement paste is drastically influenced at w/c of 0.35 while this impact is gradually fading out as the w/c approaches 0.425. It is well established in the literature that the cement pastes prepared at lower w/c < 0.42 may undergo self-desiccation process since not sufficient water is available for continuation of hydration process [27]. Bentz et al.'s findings are consistent with the results provided by Pane et al. in regards to impact of w/c on HOH of cement paste [28].

This research aims to establish equations predicting one, three and seven day HOH of Portland cements using cement phase composition and fineness at constant water to cement ratio of 0.5 and constant isothermal bath temperature of 23 °C. Blaine fineness and particle size distribution of candidate cements (as-received and ground cements (1) through (4)) was measured, and their suitability as a measure of cement fineness to develop the HOH equations was studied. Validation of the proposed equations was conducted by comparing the HOH of eight as received Portland cements (cements A through H) measured by isothermal conduction calorimetry with the calculated heat using the proposed equations. The suitability of the proposed equations to predict

the HOH was examined using statistical analysis and by establishment of paired comparison t-test confidence intervals on the predicted and measured HOH. The proposed equations can be used to identify Portland cements with high HOH which have the potential to cause thermal cracking in mass concrete elements. Also the proposed equations can be implemented to correlate the HOH with other properties of Portland cement for the prediction of physical and chemical properties and quality control of manufactured Portland cement and concrete [29].

3.2 Experimental

Four ASTM Portland cements (cements (1) through (4)) with different mineralogical composition were selected. The cements were ground separately with ethanol 200 proof absolute 99.5% pure in an air tight jar using McCrone micronizing mill [30] for 1.5, 3, 6 and 9 minutes to obtain varied finenesses. Ethanol was chosen as a slurry liquid to lessen the effect of grinding heat on temperature sensitive phases, including gypsum. Each grinding mix contained six grams of cement and ten grams of ethanol for optimum grinding efficiency. Wet grinding assists in homogeneity of the ground cement as well as reducing the oxidation and deformation of crystal lattice structure [30-31]. After the grinding operation, the slurry mix was vacuum filtered with an ultrafine Durapore membrane filter with 0.45 μ m mesh, and a Buchner funnel was used to extract the ethanol from the mix [32]. The ground cements were then oven dried at 43 °C for 90 minutes to remove as much ethanol as possible from the mix and then desiccated for 24 hours. It was understood that 43°C oven drying of ground cement does not have phase shifting effect, due to temperature, on gypsum since conversion from gypsum to hemihydrate or anhydrate occurs at higher temperatures [33]. At the time of removal of ground cements from desiccators, they were manually ground with spatula to a homogenous soft powder and stored in dry watertight plastic containers until testing.

Blaine fineness of cements was measured by an air permeability apparatus conforming to ASTM C-204 [34]. Particle size distribution of cements was determined using a Horiba laser scattering particle size analyzer (LA-950) in triplicate runs on all the samples [35-36]. Describing the laser diffraction method, when light hits a cement particle, the diffracted light is generated from the particle. Based on the light scattering theory, the diameter of cement particle is determined based on the scattered light strength while the particle's circumference length and the incoming light's wavelength are compared. Particle size diameter parameter α ($\alpha=\pi D/\lambda$) and particle refractive index dictate the scattered light strength. Before conducting the measurements, HORIBA instrument was adjusted to obtain 5000 data measurements per second with 15 iterations. Refractive index of 1.7-1.0i was specified for the diffraction measurements of cement particles. This value was obtained from the "Certification of SRM 114q: Part II (Particle size distribution), NIST Special Publication 260-166" conforming to the HORIBA LA-950 user's manual. The particle size distribution measurements were conducted in automatic mode and on dry cement powder, implementing a small nozzle at 0.3 (MPa) of air pressure. Maximum standard deviation (on cumulative volume (%)) on difference of average of three runs and each run of laser diffraction measurement for each sample was calculated as 0.6% indicating very insignificant deviation and strong repeatability of the measurements.

A TAMAIR isothermal conduction calorimetry manufactured by TA instruments was implemented to measure the HOH of cements in accordance with ASTM C-1702, method A, internal mixing, [13] at 23 °C isothermal bath temperature. Internal mixing provides the user the ability to record the HOH of cements immediately from the time of mixing of water with cement. Internal mixing was conducted by 10 seconds of water injection into the admixer ampoule followed by 60 seconds of manual constant uniform internal mixing (13 full turns) using the

designated admixer. Further detailed information regarding this methodology is available in [2]. Room temperature was maintained close to the calorimetry bath temperature to avoid any interruption of heat exchange between the water in the admixer syringe and the surrounding environment at the time of lowering the admixer into calorimetry. Water to cement ratio of 0.5 was selected to avoid self-desiccation of cement paste [27]. All the HOH measurements were performed in duplicate runs to ensure the precision of results. It is noteworthy that all the duplicate runs have less than 1% heat difference from the average of the two runs at one, three and seven day hydration ages. HOH measurements are interestingly repeatable and heat flow curve generated from the first and second runs, for each specimen, overlap throughout the complete hydration period with the maximum 30 ($\mu\text{W/g}$) heat flow deviation from each other at any hydration age (with the exception of the first 15-20 minutes of initial stage of hydration). It should be noted that shape of the heat flow curve at the initial stage of hydration may be affected by the speed of internal mixing using the designated admixer, though the cumulative heat shall merge for both first and second runs after approximately an hour from the hydration process initiation. Figure 3.1 clearly shows the repeatability of the HOH measurements as indicated by transparent overlapping of the first and second heat flow runs for two specimens used in this study.

Mineralogy of cements was studied using X-ray diffraction. The diffractometer used in this study was a PANalytical Cubix Pro coupled with PANalytical X'Pert Industry and HighScore Plus softwares for crystalline phase analysis. Softwares implement Rietveld refinement simulation for phase analysis and quantification. The instrument was equipped with accelerating detector, capable of collecting a suitable X-ray pattern scan for quantification purposes, in less than six minutes. The X-ray tube was operated at a current of 40 mA and a voltage of 45 KV. The 2θ scan range was set for $5-60^\circ$ using a step size of 0.012° . The X-ray pattern of each sample was obtained

in triplicate runs. For cements (1) through (4), the quantity of each crystal phase was determined as the average of the Rietveld refinement result of three runs of as received cements and 12 runs of ground cements, individually, for each cement. For cements A through H, the quantity of each crystal phase was determined as the average of the Rietveld refinement result of three runs of as received cement, individually, for each cement.

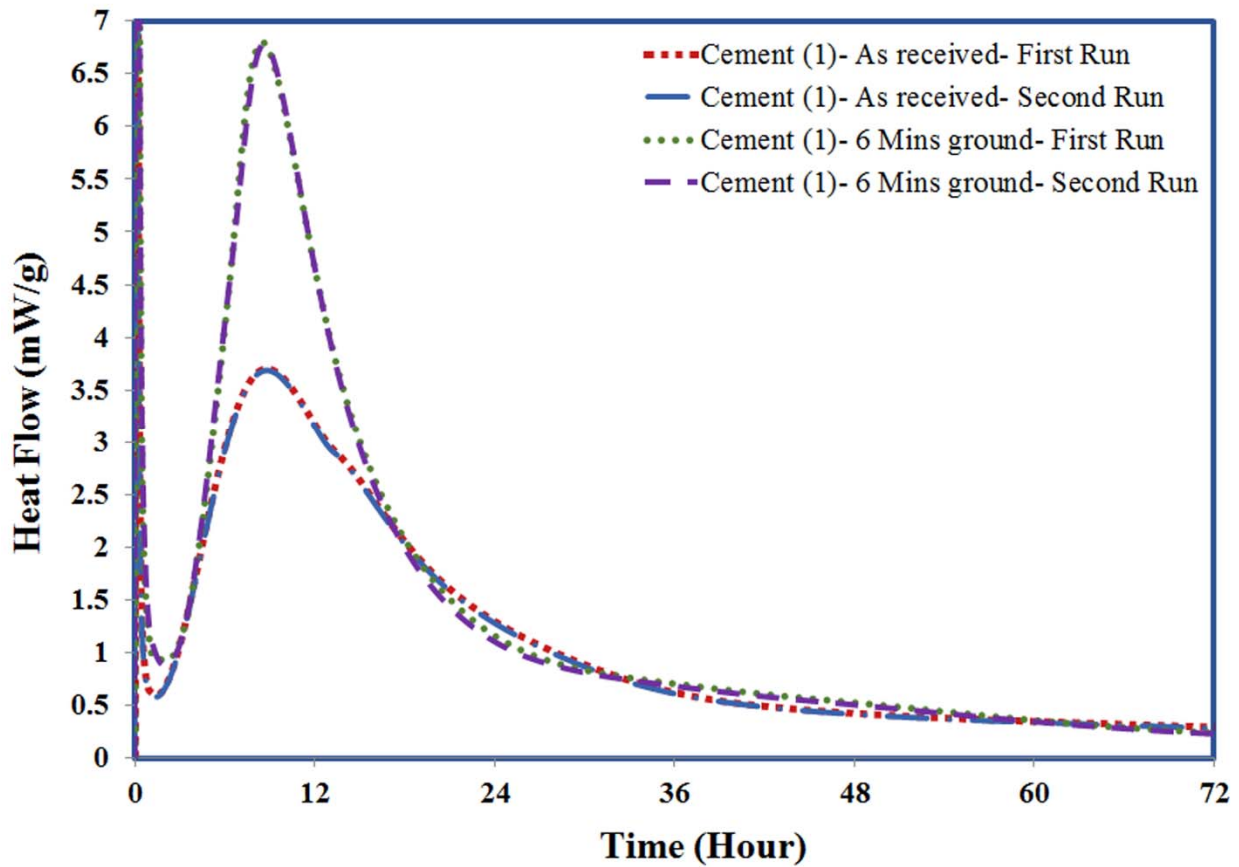


Figure 3.1 Evaluation of the repeatability of the heat flow measurements

3.3 Results and Discussion

3.3.1 X-ray Diffraction and Phase Quantification of Cements (1) Through (4)

X-ray patterns of cements (1) through (4) were measured and their crystal phase quantification (using Rietveld refinement simulation) were determined in our research lab. The X-ray patterns are shown in Figure 3.2 Rietveld refinement simulation allows direct quantification of

Portland cement crystalline phases. Improved repeatability and reproducibility of the results can be observed from the method and prior research [37]. This method uses full profile fitting simulation to calculate the quantity of each phase associated with the peaks at specific 2θ locations. It is noteworthy that implementation of automatic softwares (PANalytical X'Pert Industry and HighScore Plus) eases the use of the Rietveld method by iteratively comparing the X-ray pattern of the Portland cement sample to the X-ray pattern of each reference phase in the data base (ICDD or ICSD) [38].

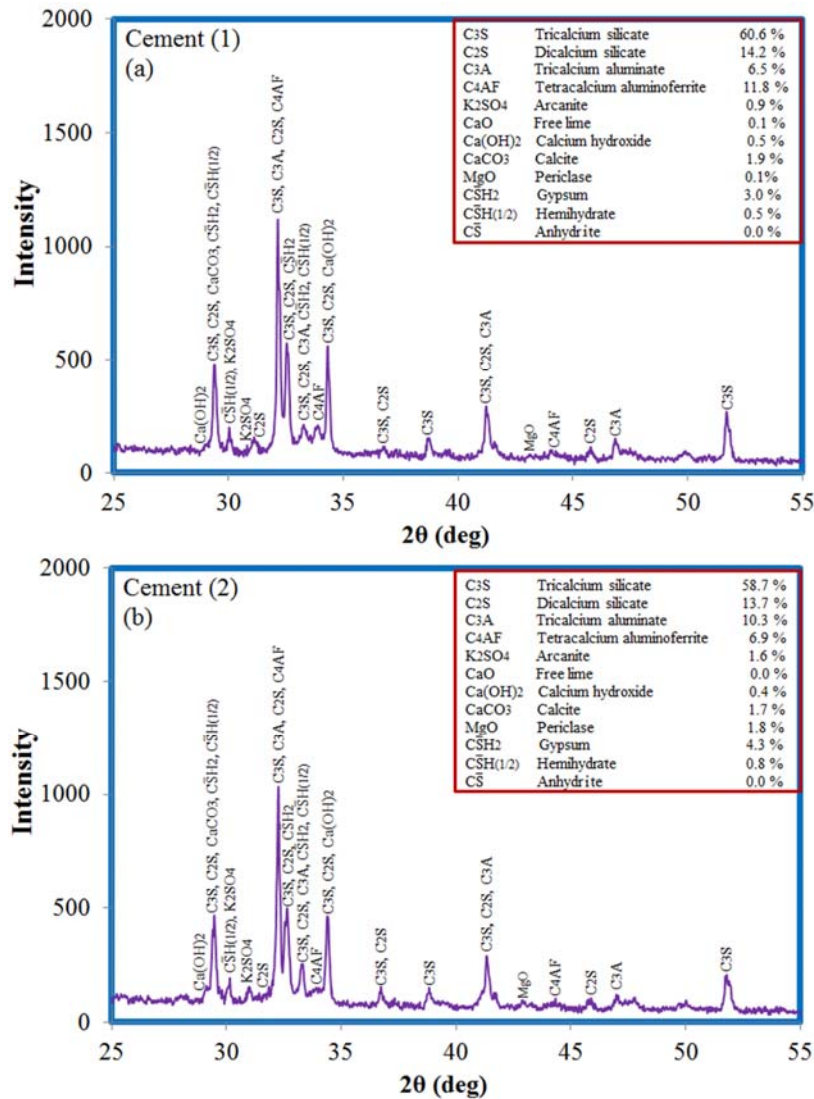


Figure 3.2 X-ray patterns and Rietveld refinement quantification of as received and ground cements, (a) cement (1), (b) cement (2), (c) cement (3), (d) cement (4)

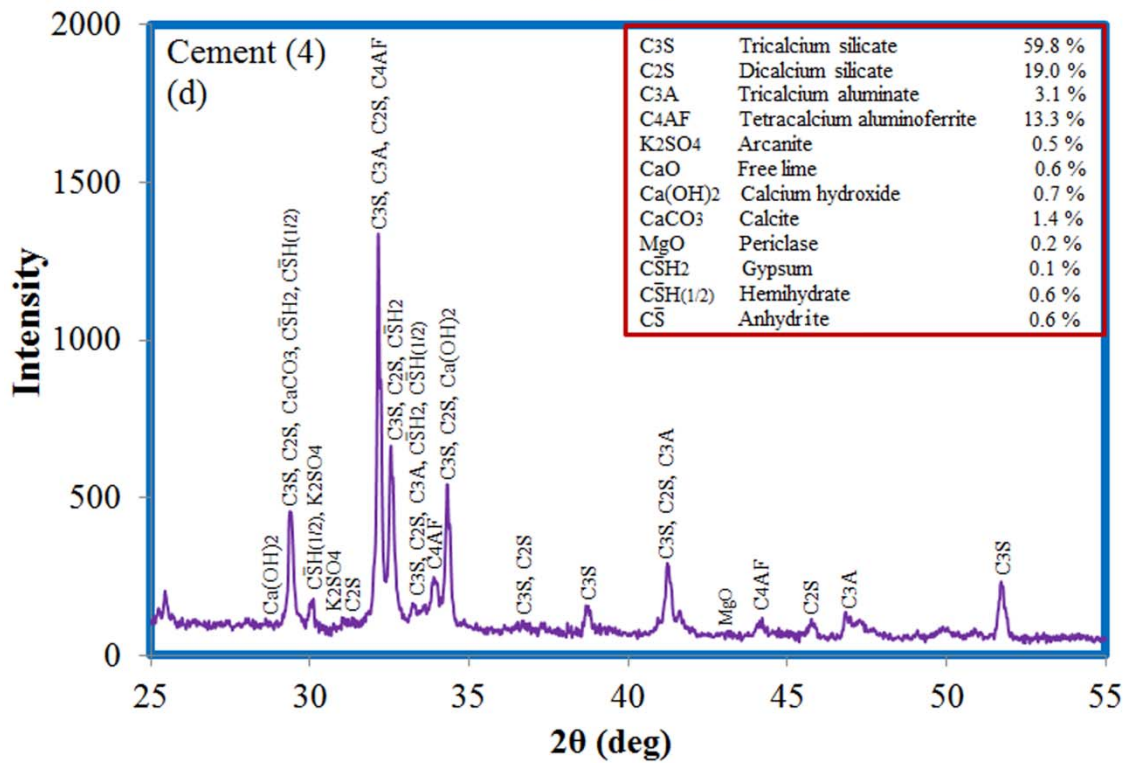
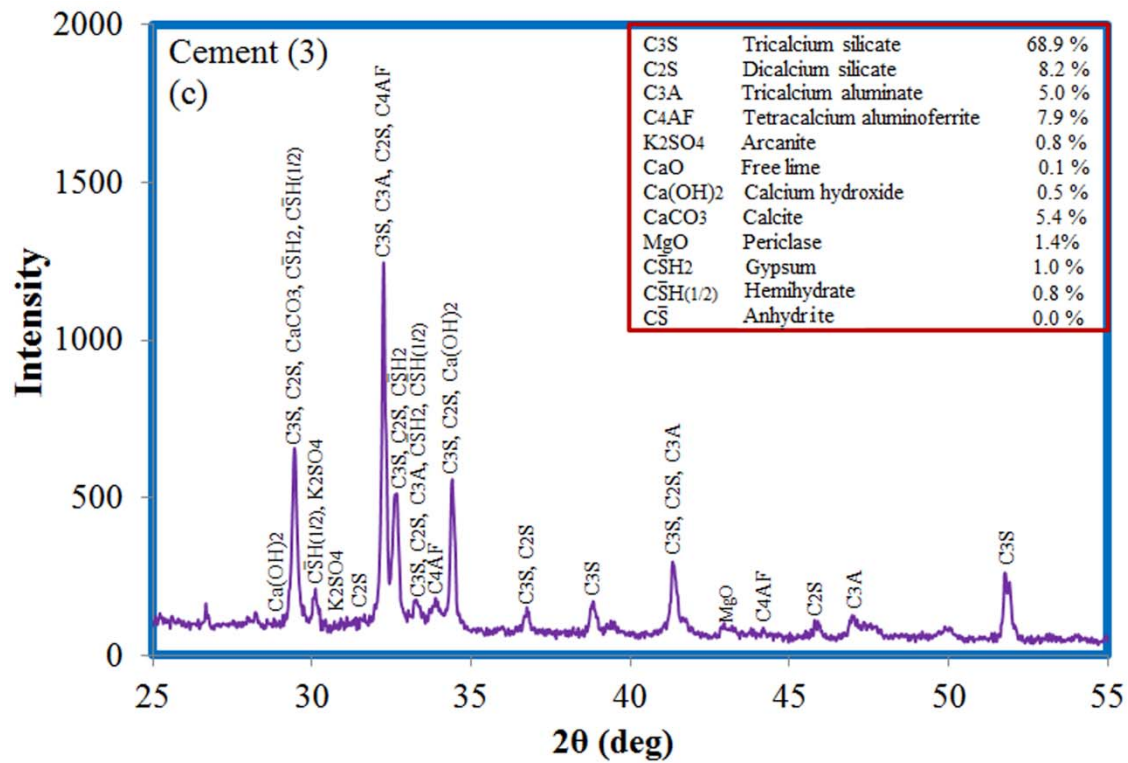


Figure 3.2 (Continued)

To quantify the crystal phases for each cement, 12 crystal phases of Alite (C₃S), Belite (C₂S), Ferrite (C₄AF), Tricalcium aluminate (C₃A), Periclase (MgO), Arcanite (K₂SO₄), Free lime (CaO), Portlandite (Ca(OH)₂), Calcite (CaCO₃), Gypsum (CaSO₄·2H₂O), Hemihydrate (CaSO₄·0.5H₂O) and Anhydrite (CaSO₄) were specified. The peaks corresponding to major crystalline phases are labeled and the quantities are indicated accordingly. The quantities of major phases are ranging from 58.7- 68.9% (for C₃S), 3.1- 10.3% (for C₃A), 8.2- 19% (for C₂S) and 6.9- 13.3% (for C₄AF) between cements (1) through (4) as outlined in Table 2.1.

Table 3.1 Major phase composition of cements (1) through (4)

Cement ID	C ₃ S, %	C ₃ A, %	C ₂ S, %	C ₄ AF, %
Cement (1)	60.6	6.5	14.2	11.8
Cement (2)	58.7	10.3	13.7	6.9
Cement (3)	68.9	5.0	8.2	7.9
Cement (4)	59.8	3.1	19.0	13.3

3.3.2 Particle Size Distribution of As-received and Ground Cements (1) Through (4)

Particles size distribution of as-received and ground cements (1) through (4) used to establish the proposed HOH equations are shown in Figure 3.3 and summarized in Table 3.2.

The laser scattering particle size analyzer, implemented in this study, determines the cement mean particle size based on the Equation (3.1) [35].

$$\text{Mean diameter} = \frac{\sum (q(J) \cdot X(J))}{\sum q(J)} \quad \text{Eq. (3.1)}$$

J: Particle diameter division number

q (J): Frequency distribution value (%)

X (J): Jth particle diameter range's representative diameter (μm)

Mean particle size for cement (1) is changing from 12.90μm to 5.53μm, for cement (2) from 14.35μm to 5.21μm, for cement (3) from 15μm to 3.82μm and for cement (4) from 13.15μm to 6.17μm. The span indicating the width of the particle size distribution curve can be calculated

based on the Equation (3.2) [36].

$$\text{Span} = \frac{D_{90} - D_{10}}{D_{50}} \quad \text{Eq. (3.2)}$$

D_{90} , D_{50} and D_{10} refer to the diameters which 90%, 50% and 10% of the cement bulk (by volume), respectively, is smaller than that.

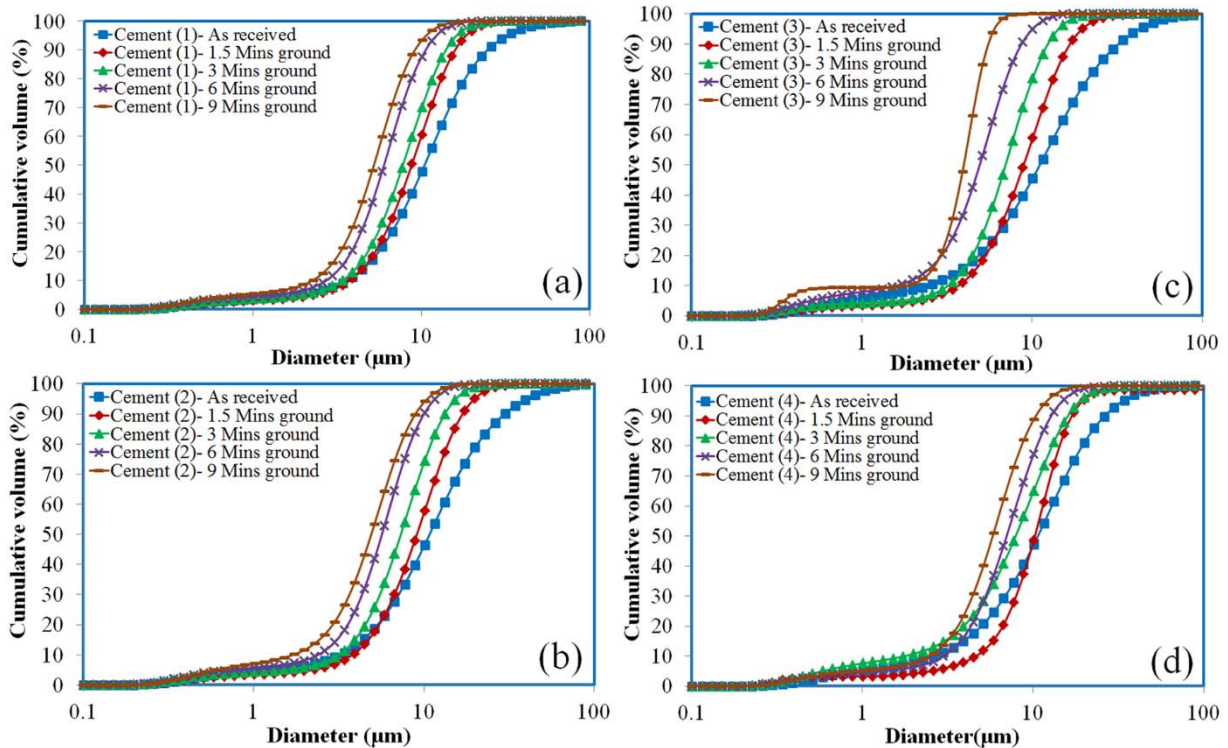


Figure 3.3 Particle size distribution of as received and ground cements, (a) cement (1), (b) cement (2), (c) cement (3), (d) cement (4)

As summarized in Table 3.2 and shown in Figure 3.3, the method of grinding implemented for this study narrowed the particle size distribution curve; therefore, the range of cements' particle size becomes closer to the mean. It is observed that grinding has a distinguishing effect on D_{90} for cements ground for nine minutes as D_{90} appeared as $9.23\mu\text{m}$, $8.92\mu\text{m}$ and $10.43\mu\text{m}$ for cements (1), (2) and (4), respectively, while it is $5.59\mu\text{m}$ for cement (3). Cement (3) contains the highest C_3S amount of 68.9% and low C_2S and C_4AF amounts of 8.2% and 7.9%, respectively among all

the ground cements. Also, D₁₀ for cements (2) and (3) ground for nine minutes is reported as 1.7 μ m and 1.8 μ m, while it is 2.25 μ m and 2.44 μ m for cements (1) and (4), respectively. Cements (2) and (3) have lower sum amount of C₂S and C₄AF compared to cements (1) and (4). It is understood that grindability of cement is related to packing density of each individual phase. C₃S crystals show elongated habit; and are less densely packed compared to C₂S crystals. Brittle index calculated from the measurements of the impression made in each phase by Vickers microindenter conducted by David Lawrence [39] indicates the highest brittle index of 4.7 for C₃S followed by 2.9 for C₃A and 2 for C₂S and C₄AF. Brittle index is defined as the ratio of elastic strain energy to irreversible strain energy, corresponding to the peak point of the σ - ϵ curve [40]. It is perceived that cements with high amount of C₃S and low amounts of C₂S and C₄AF have higher grindability potential.

Table 3.2 Particle size distribution of as-received and ground cements (1) through (4)

ID	Mean(μ m)	Median(μ m)	Span	D10 (μ m)	D50 (μ m)	D90 (μ m)
Cement (1), as received	12.90	10.45	2.03	3.61	10.45	24.86
Cement(1), 1.5mins ground	9.42	8.77	1.40	3.74	8.77	16.00
Cement (1), 3mins ground	8.34	7.78	1.38	3.40	7.78	14.11
Cement (1), 6mins ground	6.39	6.00	1.33	2.71	6.00	10.69
Cement (1), 9mins ground	5.53	5.23	1.33	2.25	5.23	9.23
Cement (2), as received	14.35	10.78	2.46	3.21	10.78	29.74
Cement (2), 1.5mins ground	9.86	9.08	1.45	3.79	9.08	16.92
Cement (2), 3mins ground	7.85	7.31	1.39	3.13	7.31	13.27
Cement (2), 6mins ground	5.98	5.66	1.35	2.38	5.66	10.02
Cement (2), 9mins ground	5.21	4.90	1.47	1.70	4.90	8.92
Cement (3), as received	15.00	11.11	2.68	2.43	11.11	32.21
Cement (3), 1.5mins ground	9.75	8.94	1.47	3.68	8.94	16.79
Cement (3), 3mins ground	7.45	6.99	1.33	3.20	6.99	12.46
Cement (3), 6mins ground	5.14	14.93	1.44	1.59	14.93	8.70
Cement (3), 9mins ground	3.82	3.97	0.95	1.80	3.97	5.59
Cement (4), as received	13.15	10.67	2.22	2.63	10.67	26.30
Cement (4), 1.5mins ground	11.97	10.25	1.21	4.60	10.25	16.96
Cement (4), 3mins ground	8.65	7.90	1.81	1.76	7.90	16.08
Cement (4), 6mins ground	7.53	7.00	1.41	2.98	7.00	12.83
Cement (4), 9mins ground	6.17	5.80	1.38	2.44	5.80	10.43

3.3.3 Development of Proposed Heat of Hydration Equations

TAMAIR isothermal conduction calorimetry was implemented to measure the HOH of cements at w/c=0.5 and isothermal bath temperature of 23 °C. The heat flow pattern obtained from the calorimetry can be used to study the hydration stages of the Portland cement. Integration of the area under the heat flow curve can be specified as the cumulative heat at varying hydration ages and used to develop the equations predicting the HOH at one, three and seven day hydration ages.

Initially, the effect of cement fineness on HOH was studied by measuring the Blaine fineness of cements (1) through (4) in the as received and ground forms in accordance with ASTM C204 specification. The HOH of cements (1) through (4) (in as received and ground forms) is plotted versus the Blaine fineness and is shown in Figure 3.4 and summarized in Table 3.3 Each line in the figure depicts different grinds of the same cement while the cement composition remained constant. Coefficients of determination (R^2) based on linear regression theory are shown, for each cement, in the figure. Coefficients of determination (R^2) are in the range of [0.75-0.94], [0.69-0.86], [0.64-0.83] for one, three and seven day hydration ages, respectively. Based on the (R^2) provided, it is unlikely to find strong linear correlation between the HOH and the Blaine fineness.

The cement mean particle also has the potential to correlate with the HOH to develop the equations predicting the HOH. In prior research, mean particle size was noted as an approximate average of D₁₀, D₅₀, and D₉₀ [41]. To examine the implementation of mean particle size as a measure of cement fineness, the determined HOH of as received and ground cements (1) through (4) at one, three and seven day hydration ages is plotted versus mean particle size and is shown in Figure 3.5. Each line in the figure depicts the different grinds of the same cement while cement composition remained constant. Coefficients of determination (R^2), based on the linear regression

theory, are shown in the figure for each cement. As it is evident from the figure, R^2 ranges from 0.92-0.99 for all the cements (1) through (4) at one, three and seven day hydration ages. The slope of the line is steeper for one day HOH relative to three and seven days indicating that cement fineness has more significant effect on one day HOH compared to three and seven days. It can be concluded from the calculated R^2 that, in order to develop the equations, mean particle size is a better parameter compared to Blaine fineness to correlate with the HOH. Accordingly, equation (3.3) can be offered as a general linear regression equation predicting one, three and seven day HOH of Portland cements.

$$\text{Cumulative HOH (at 1, 3 or 7 days)} = (\text{HOH}) \text{ Intercept} + \text{Slope} * (\text{mean particle size}) \quad \text{Eq. (3.3)}$$

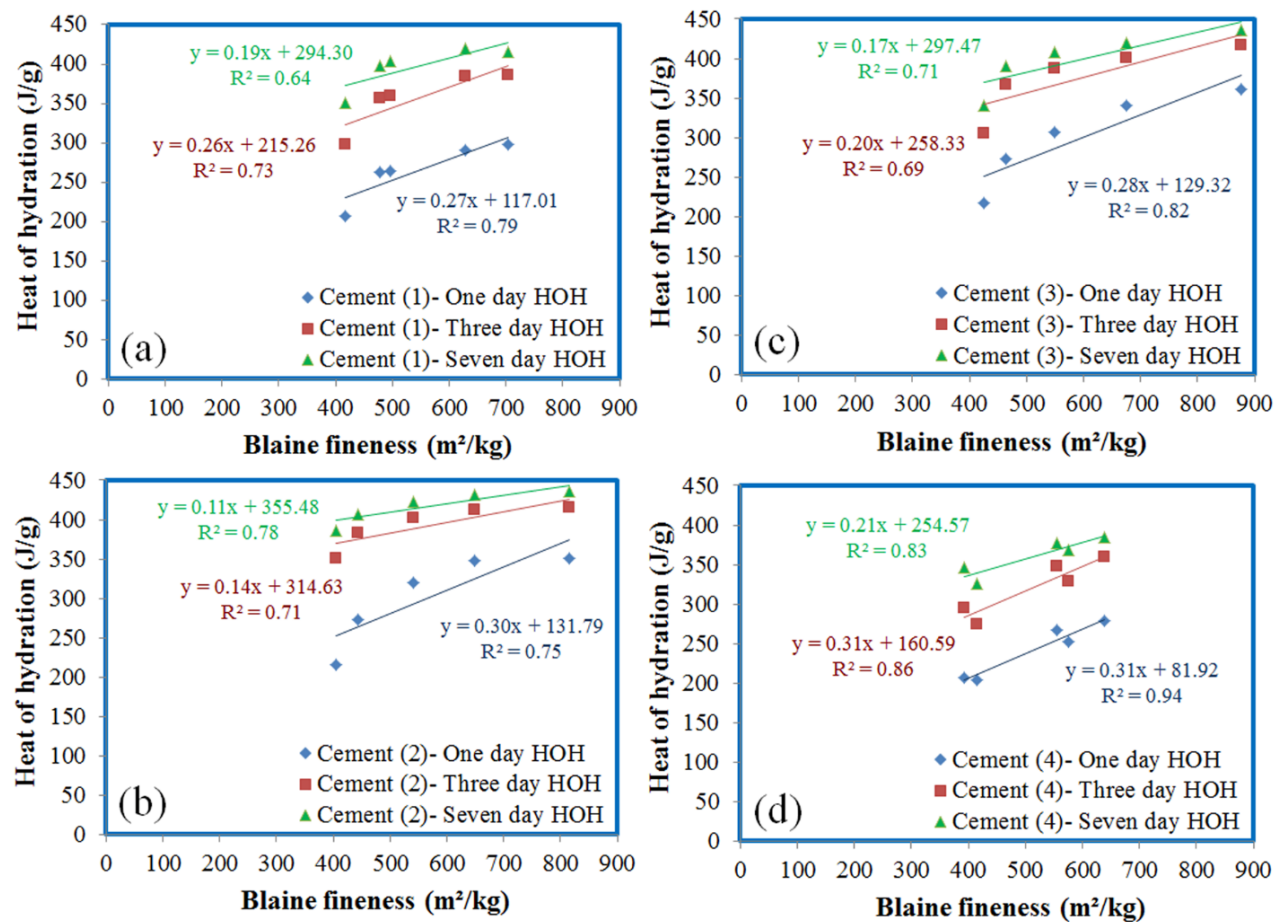


Figure 3.4 Cement heat of hydration versus Blaine fineness, (a) cement (1), (b) cement (2), (c) cement (3), (d) cement (4)

Table 3.3 Measured Blaine fineness, mean particle size, one; three and seven day heat of hydration for as-received and ground cements (1) through (4)

ID	Blaine fineness (m ² /kg)	Mean particle size (μm)	Measured one day HOH (J/g)	Measured three day HOH (J/g)	Measured seven day HOH (J/g)
Cement (1), as received	417	12.90	207	298	350
Cement(1), 1.5mins	479	9.42	262	356	397
Cement (1), 3mins	497	8.34	264	359	403
Cement (1), 6mins	628	6.39	290	384	420
Cement (1), 9mins	703	5.53	297	385	415
Cement (2), as received	405	14.35	216	350	386
Cement (2), 1.5mins	444	9.86	273	383	407
Cement (2), 3mins	542	7.85	320	402	423
Cement (2), 6mins	648	5.98	349	413	432
Cement (2), 9mins	816	5.21	350	415	435
Cement (3), as received	426	15	217	306	340
Cement (3), 1.5mins	463	9.75	273	367	390
Cement (3), 3mins	550	7.45	306	387	409
Cement (3), 6mins	675	5.14	341	401	419
Cement (3), 9mins	876	3.82	362	417	436
Cement (4), as received	414	13.15	204	274	326
Cement (4), 1.5mins	392	11.97	207	295	346
Cement (4), 3mins	573	8.61	250	328	367
Cement (4), 6mins	555	7.53	267	348	377
Cement (4), 9mins	638	6.17	279	360	385

The hydration of Portland cement consists of a series of reactions between cement phases and water. The HOH of cements is mainly controlled by the four major phases of C₃S, C₃A, C₂S and C₄AF [1]. As indicated in Figure 3.5, HOH of a specific cement is a linear function of mean particle size at ages of one, three or seven days, individually; also the change in slope and (HOH) intercept, for each cement, is the reflection of cement mineralogy. In this regard, the (HOH) intercept and slope for each cement can be defined as a linear regression of C₃S, C₃A, C₂S and C₄AF phases, for each hydration ages of one, three and seven days , as indicated in Equations (3.4)

and (3.5). In this regard, Solver command in Microsoft Excel 2010 and also the least squares method can be used to determine and optimize the coefficients (A_1 through D_1 & A_2 through D_2) based on the actual intercepts and slopes results (as shown in Figure 3.5) for cements (1) through (4) at three hydration ages of one, three and seven days. Solver command in Microsoft Excel functions based on the Generalized Reduced Gradient (GRG2) Algorithm for optimizing nonlinear problems code.

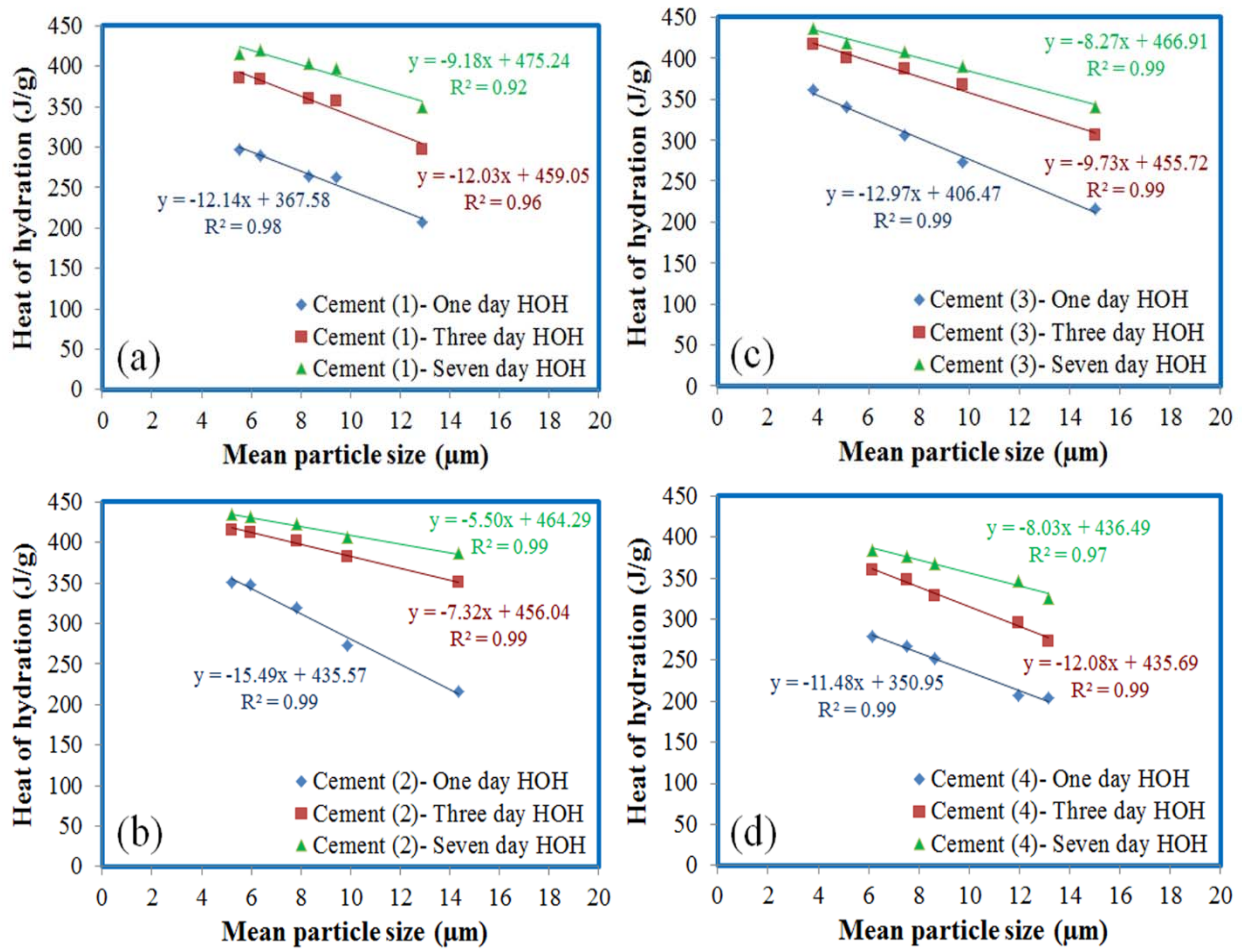


Figure 3.5 Cement heat of hydration versus mean particle size, (a) cement (1), (b) cement (2), (c) cement (3), (d) cement (4)

$$(\text{HOH}) \text{ Intercept} = A_1 (C_3S) + B_1 (C_3A) + C_1 (C_2S) + D_1 (C_4AF) \quad \text{Eq. (3.4)}$$

$$\text{Slope} = A_2 (C_3S) + B_2 (C_3A) + C_2 (C_2S) + D_2 (C_4AF) \quad \text{Eq. (3.5)}$$

Coefficients of determination (R^2) for actual versus calculated (based on optimized coefficients) intercepts and slopes, for cements (1) through (4) as indicated in Table 3.4, show an interesting fit ($R^2 > 0.98$) for cements (1) through (4) for hydration ages of three and seven days.

After determining the coefficients of A1 through D1 & A2 through D2, Equations (3.4) and (3.5) can be inputted into Equation (3.3), to develop the HOH Equations of (3.6), (3.7) and (3.8) for one, three and seven day hydration ages.

$$1\text{Day HOH (J/g)} = (476 - 13.35\text{MPS}) C_3S + (1290 - 58.41\text{MPS}) C_3A + (99 - 6.94\text{MPS}) C_2S$$

Eq. (3.6)

$$3\text{Day HOH (J/g)} = (521 - 6.84\text{MPS}) C_3S + (933 - 0.55\text{MPS}) C_3A + (127 + 20.04\text{MPS}) C_2S + (534 - 88.55\text{MPS}) C_4AF$$

Eq. (3.7)

$$7\text{Day HOH (J/g)} = (517 - 6.53\text{MPS}) C_3S + (1099 - 11.73\text{MPS}) C_3A + (35.18\text{MPS}) C_2S + (722 - 78.59\text{MPS}) C_4AF$$

Eq. (3.8)

Mean particle size should be noted as μm and the quantity of each phase must be inputted as a fraction. Validation of the proposed Equations (3.6), (3.7) and (3.8) is discussed in the following section.

Table 3.4 Coefficients of determination (R^2) for actual versus calculated intercepts and slopes for cements (1) through (4)

Coefficients of determinations (R^2) for actual versus calculated intercepts and slopes		
	Intercept	Slope
One day heat	0.88	0.85
Three day	1	1
Seven day	0.98	1

Equations (3.6), (3.7) and (3.8) can be combined into a more general expression as presented in Equation (3.9). To develop Equation (3.9), each coefficient in Equations (3.6), (3.7) and (3.8) was plotted as a function of time and the corresponding second order polynomial equations was fitted

into the data points to define each coefficient as a function of time (day), subsequently, each coefficient was placed in the general format of Equation (3.6), (3.7) or (3.8) to develop Equation (3.9).

$$\text{HOH}_D = [(-3.92(D^2) + 38.17(D) + 441.75) - (0.53(D^2) - 5.37(D) + 18.19)\text{MPS}]C_3S + [(36.67(D^2) - 325.17(D) + 1578.5) - (5.29(D^2) - 50.08(D) + 103.2)\text{MPS}]C_3A + [(-7.63(D^2) + 44.5(D) + 62.13) - (1.62(D^2) - 19.96(D) + 25.28)\text{MPS}]C_2S + [(-36.67(D^2) + 413(D) - 377) - (-7.79(D^2) + 75.45(D) - 67.66)\text{MPS}]C_4AF \quad \text{Eq. (3.9)}$$

where “D” corresponds to the hydration age (1, 3 or 7 days)

3.3.4 Validation of Proposed Heat of Hydration Equations

Validation of the proposed Equations (3.6), (3.7) and (3.8) is conducted by comparing the measured HOH of eight as received commercial Portland cements (cements A through H) with the predicted heat by the proposed Equations (3.6), (3.7) and (3.8). The Blaine fineness, mean particle size, mineralogical composition and HOH of the cements were determined using the same experimental procedures and instruments used to characterize cements (1) through (4). The pertaining data are summarized in Table 3.5.

Table 3.5 Measured Blaine fineness, mean particle size, X-ray Rietveld phase quantification, one; three and seven day heat of hydration of as received cements A through H

Cement ID	Blaine fineness (m ² /kg)	Mean particle size (µm)	C ₃ S	C ₃ A	C ₂ S	C ₄ AF	Measured one day HOH (J/g)	Measured three day HOH (J/g)	Measured seven day HOH (J/g)
			Expression %						
Cement A	612	10.05	61.7	6.9	14.0	12.7	252	341	385
Cement B	530	10.27	58.8	11.2	13.3	5.9	286	383	407
Cement C	575	8.65	58.6	2.9	20.1	13.4	252	329	368
Cement D	494	10.41	61.9	5.2	15.8	9.6	252	342	384
Cement E	389	14.45	57.4	4.5	11.4	13.2	177	234	278
Cement F	392	13.01	61.3	6.1	11.3	10.4	211	297	345
Cement G	414	13.69	68.3	4.3	8.9	9.6	206	303	343
Cement H	405	15.59	63.5	5.6	13.7	12.6	189	270	328

The paired-comparison t-test hypothesis [42] was implemented to determine the 95% confidence interval on predicted (by Equations (3.6) through (3.8)) and measured HOH of cements A through H as outlined in Table 3.6 The difference between predicted and measured HOH of cements A through H, at hydration ages of one, three and seven days, is shown in Figure 3.6.

Table 3.6 Statistical analysis on cements A through H for evaluation of proposed equations (3.6) through (3.8)

Hydration age	Average of “predicted minus measured” heat (J/g)	Standard Deviation of “predicted minus measured” heat (J/g)	(R ²) of “predicted versus measured” heat(J/g)	Paired comparison t-test lower confidence limit	Paired comparison t-test upper confidence limit
One day	3	9	0.95	-5	10
Three	1	3	1	-2	4
Seven	1	6	0.98	-4	6

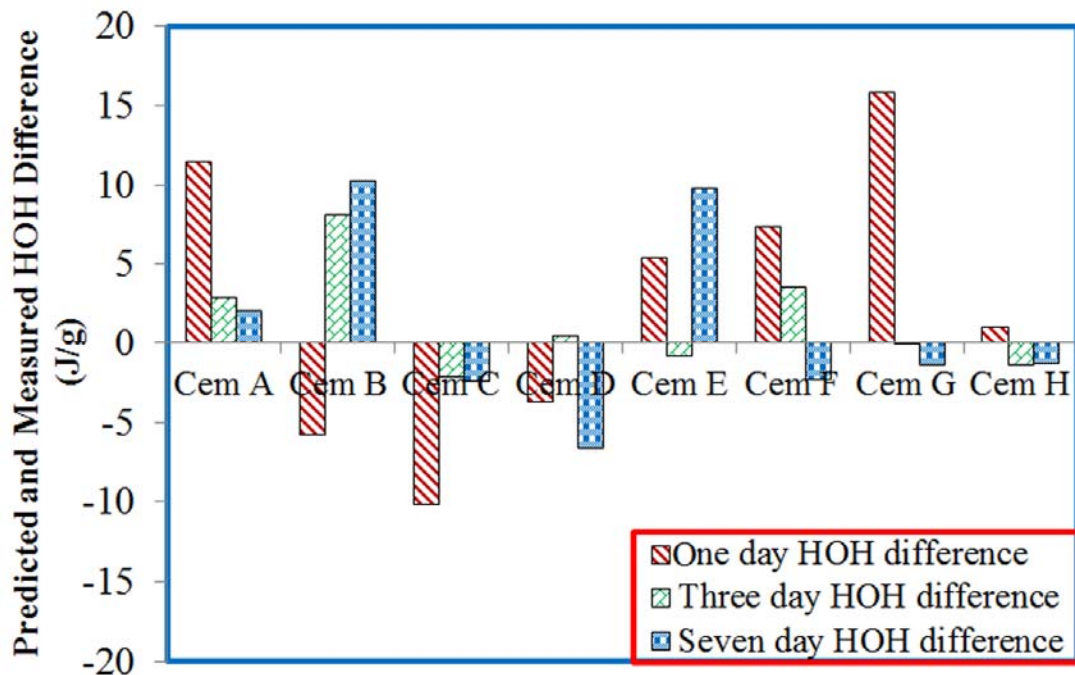


Figure 3.6 Predicted and measured heat of hydration difference for as received cements A through H, using equations (3.6) through (3.8)

The proposed Equation (3.6) “one day HOH prediction”, Equation (3.7) “three day HOH prediction” and Equation (3.8) “seven day HOH prediction”, overestimate the HOH, on average, by +3, +1, +1 J/g, respectively. The standard deviation of “predicted minus measured heat” at hydration ages of one, three and seven days are calculated as 9, 3 and 6 J/g, respectively.

The 95% confidence interval on predicted and measured HOH were calculated as [-5, 10], [-2, 4] and [-4, 6] for hydration ages of one, three and seven days, respectively. It is understood that the smaller 95% confidence interval shows the higher accuracy of the equation to predict the HOH [2, 42].

It appears that Equation (3.7) can more accurately predict the HOH (at three day hydration age), as it has smaller confidence interval, smaller standard deviation of “predicted minus measured heat” compared to Equations (3.6) and (3.8) implemented to predict the HOH at one and seven day hydration ages, respectively.

It is concluded that all the three proposed Equations (3.6), (3.7) and (3.8) show good accuracy to predict the HOH at hydration ages of one, three and seven days, while Equation (3.7) occurs to be a better predictor of HOH relative to the other two proposed equations.

3.3.5 Evaluation of the Equations Predicting the Seven Day HOH Proposed by the Authors of This Paper and Also, Available in the Literature

This section will discuss the equations developed by the authors of this paper and also by other researchers to predict the seven day HOH of Portland cements. Per ASTM standard specifications, ASTM C150 [43] and ASTM C1600 [44] have set limits per optional physical requirements on seven day HOH of cements while ASTM C595 [45] and ASTM C1157 [46] have set limits per physical requirements on seven day HOH of cements. ASTM standard specifications assigned the [14] as the procedure to measure the seven day HOH of Portland cement for standard

purposes. Following this statement, several researchers attempted to predict the seven day HOH of Portland cement based on the cement composition, cement fineness and/or physical properties of cement paste or mortar.

Poole developed Equation (3.10) based on the HOH of individual compounds published in “Lea’s chemistry of cement” [24, 47]. Equation (3.10) consists of the four major phases of C₃S, C₃A, C₂S and C₄AF as the main contributors to the seven day HOH of cement. This equation does not include the effect of cement fineness as a variable affecting the seven day HOH of cements.

$$\text{Seven day HOH (J/g)} = (15.55) C_3A + (2.21) C_3S + (0.42) C_2S + (5.82) C_4AF \quad \text{Eq. (3.10)}$$

Poole (Poole 2009 [24]) developed Equation (3.11) from a stepwise linear regression calculation on the seven day HOH, measured by heat of solution calorimetry [14], of 38 cements data that he obtained from the CCRL (16 cements) and U.S. Army Corps of Engineers Research and Development Center (22 cements). He noted that the variables were incorporated into the equation as long as they were statistically significant at a probability of 0.05. He concluded that only C₃S and C₃A were found to be statistically significant. This equation was the basis to establish the maximum limit of 100 on the quantity of (C₃A + 4.75 C₃A) in ASTM C150 to maintain the seven day HOH (measured based on ASTM C186) of type II (MH) and type II (MH)A under 335 (J/g). The range of the Blaine fineness of the cements used to calibrate the equation falls within 2640- 4360 cm²/g. The quantities of the major phases of cements (potential phase composition) were determined using Bogue equations [43].

$$\text{Seven day HOH (J/g)} = (133.9) + (9.36) C_3A + (2.13) C_3S \quad \text{Eq. (3.11)}$$

Poole [24] developed Equation (3.12) from the linear regression analysis on seven day HOH data obtained from the Verbeck and Foster’s research study [23] The seven day HOH was determined using the heat of solution calorimetry. Water to cement ratio of 0.4 was chosen to prepare the cement pastes. The Blaine fineness of the cements used to calibrate the equation falls

within the range of 2850-4900 cm²/g. Poole incorporated Blaine fineness as a variable into the Equation (3.12) as he found it statistically significant variable affecting the seven day HOH of cement.

$$\text{Seven day HOH} = 1.98 + (11.44) C_3A + (1.53) C_3S + (0.4) \text{ Blaine fineness} \quad \text{Eq. (3.12)}$$

Poole's equation indicates approximately 0.4 J/g increase/decrease in seven day HOH per unit m²/kg change (increase/decrease) of Blaine fineness. Mathematical analysis conducted by the authors of this paper on four cements with varied finenesses and mineralogical composition (HOH and Blaine fineness of the cements are outlined in Table 3.3) indicates approximately 0.23, 0.12, 0.21 and 0.26 J/g change in seven day HOH, respectively for cements one through four, per unit m²/kg change of Blaine fineness. As it is evident from the results, change in seven day HOH per unit change of Blaine fineness is significant and influenced by the phase composition of the studied cements. The results indicate that change in seven day HOH per unit change in Blaine fineness is less significant for cements with higher amount of C₃A (cement 2) and is substantial for cements with lower amount of C₃A (cement 4).

Taylor [48] developed Equation (3.13) from the linear regression analysis on seven day HOH and potential phase composition (determined based on the Bogue equations) of several cements. He did not mention the quantity of the phases of the cements and also their finenesses used to calibrate his equation. He noted that the seven day HOH of the cement pastes were measured using heat of solution calorimetry and at water to cement ratio of 0.4.

$$\text{Seven day HOH} = (1556) C_3A + (222) C_3S + (42) C_2S + (494) C_4AF \quad \text{Eq. (3.13)}$$

The suitability of the proposed Equations (3.8), (3.10), (3.11), (3.12) and (3.13) to predict the seven day HOH of Portland cements was assessed by inputting the mineralogy and fineness of the cements A through H, as outlined in Table 3.5, in each equation and comparing the predicted HOH with the measured HOH of cements A through H. The difference between the predicted (by

the proposed equations) and measured seven day HOH of Portland cements of A through H is shown in Figure 3.7.

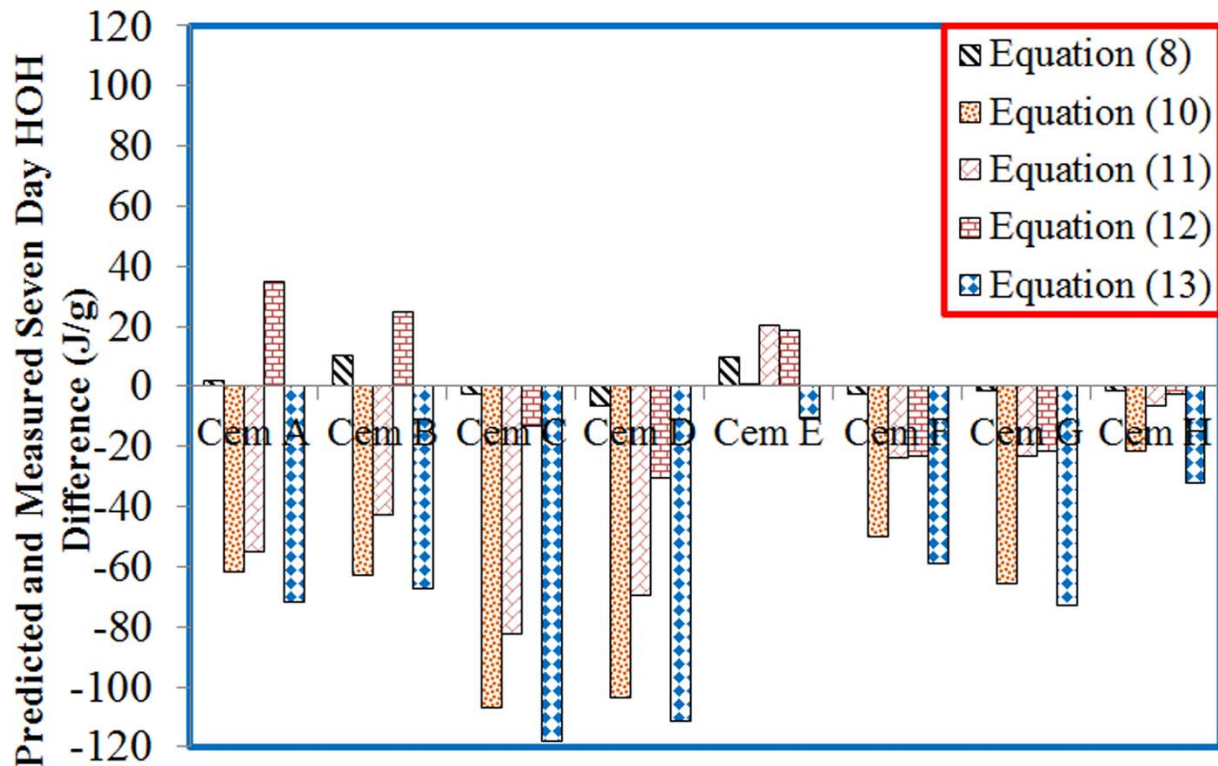


Figure 3.7 Predicted and measured seven day heat of hydration difference for as-received cements A through H, using equations (3.8) through (3.13)

For each proposed equation, predicting the seven day HOH, 95% confidence interval (based on the paired-comparison t-test hypothesis), [2, 42]) was determined on predicted and measured seven day HOH of cements A through H, as outlined in Table 3.7 Paired comparison t-test greatly improves the precision by making comparisons within matched pairs (blocks of measured and predicted HOH) of experimental cements. This method eliminates the error associated with the differences of phase composition and fineness between cements, as an additional source of variability. The paired comparison t-test confidence interval can be calculated using the following equation:

$$\bar{d} \pm t_{0.025,n} \cdot S_d / \text{Sqrt}(n) \quad \text{Eq. (3.14)}$$

\bar{d} : Average of the difference between predicted and measured HOH of studied cements

$t_{0.025,n}$: t-statistics corresponding to 95% confidence interval & (n) studied cements

S_d : Standard deviation on difference between predicted and measured HOH of studied cements

The average and standard deviation of “predicted minus measured seven day HOH” of cements A through H were calculated for each proposed equation and are outlined in Table 3.7. It appears that Equation (3.8) overestimate the seven day HOH, on average, by +1 J/g while Equations (3.10), (3.11), (3.12) and (3.13) underpredict it by -59, -35, -1, and -68 J/g, respectively. The standard deviations of the “predicted minus measured seven day HOH” were calculated as 6, 37, 34, 25 and 36 J/g for Equations (3.8), (3.10), (3.11), (3.12) and (3.13), respectively.

Table 3.7 Statistical analysis on cements A through H for evaluation of proposed equations (3.8) through (3.13)

Equation #	Average of “predicted minus measured” heat (J/g)	Standard Deviation of “predicted minus measured” heat (J/g)	(R ²) of “predicted versus measured” heat(J/g)	Paired comparison t-test lower confidence limit	Paired comparison t-test upper confidence limit
Eq. (3.8)	1	6	0.98	-4	6
Eq. (3.10)	-59	37	0.22	-90	-28
Eq. (3.11)	-35	34	0.30	-64	-7
Eq. (3.12)	-1	25	0.74	-22	19
Eq. (3.13)	-68	36	0.25	-98	-38

It appears that Equation (3.8) shows the smallest 95% confidence interval of [-4, 6] on predicted and measured seven day HOH of cements compared to Equations (3.10), (3.11), (3.12), and (3.13) with the confidence intervals of [-90, -28], [-64, -7], [-22, 19] and [-98, -38], respectively. It can be concluded that the following reasons may result in the Equation (3.8) to be a better predictor of seven HOH of Portland cements relative to other Equations (3.10), (3.11), (3.12) and (3.13).

- Equation (3.8) was developed based on the mineralogical composition (quantitative X-ray diffraction (QXRD), direct method) of the Portland cements while Equations (3.10), (3.11), (3.12) and (3.13) were established based on the potential phase composition (using Bogue equations) of the cements. It is well established in the literature that the Bogue equations may cause erroneous results when quantifying the major phases in Portland cement [32, 48].
- Cement mean particle size is incorporated into Equation (3.8) as a measure of cement fineness while Equations (3.10), (3.11) and (3.13) do not contain any measure of cement fineness as a variable factor affecting the seven day HOH of Portland cements.
- HOH of Portland cements (1) through (4) (used to calibrate Equations (3.6), (3.7) and (3.8)) and also HOH of cements A through H were determined at water to cement ratio of 0.5 while the HOH of cements used to calibrate Equations (3.10) through (3.13) were determined at water to cement ratio of 0.4. Higher water to cement ratio may provide more available water for wetting and hydration of Portland cement, though the change of water to cement ratio from 0.4 to 0.5 may not significantly affect the HOH of cement paste at seven day hydration age [26].
- HOH measurements using isothermal conduction calorimetry shows better precision compared to solution calorimetry for both within laboratory and between laboratory HOH results [13].

3.4 Conclusions and Proposed Future Work

This paper addressed the development of empirical equations predicting the heat of hydration of Portland cement at one, three and seven day hydration ages. The main results are summarized as follows:

- The proposed equations can be used to identify Portland cements with the potential to cause thermal cracking in mass concrete elements. Also, the equations can be used to correlate the

heat of hydration with other properties of Portland cement for quality control and prediction of physical and chemical properties of manufactured Portland cement and concrete.

- Cement fineness plays critical role in the heat of hydration of Portland cements.
- Mean particle size is a better measure of cement fineness relative to Blaine fineness to correlate with the heat of hydration of Portland cement to establish equations predicting the heat at one, three and seven day hydration ages.
- Heat of hydration of Portland cement at one, three and seven day hydration ages is a linear function of cement mean particle size when the composition is maintained constant at constant isothermal bath temperature of 23 °C and water to cement ratio of 0.5.
- Equations predicting one, three and seven day heat of hydration of Portland cement can be established based on the Portland cement major phases of C₃S, C₃A, C₂S, C₄AF and cement mean particle size.
- The proposed Equations (3.6), (3.7) and (3.8) can predict the heat of hydration at one, three and seven day hydration ages with good accuracy for Portland cements for which major phases (C₃S, C₂S, C₃A, C₄AF) and mean particle size fall within the range of cements (1) through (4) used to calibrate the proposed equations.

Proposed future work is outlined in the following.

The HOH equations developed in this paper can be modified to reflect the effect of combination of (w/c), temperature, cement fineness, cement composition and pozzolanic cementitious materials content on HOH. The following general equation can be proposed.

$$\text{HOH}(X, Y, Z) = A.X + B.Y + C.Z$$

X: (w/c), Y= Temperature (°C), Z= Cement fineness (m²/kg or mean particle size)

$$A = A_1 \cdot (C_3S) + B_1 \cdot (C_3A) + C_1 \cdot (C_2S) + D_1 \cdot (C_4AF) + E_1 \cdot (CaO_{\text{fly ash or slag}}) + F_1 \cdot (SiO_2_{\text{fly ash or slag}}) + G_1 \cdot (\text{Silica fume})$$

$$B = A_2 \cdot (C_3S) + B_2 \cdot (C_3A) + C_2 \cdot (C_2S) + D_2 \cdot (C_4AF) + E_2 \cdot (CaO_{\text{fly ash or slag}}) + F_2 \cdot (SiO_2_{\text{fly ash or slag}}) + G_2 \cdot (\text{Silica fume})$$

$$C = A_3 \cdot (C_3S) + B_3 \cdot (C_3A) + C_3 \cdot (C_2S) + D_3 \cdot (C_4AF) + E_3 \cdot (CaO_{\text{fly ash or slag}}) + F_3 \cdot (SiO_2_{\text{fly ash or slag}}) + G_3 \cdot (\text{Silica fume})$$

Quantity of each phase must be inputted as a fraction.

Significant number of HOH experiments need to be conducted to measure the HOH at varied “w/c= 0.3, 0.4 and 0.5”, “temperature= 23, 30 and 40 °C”, “Cement fineness= at least 4 different cement finenesses”, “four Portland cements covering high and low quantities of major phases of C₃S, C₃A, C₂S, C₄AF”, “Pozzolanic materials (slag, fly ash) = pozzolanic materials with high and low CaO and SiO₂ content”, “Silica Fume= high and low quantities”. For this instance, the number of HOH experiments in duplicate runs will be: N= 2 x 3 x 3 x 4 x 10 = 720. Solver command in Microsoft Excel can be implemented to optimize the coefficients of A₁ through G₁, A₂ through G₂ and A₃ through G₃ based on the known cement composition, cement fineness, (w/c), temperature, pozzolanic cementitious materials content.

It is important to note that development of equations capable of predicting the HOH at 28 days is a possible option which requires extension of the HOH measurements up to 28 days.

3.5 References

- [1] Odler, Ivan. "Hydration, setting and hardening of Portland cement." *Lea's Chemistry of Cement and Concrete* 4 (1998): 241-297.
- [2] Zayed, A., Ahmadreza Sedaghat, and Paul Sandberg. "Measurement and prediction of heat of hydration of portland cement using isothermal conduction calorimetry." *Journal of Testing and Evaluation* 41.6 (2013): 1-8.
- [3] Sedaghat, Ahmadreza, et al. "Investigation of physical properties of graphene-cement composite for structural applications." *Open Journal of Composite Materials* 2014 (2014).
- [4] Zayed, Abla, et al. "Effects of portland cement particle size on heat of hydration." (2014).
- [5] Kaszyńska, Maria. "Early age properties of high-strength/high-performance concrete." *Cement and Concrete Composites* 24.2 (2002): 253-261.
- [6] Kumar, Aditya, et al. "Simple methods to estimate the influence of limestone fillers on reaction and property evolution in cementitious materials." *Cement and Concrete Composites* 42 (2013): 20-29.
- [7] Schindler, Anton Karel. "Concrete hydration, temperature development, and setting at early-ages." (2011).
- [8] Bentz, Dale P., Gaurav Sant, and Jason Weiss. "Early-age properties of cement-based materials. I: Influence of cement fineness." *Journal of Materials in Civil Engineering* 20.7 (2008): 502-508.
- [9] Portland Cement Association. "Concrete Technology Today, vol. 18." (1997).
- [10] Oey, Tandr e, et al. "The filler effect: the influence of filler content and surface area on cementitious reaction rates." *Journal of the American Ceramic Society* 96.6 (2013): 1978-1990.
- [11] Kumar, Aditya, Shashank Bishnoi, and Karen L. Scrivener. "Modelling early age hydration kinetics of alite." *Cement and Concrete Research* 42.7 (2012): 903-918.
- [12] Kumar, Aditya, et al. "A comparison of intergrinding and blending limestone on reaction and strength evolution in cementitious materials." *Construction and Building Materials* 43 (2013): 428-435.
- [13] ASTM C1702-09a. (2010). "Standard test method for measurement of heat of hydration of hydraulic cementitious materials using isothermal conduction calorimetry." ASTM International, West Conshohocken, PA, USA.
- [14] ASTM C186-05. (2010). "Standard test method for heat of hydration of hydraulic cement." ASTM International, West Conshohocken, PA, USA.

- [15] Poole, Toy. Revision of test methods and specifications for controlling heat of hydration in hydraulic cement. No. PCA R&D Serial No. 2007. Portland Cement Association, (2007).
- [16] Wadsö, Ingemar. "Isothermal microcalorimetry near ambient temperature: an overview and discussion." *Thermochimica Acta* 294.1 (1997): 1-11.
- [17] Kumar, Mukesh, Sanjay K. Singh, and N. P. Singh. "Heat evolution during the hydration of Portland cement in the presence of fly ash, calcium hydroxide and super plasticizer." *Thermochimica Acta* 548 (2012): 27-32.
- [18] Xu, Qinwu, et al. "Modeling hydration properties and temperature developments of early-age concrete pavement using calorimetry tests." *Thermochimica Acta* 512.1 (2011): 76-85.
- [19] Killoh, D. C. "A comparison of conduction calorimeter and heat of solution methods for measurement of the heat of hydration of cement." *Advances in Cement Research* 1.3 (1988): 180-186.
- [20] Woods, Hubert, Harold H. Steinour, and Howard R. Starke. "Effect of composition of Portland cement on heat evolved during hardening." *Industrial & Engineering Chemistry* 24.11 (1932): 1207-1214.
- [21] Woods, H., H. H. Steinour, and H. R. Starke. "Heat evolved by cement in relation to strength." *Engineering News-Record* 1933 (1933): 431-433.
- [22] Lerch, Wm, and Robert Herman Bogue. "The heat of hydration of Portland cement pastes." Portland Cement Association Fellowship, (1934).
- [23] Verbeck, George J., and Cecil W. Foster. "Long-time study of cement performance in concrete: chapter 6. The heat of hydration of the cements." *Proceeding of American Society of Testing and Materials*. Vol. 50. (1950).
- [24] Poole, Toy S. "Predicting seven-day heat of hydration of hydraulic cement from standard test properties." *Journal of ASTM International* 6.6 (2009): 1-10.
- [25] Bentz, Dale P. "Blending different fineness cements to engineer the properties of cement-based materials." *Magazine of Concrete Research* 62.5 (2010): 327-338.
- [26] Bentz, Dale P., Max A. Peltz, and John Winpigler. "Early-age properties of cement-based materials. II: Influence of water-to-cement ratio." *Journal of Materials in Civil Engineering* 21.9 (2009): 512-517.
- [27] Mindess, S., J. F. Young, and D. Darwin. "Concrete, 2nd Edition Prentice Hall." *Englewood Cliffs, NJ* (2002).

- [28] Pane, Ivindra, and Will Hansen. "Investigation of blended cement hydration by isothermal calorimetry and thermal analysis." *Cement and Concrete Research* 35.6 (2005): 1155-1164.
- [29] Ali, M. Memari, A. Kremer Paul, and A. Behr Richard. "Relating compressive strength to heat release in mortars." *Advances in Civil Engineering Materials* 1.1 (2012): 1-14.
- [30] "The McCrone Sample preparation kit." McCrone Microscope & Accessories. Web. 24 Feb. (2014).
- [31] Hurst, Vernon J., Paul A. Schroeder, and Robert W. Styron. "Accurate quantification of quartz and other phases by powder X-ray diffractometry." *Analytica Chimica Acta* 337.3 (1997): 233-252.
- [32] Stutzman, Paul E. "Guide for X-ray powder diffraction analysis of Portland cement and clinker." US Department of Commerce, Technology Administration, National Institute of Standards and Technology, Office of Applied Economics, Building and Fire Research Laboratory, (1996).
- [33] Hudson-Lamb, D. L., C. A. Strydom, and J. H. Potgieter. "The thermal dehydration of natural gypsum and pure calcium sulphate dihydrate (gypsum)." *Thermochimica Acta* 282 (1996): 483-492.
- [34] ASTM C204-07. (2010). "Standard test methods for fineness of hydraulic cement by air-permeability apparatus." ASTM International, West Conshohocken, PA.
- [35] Horiba Instruments Incorporated, "Laser Scattering Particle Size Distribution Analyzer LA 950 Instruction Manual." <www.horibalab.com> (accessed 02/24/ 2014).
- [36] Horiba Scientific, "A guidebook to particle size analysis." <http://www.horiba.com/fileadmin/uploads/Scientific/Documents/PSA/PSA_Guidebook.pdf> (accessed 02/24/2014).
- [37] Le Saoût, Gwenn, Vanessa Kocaba, and Karen Scrivener. "Application of the Rietveld method to the analysis of anhydrous cement." *Cement and Concrete Research* 41.2 (2011): 133-148.
- [38] Scrivener, K. L., et al. "Quantitative study of Portland cement hydration by X-ray diffraction/Rietveld analysis and independent methods." *Cement and Concrete Research* 34.9 (2004): 1541-1547.
- [39] Lawrence, C. David. "The constitution and specification of Portland cements." *Leas's Chemistry of Cement and Concrete, 4th ed. Edited by PC Hewlett. Butterworth-Heinemann, UK* (1998): 131-193.

- [40] Brandt, Andrzej M. Cement-based composites: materials, mechanical properties and performance. CRC Press, (2009).
- [41] Azari, Haleh. Statistical modeling of cement heat of hydration using phase and fineness variables. National Cooperative Highway Research Program, Transportation Research Board of the National Academies, (2010).
- [42] Montgomery, Douglas C. "Design and analysis of experiments." John Wiley & Sons, (2008).
- [43] ASTM C150/C150M. (2009). "Standard specification for Portland cement." ASTM International, West Conshohocken, PA. USA.
- [44] ASTM C1600/C1600M-08. (2008). "Standard specification for rapid hardening hydraulic cement." ASTM International, West Conshohocken, PA. USA.
- [45] ASTM C595/C595M-10. (2010). "Standard specification for blended hydraulic cements." ASTM International, West Conshohocken, PA. USA.
- [46] ASTM C1157/C1157-10. (2010). "Standard performance specification for hydraulic cement." West Conshohocken," ASTM International, PA. USA.
- [47] Lea, F. M. "The Chemistry of cement and concrete." chemical Publishing Co." Inc., New York (1971).
- [48] Taylor, Harry FW. Cement chemistry. Thomas Telford, (1997).

CHAPTER 4³: INVESTIGATION OF PHYSICAL PROPERTIES OF GRAPHENE-CEMENT COMPOSITE FOR STRUCTURAL APPLICATIONS

4.1 Introduction

Concrete is a composite material of aggregates and binders where binding materials are primarily a combination of portland cement, pozzolanic materials and water [1, 2]. Hydration of cement generates heat due to the exothermic nature of the hydration process. The phases mainly responsible for heat generation during the hydration process are tricalcium silicate (C_3S), dicalcium silicate (C_2S), tricalcium aluminate (C_3A) and tetracalcium aluminoferrite (C_4AF) [2, 3]. The hydration process of portland cement depends on several factors or parameters such as cement mineralogical composition, particle size distribution, water to cement ratio and curing temperature. Due to the exothermic nature of the reaction combined with poor heat dissipation in massive concrete elements, the hydration process results in a temperature gradient between the inner core and the outer surface of the element [4]. The high temperature gradient is known to result in large tensile stresses that may exceed the tensile strength of concrete thus leading to thermal cracking. The temperature gradient minimization in an element could be achieved through lowering the temperature rise due to hydration and/or improving heat dissipation by increasing thermal conductivity of concrete. Improving the paste thermal conductivity reduces the temperature gradient in the concrete element, thus reducing the probability of concrete thermal cracking [5].

³ Note. "Investigation of Physical Properties of Graphene-Cement Composite for Structural Applications" A. Sedaghat, M.K. Ram, A. Zayed, R. Kamal, N. Shanahan, 2014, Open Journal of Composite Materials, Vol.4 No.1(2014), Article ID:41685, DOI:10.4236/ojcm.2014.41002.

Recent research indicates the possibility of using nanomaterials (carbon nanotube, graphene, titanium oxide, nanosilica, and nanoalumina) in civil infrastructure applications; however, costly process and low production of such materials may limit such applications [6]. Incorporation of nanomaterials changes the macroscopic properties of the main binder; namely, Portland cement paste [7]. Introduction of nanomaterials in cement paste reduces the porosity and rate of hydration leading to the development of stronger and more durable products [7]. The structure of the hydrated gel is also affected by the introduction of nanomaterials at a nano-level [8, 9]. The long term creep properties of cement paste are dependent on the density of calcium silicate hydrate which is the main hydration product. Introduction of nanomaterials in concrete using an electromutagenic process modifies the microstructure of high performance concrete without changing the dimensions or appearance [10]. High surface area of the nanomaterials makes them efficient in controlling the propagation of microcracks in cementitious composite materials. Defects present in the lattice structure of the carbon nanotubes, provide potential sites for formation of carboxyl ($-\text{COOH}$) and hydroxyl ($-\text{OH}$) species and creation of bonding to the hydrated cement [11]. It is demonstrated that graphene-oxide (GO) nanosheets may reduce the brittleness and enhance toughness, tensile and flexural strength of the hydrated cement composite. GO can regulate cement hydration and distinctly affect the mechanical properties of hydrated cement composite [12].

In addition to increasing strength, preventing cracking and reducing porosity, nanomaterials are useful as anti-corrosive agents in reinforced concrete. Recently, it has been shown that titanium addition to cementitious binders results in triggering self-cleaning process in cement pastes [13]. Carbon nanotubes, nanoflakes or carbon block additions were used in electromagnetic shielding applications [14]. Carbon nanotubes, with extremely high aspect ratios

(length to diameter ratio), are distributed in a much finer scale relative to other common fibers resulting in efficient bridging in hydrated cement composite and reduction of microcrack propagation [15]. The functionalized carbon nanotubes (F-CNT), showing hydrophilic behavior, can interfere with the cement hydration mechanism and may improve or reduce the performance of hydrated cement. The extent of this process is dependent upon the amount of F-CNT incorporated into the composite mix [16].

Nanomaterials such as nanoalumina are found to improve the flexural strength of concrete [17, 18]. Titanium and nanosilica enhance abrasion resistance and flexural strength [19, 20]. Nanosilica has been effective in promoting early precipitation of calcium silicate hydrate thus shortening the induction period [21, 22]. Incorporation of nanomaterials affects the cement hydration process and the rate of formation of hydration products enhancing the quality performance of concrete.

Graphene, a 2-D π -conjugation, has several extraordinary physical properties such as high thermal conductivity, high electrical conductivity, high surface area (2630 m²/g), high elastic modulus and amphi-polar electric field effect [23- 25]. Graphene forms a colloidal mixture and has also been used in making nanocomposites with conducting polymer for supercapacitor applications [26- 28]. In the current study, graphene was introduced as a partial replacement of Portland cement at various ratios to understand its effect on the heat dissipation in cementitious paste during the cement hydration. Thermal diffusivity and electrical conductivity of the hydrated cement paste incorporating different quantities of graphene were measured to understand thermal and electrical properties of the composite. SEM and X-ray diffraction methods were used to understand the physical and structural properties of the graphene-cement composite.

4.2 Experimental

4.2.1 As-received Materials

A commercially available portland cement and graphene platelets of 110x110x0.12 nm (Angstrom Materials, N008-100-N) were used in this study. All other chemicals and materials were used as purchased without any modifications.

4.2.2 Composite Materials Preparation

Hydrated graphene-cement mixes were prepared using a commercial mixer (Speedmixer DAC 150.1 FVZ) with constant water to solid ratio of 0.5 and at ambient temperature of 23 ± 2 °C. Sufficient workability of the mix could be obtained at a water to solid ratio of 0.5. The composite was mixed for 3 minutes in the Speedmixer operated at 3500 RPM. The mixes were poured into small containers and wrapped with plastic tape to avoid evaporation of water and desiccation. The mixes were cured for 44 hours from the mixing time. This hydration time was selected as it corresponds to the approximate average time at which the concrete element experiences a large temperature gradient between its inner core and outer surface [5].

4.2.3 Materials Characterization

The main constituent responsible for temperature rise in a concrete element is Portland cement due to the exothermic nature of its reaction with water. In defining temperature rise in mass elements, equally important to the ability to dissipate the heat is the amount of heat generated by Portland cement hydration. Cement fineness and mineralogy are the main contributors to the total heat generated through the cement hydration process. In conducting the current research, it is therefore important to characterize the as-received cement properties that are of significance to temperature rise; namely, cement fineness and mineralogy. Mineralogical composition of Portland cement was studied using X-ray diffraction. The diffractometer used in this study was a

PANalytical Cubix Pro coupled with HighScore Plus software for crystalline phase analysis. The software uses Rietveld analysis for phase quantification. The tube was operated at a current of 40 mA and a voltage of 45 KV. The scan range was set for 2θ of 8-70° using a step size of 0.014° with the time per step of 10 seconds. For hydrated composites and powdered specimens, rutile was added as an internal standard at 10 % by weight of the sample for qualitative comparison. Additionally, heat of hydration measurements on Portland cement was conducted using *TAMAIR* isothermal conduction calorimeter instrument with 8-twin channels at a bath temperature of 23°C. The test was conducted in accordance with the internal mixing procedure as outlined in the ASTM C1702 [29]. A Horiba LA-950 laser scattering particle size analyzer was used to assess the particle size distribution of the as- received cement.

The microstructure of the hydrated graphene-cement composites was examined using Hitachi SU-70 scanning electron microscope. For electrical conductivity measurements, cylindrical pellets of ground hydrated graphene-cement composites were prepared with a constant mass of 0.63 grams, a circular diameter of 13.07 mm and a thickness of 2.6 ± 0.1 mm. The pellets were oven dried at 105°C to eliminate the contribution of evaporable water to electrical conductivity. The pellets were gradually loaded up to 10 kips in a period of 3 minutes then unloaded for another 3 minutes before taking measurements. The electrical conductivity of the pellets was measured by setting them between two metal plates. The current was measured at different voltages using a Keithley electrometer 2400. The conductivity was calculated based on the current, voltage and the dimensions of the pellet samples.

In examining the effectiveness of graphene to improve concrete heat dissipation, thermal diffusivity was also measured. Hydrated graphene-cement composite specimens with thickness of 1.5 ± 0.05 mm and diameter of 10 ± 0.1 mm were prepared and cured for 44 hours. Thermal diffusivity

was determined using Linseis (c) XFA500 instrument conforming to ASTM E-1461, DIN 30905 and DIN EN 821 specifications. The instrument provides results with $\pm 5\%$ accuracy for most homogenous materials tested based on the flash method procedure [30].

Figure 4.1 reveals the morphology of hydrated graphene-portland cement and possible nanocomposite structure using SEM technique. The emphasis is given to how the graphene is attached to the main Portland cement hydration products such as calcium silicate hydrate and calcium hydroxide.

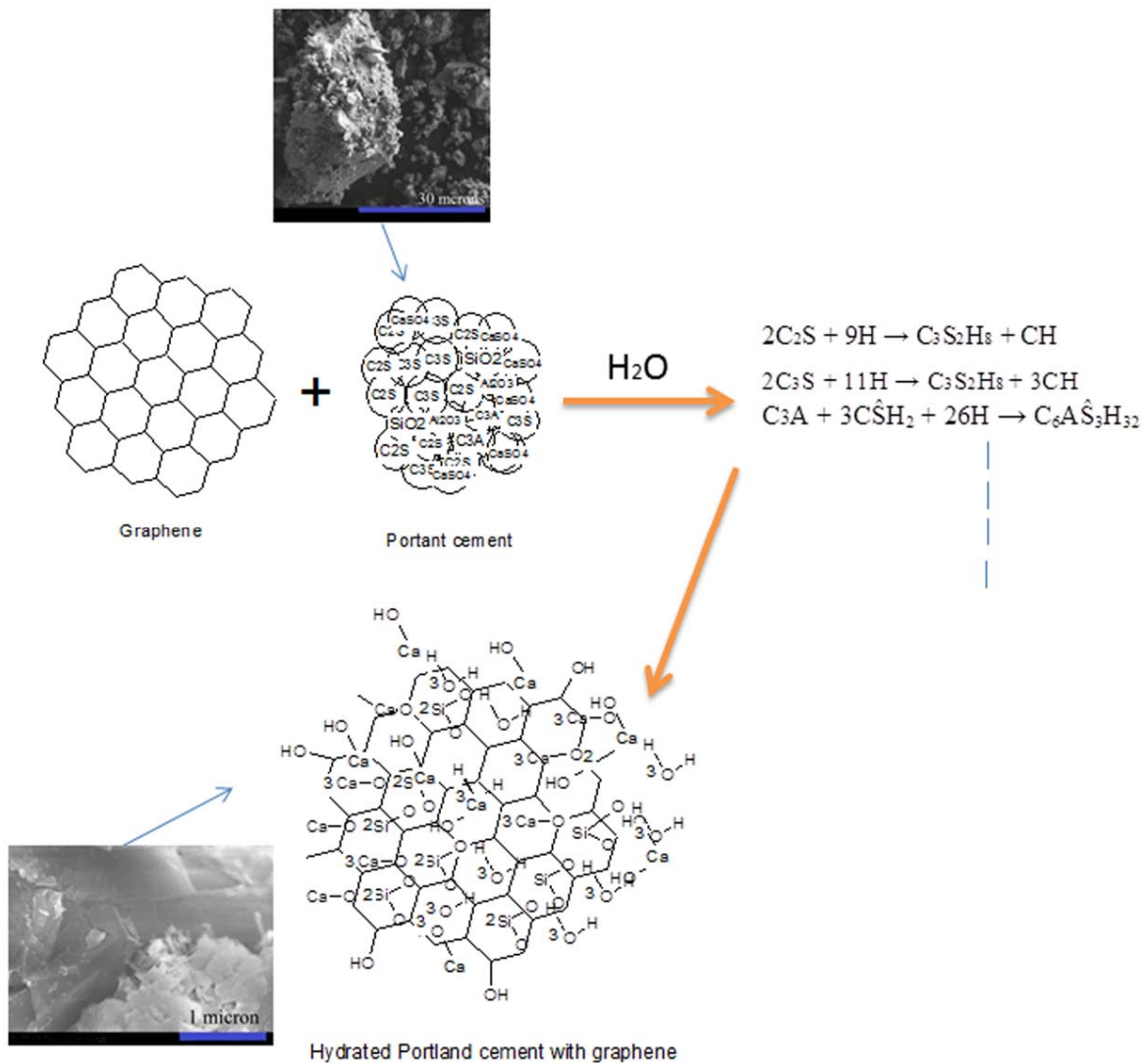


Figure 4.1 Schematic of hydrated graphene-cement composite and possible nanocomposite structure

4.3 Results and Discussion

4.3.1 Cement Characterization

The X-ray diffraction pattern of the as-received cement is presented in Figure 4.2. Rietveld analysis indicates that the amounts of the main crystalline phases are: alite=59.7%, belite=12.6%, tricalcium aluminate=11.2%, tetracalcium alumino-ferrite=6.0%, gypsum=3.6%, calcite=2.3%, periclase=1.7% and arkanite=1.6%. The amount of tricalcium aluminate (C_3A) present in this cement is high and it is therefore expected that this cement would generate higher heat of hydration compared to moderate-heat cements. ASTM C-150 [31] sets a maximum of 8% on C_3A for moderate-heat Portland cements. It is therefore anticipated that a concrete element incorporating this cement could generate a higher temperature gradient unless there is significant improvement in heat dissipation to counteract the effect of higher heat generation.

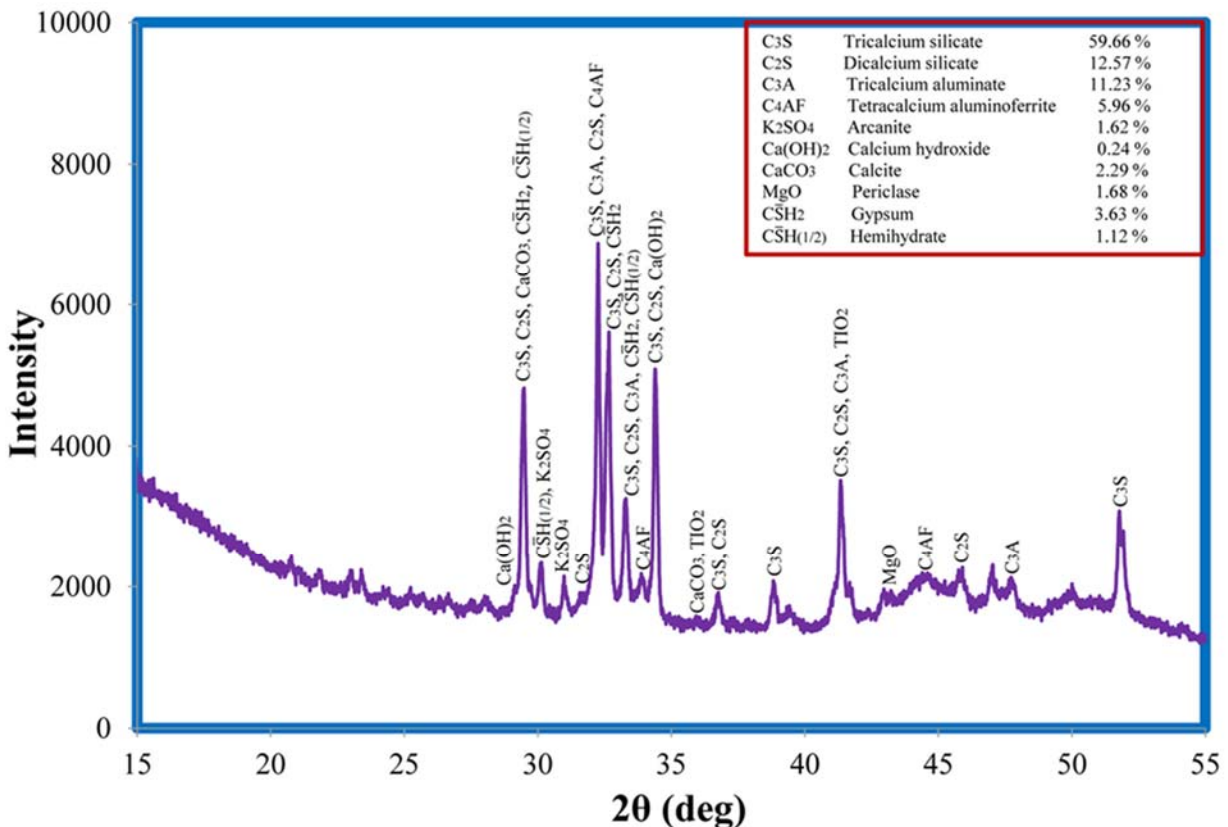


Figure 4.2 Mineralogical analysis of as-received cement using XRD

The particle size distribution analysis presented in Figure 4.3 indicates that the cement has a mean, median, mode and standard deviation of $10.27\mu\text{m}$, $9.08\mu\text{m}$, $10.82\mu\text{m}$ and $6.97\mu\text{m}$ respectively, with 70.5% of the as-received cement particles laying within one standard deviation of the reported mean. The reported value of the mean is the equivalent spherical diameter of the cement particles measured on volume basis. It is noteworthy that advanced Horiba hardware and software do not require normal or Rosin-Rammler [32] distribution assumptions to establish the particle size distribution curve.

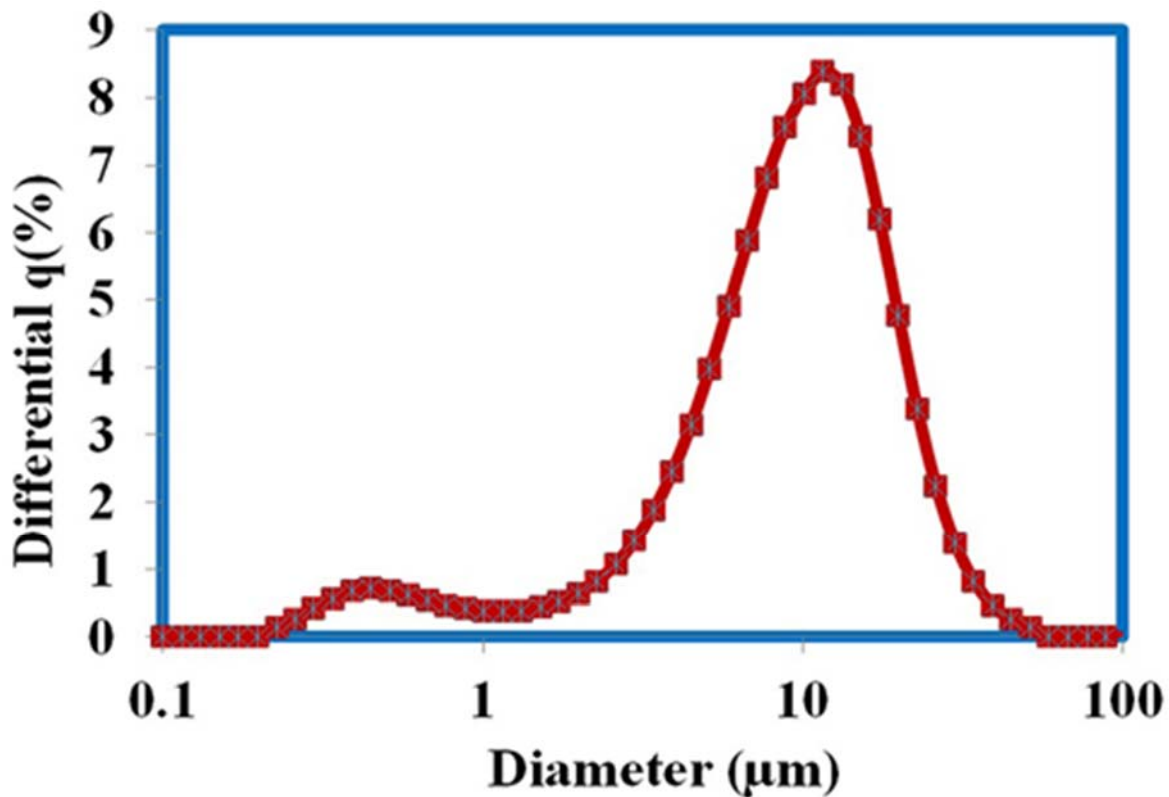


Figure 4.3 Particle size distribution of as-received cement

Figure 4.4 shows the total heat generated at seven days of hydration for Portland cement paste to be 406 J/g . The data indicate that more than 75% of the seven-day heat of hydration is generated during the first 48 hours. This implies that the potential for temperature rise is more important during the first few days. It also indicates the significance of increasing thermal diffusivity during the first few days to reduce the cracking potential of a massive concrete element.

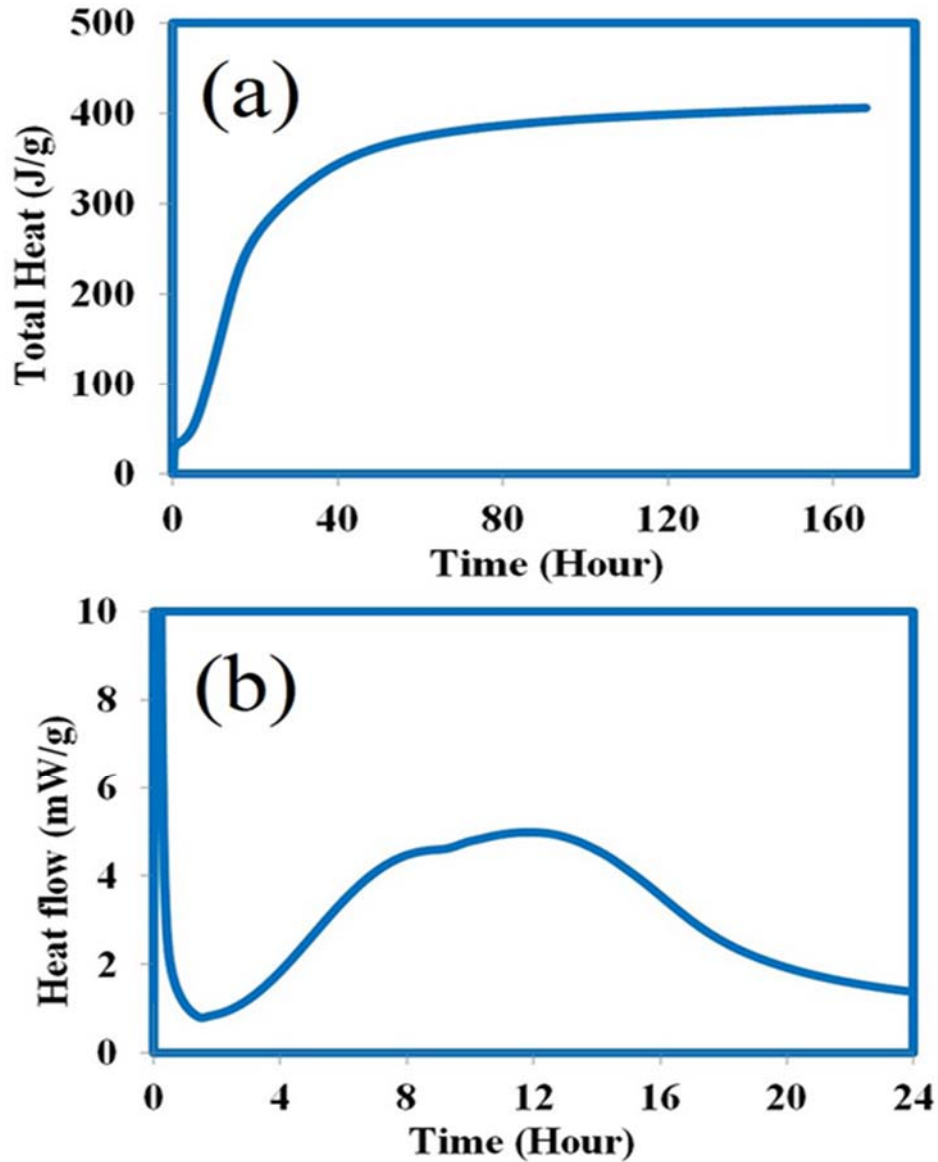


Figure 4.4 Cement paste (a) total heat & (b) heat flow

4.3.2 X-ray Diffraction and Rietveld Analysis

X-ray diffraction patterns of cement and graphene-cement composites are presented in Figure 4.5 for hydrated and anhydrous specimens. Rutile was added to the specimens as an internal standard at a 10% by weight of the solids. Figure 4.5(a) shows the XRD patterns of anhydrous graphene-cement composites and cement powder. The main diffraction peak for graphene occurs at a diffraction angle of 26.56° . The intensity ratio of graphene to titanium oxide ($2\theta=27.45^\circ$) increases with the increase of graphene content in the composite specimen. A hump can be

observed at 2θ of 42° - 52° and is more prominent at 10% graphene content while absent in the cement powder specimen with no graphene. Figure 4.5(b) for hydrated samples shows fewer and shorter peaks between 15° to 30° due to the chemical reaction of water with cement phases and formation of poorly crystalline calcium silicate hydrate gel in addition to other hydration phases such as calcium hydroxide and ettringite [1]. The characteristic peak of $\text{Ca}(\text{OH})_2$ at 18° is also clearly visible. The presence of a sharp peak of graphene from (002) plane, due to incremental increase of graphene in hydrated graphene-cement composite, is clearly shown at $2\theta=26.56^\circ$.

4.3.3 Temperature Treatment of Hydrated Graphene-Cement Composites

The effect of temperature on the hydrated graphene-cement samples is shown in Figure 4.6. Mixes of different ratios of graphene to cement, hydrated for 44 hours, were treated at varying temperatures of 23, 100, 400, and 600 to 750 °C. The presence of graphene in composite was studied by capturing the images of the mix at different temperatures. Figure 4.6 (A-D) shows the composites containing 0%, 1%, 5%, 10% graphene at 23°C. Figure 4.6 (E-H) shows no apparent difference in composites containing 0%, 1%, 5%, 10% graphene heated at 100°C. The varying color intensity in the pictures at different ratios of graphene is due to the incremental increase of carbon material in the composites. Presence of water in the graphene-cement mixes at 23 °C is reflected in the images as extra transparency compared to other mixes heated at higher temperatures. Figure 4.6 (I-L) shows the images of same composition of graphene-cement heated at 400 °C. The smooth structure observed in the images is probably due to the evaporation of capillary pore water and decomposition of calcium silicate hydrate in the mixes. The mixes heated beyond 400 °C are shown in Figure 4.6 (M-T). Interestingly, the graphene has been found to oxidize when heated to 600 and 750 °C. Also, calcium hydroxide decomposes in the temperature range of 400 – 500 °C.

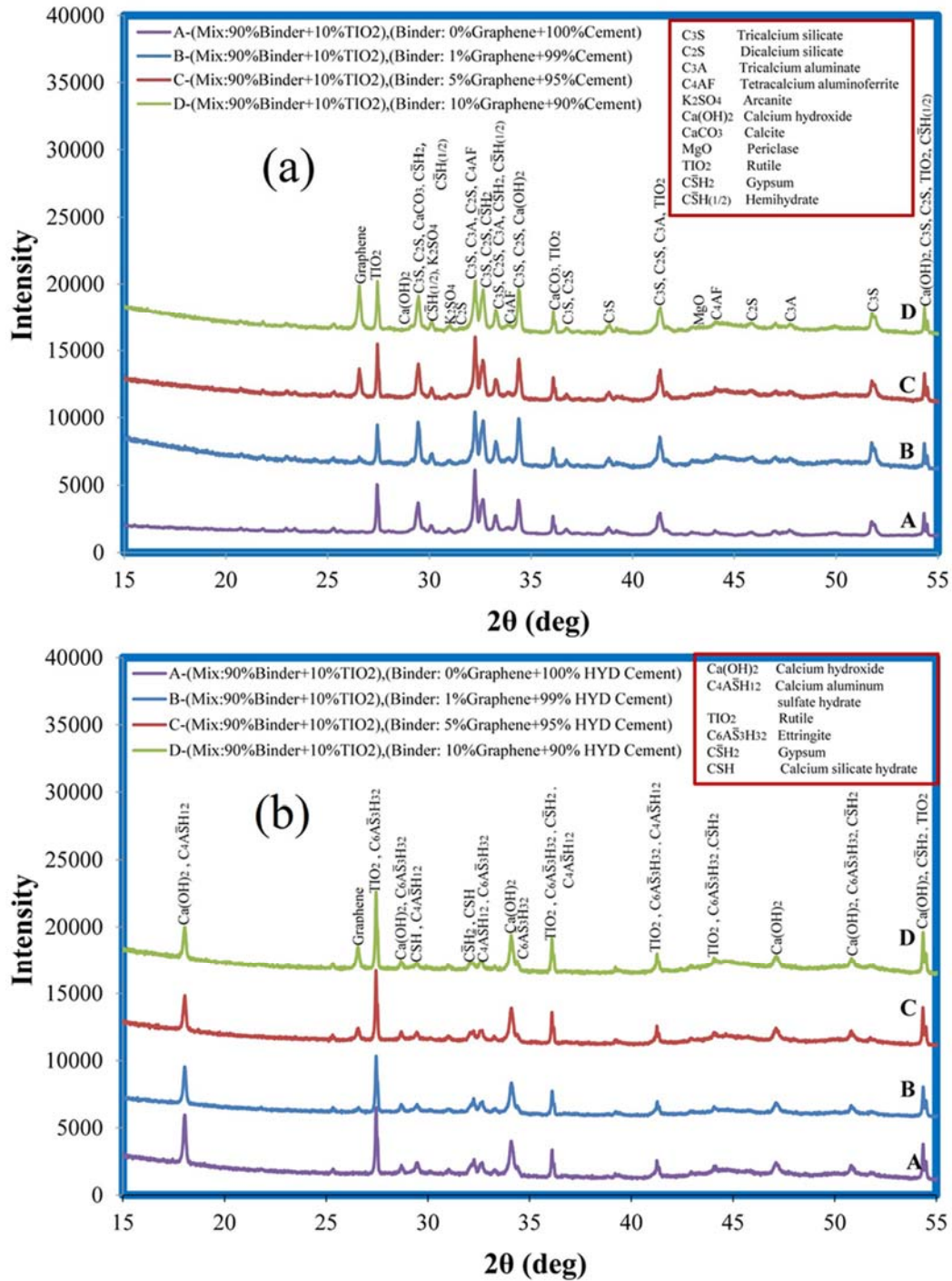


Figure 4.5 XRD patterns of cement & graphene-cement composites (a) anhydrous & (b) hydrated

It appears that the elemental metallic oxides in cement act as catalysts contributing to graphene oxidation regardless of the percentage of graphene present in the cement based composites. The hydration process may cause temperature gradient of 30 to 90° C in massive

concrete elements [5]. In this study, the hydrated graphene cement composite was examined at higher temperatures to investigate the physical changes that may occur in the composite in the event that the concrete element is exposed to external high temperatures (including fire).

4.3.4 Morphological Properties of Composite Materials in Hydration

The SEM image of the hydrated cement is shown in Figure 4.7 (A-C). The structure of the hydrated cement shows the formation of the needle-like ettringite and the sheet-like habit of calcium hydroxide ($\text{Ca}(\text{OH})_2$). Figure 4.7 (D-F) shows a mix of 1% graphene and 99% cement in the hydrated form. The structure of the 1% graphene and 99% cement mix shown in Figure 4.7 (D-F) is found to be different from the hydrated cement samples. Figure 4.7 (G-I) showing the hydrated sample of 5% graphene and 95% cement mix is more compact, with less needle-like formations, grown in the hydrated samples. The increase of graphene may decrease the porosity of the hydrated product as the graphene nanoparticles fill the micro-size capillary pores. It is also possible that graphene has an effect on the morphology of the needle-shaped ettringite. Figure 4.7 (J-L) depicts images of the hydrated 10% graphene and 90% cement mix which reveal no growth of needle-shaped structure, while the compact structure is predominant. Drastic reduction of porosity is anticipated for such a composite.

4.3.5 Electrical Conductivity Properties of Composite Materials in Hydration

Figure 4.8 and Table 4.1 show the effect of graphene content on the electrical resistivity of the hydrated graphene–cement samples. The conductivity of hydrated cement paste was approximately 10^{-8} S/m; however, incorporation of 1% of graphene changes the conductivity by 3 orders of magnitude. Interestingly, the increase in conductivity is substantial when the composite contains 5% graphene. At a graphene content of 10%, the conductivity measured was at about 10^{-2} S/m. The increase in conductivity with graphene content appears to be accompanied by a change

in electrical properties from insulating to semiconducting behavior. Such an increase in conductivity could bring about wide range of electrical applications for graphene-cement composites. The results indicate that low additions of graphene, even at 1%, could be sufficient for use in applications where electrostatic dissipation (ESD) is desirable.

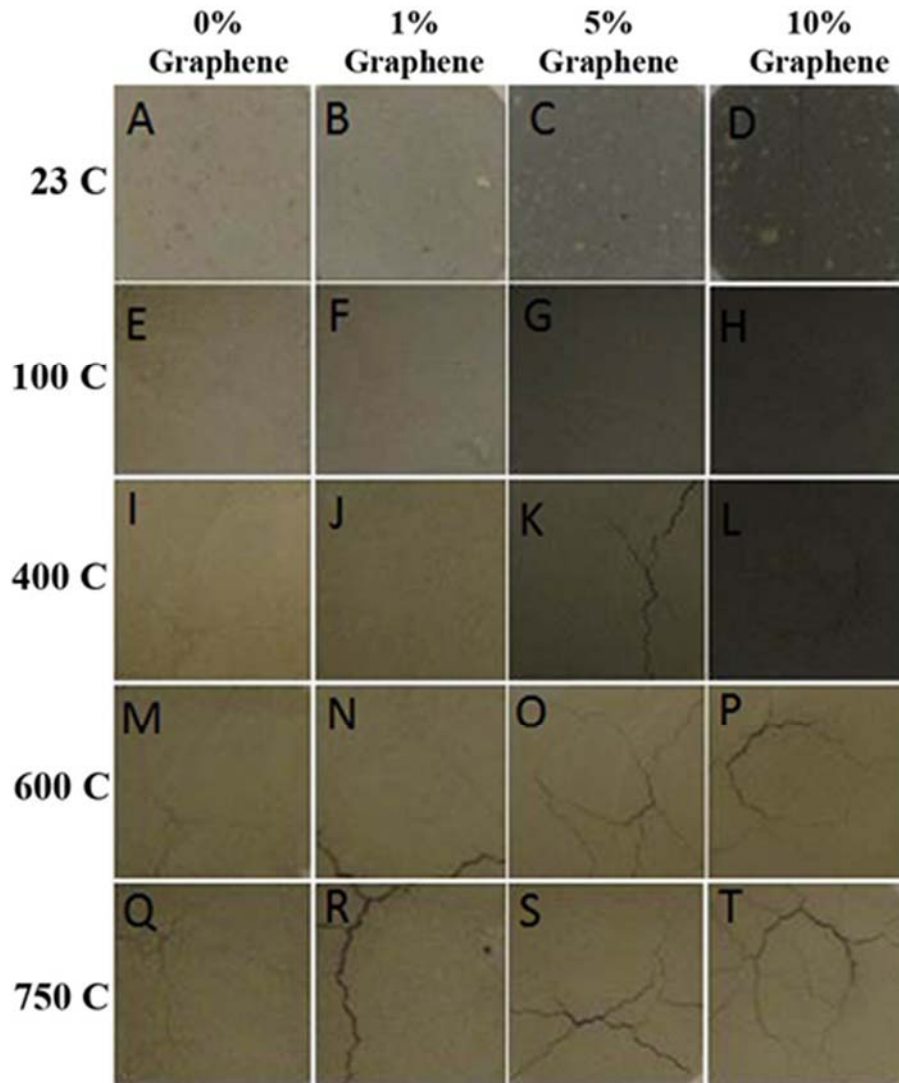


Figure 4.6 Temperature treatment of hydrated graphene-cement composites

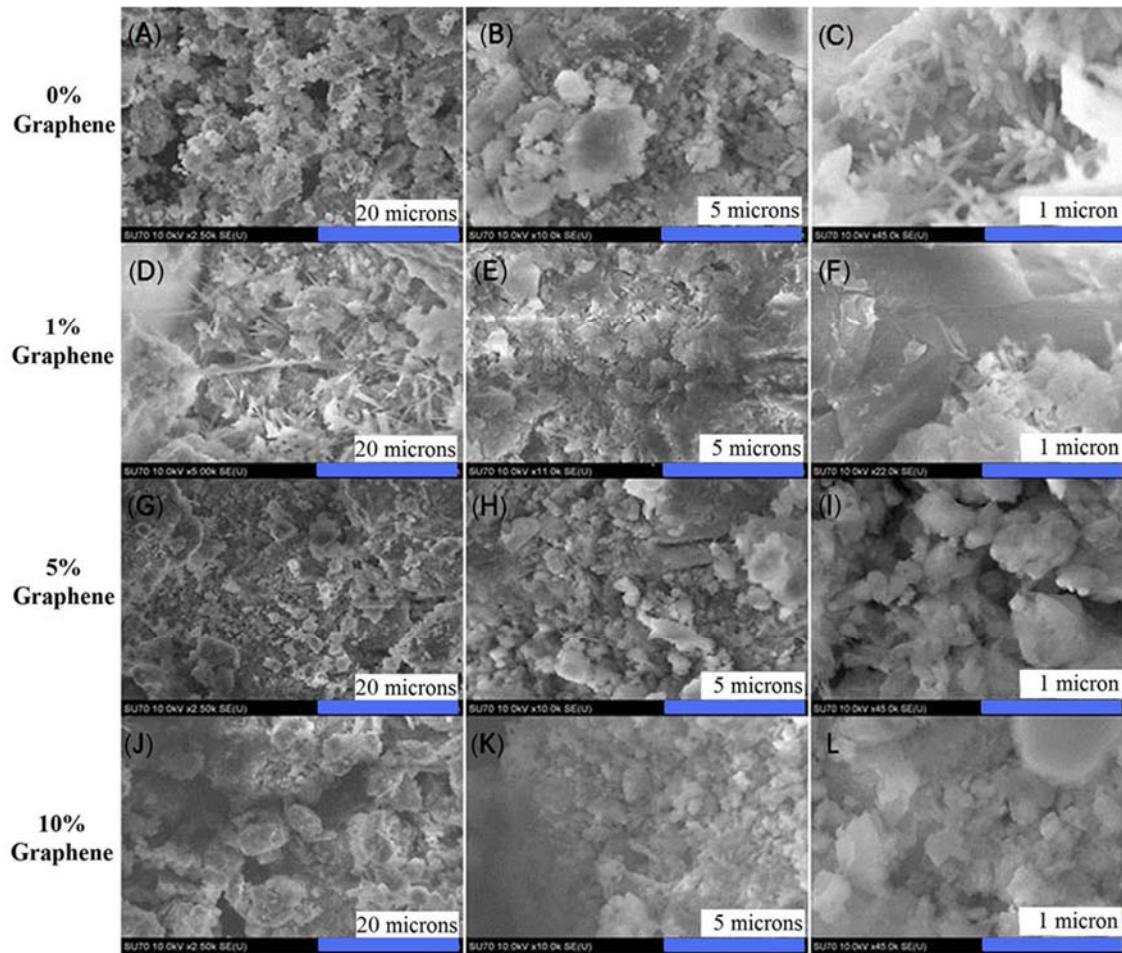


Figure 4.7 Scanning electron microscopy image of hydrated graphene-cement composite

4.3.6 Thermal Diffusivity Properties of Composite Materials in Hydration

Thermal diffusivity for the composite samples was determined using Parker's formula

[30]:

$$\alpha = \frac{0.139d^2}{t_{(1/2)}} \quad \text{Eq. (4.1)}$$

where

(α) = thermal diffusivity in (m^2/s)

$t_{(1/2)}$ = time (s) to reach 50% of maximum temperature amplitude

d = thickness of the material (m) across the direction of heat flow

About three runs were taken at every temperature for a better estimation of the thermal diffusivity for the composite samples. The hydrated graphene-cement composites were tested

under a similar range of temperatures as shown in Figure 4.9. The general trend observed here is that there is a decrease in thermal diffusivity with an increase in temperature, from 25 °C to 400 °C. It appears that the decrease in thermal diffusivity is about 35% for all the mixes, regardless of the graphene content. The data indicate that incorporation of 1% graphene did not have any significant effect on thermal diffusivity of the mix. Incorporation of 5% graphene, on the other hand, improved the thermal diffusivity by 25% at 25 °C and about 30% at 400 °C compared to the pure cement paste or the 1% graphene composite. The mix containing 10% graphene shows significant improvement in thermal diffusivity of about 75% at 25 °C and 60% at 400 °C. In general, it appears that incorporation of graphene in cement paste could significantly improve thermal diffusivity of the composite. Improvement of thermal diffusivity of cementitious pastes can reduce the temperature gradient (30- 90°C) effect due to cement hydration in mass concrete structures. This can consequently reduce the potential of massive concrete elements to experience thermal cracking thus improving thermal integrity and durability of concrete structures.

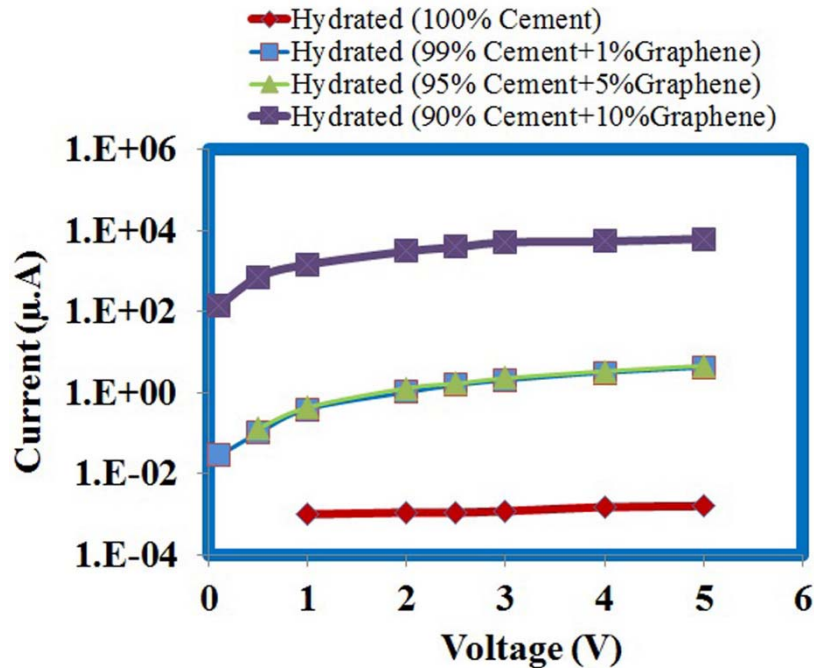


Figure 4.8 Electrical conductivity of hydrated graphene-cement composites

Table 4.1 Hydrated graphene-cement composite properties

Mix characteristics	Resistivity ($\Omega \cdot m$)	Electrical Conductivity ($S \cdot m^{-1}$)	Oven dried bulk density (g/cm^3)	Encapsulated bulk density (g/cm^3)
Hydrated (100%)	112441765	8.89E-09	1.490	1.851
Hydrated (99% Cement + 1% Graphene)	121820	8.21E-06	1.481	1.847
Hydrated (95% Cement + 5% Graphene)	94659	1.06E-05	1.463	1.838
Hydrated (90% Cement + 10% Graphene)	37	2.70E-02	1.436	1.827

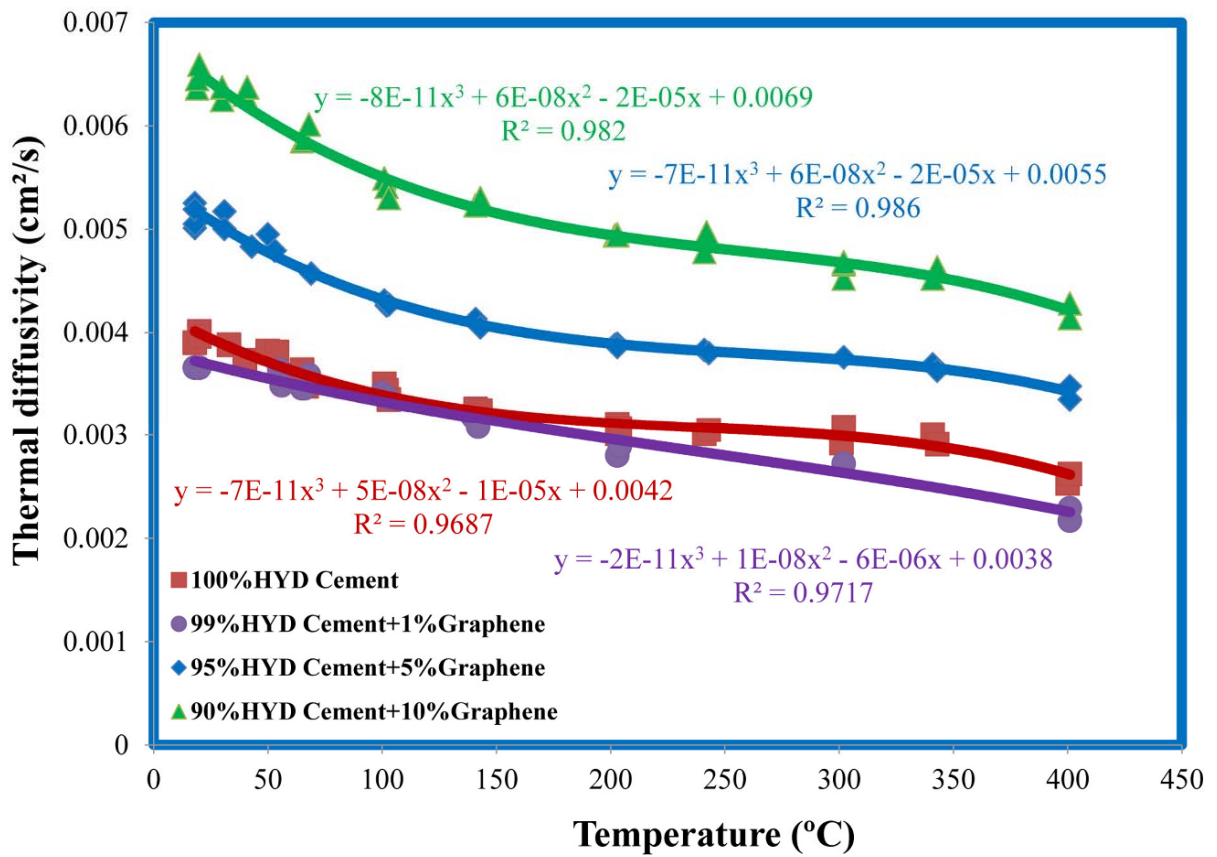


Figure 4.9 Thermal diffusivity of hydrated graphene-cement composites

4.4 Conclusions

Incorporation of graphene nanoparticles in cement paste showed interesting modifications in microstructural, morphological, electrical and thermal properties of the paste. Thermal diffusivity and electrical conductivity were found to increase with increasing the graphene content in the composite. The increase in thermal diffusivity of the hydrated graphene cement composite is a clear indication of the heat sink capacity of graphene. This effect is of significant importance especially during the exothermic reactions taking place during the initial stages of hydration of Portland cement. The hydrated graphene-cement samples indicate the presence of graphitic plane in the composite structure. The rod or needle-shaped morphology of ettringite, which is typically observed in hydrated cement paste, was less prevalent in the graphene composites and appeared to be affected by graphene content. The metal oxides in cement act as a catalyst for the oxidation of graphene at higher temperatures (600 to 750 °C), regardless of the quantity of graphene present in cement-based composite. The impact of the incremental increase of graphene on the electrical conductivity of the composites indicates the potential of using graphene in application where electrostatic dissipation (ESD) of charge is desirable.

4.5 References

- [1] Mindess, Sidney, J. Francis Young, and David Darwin. *Concrete*. (2003).
- [2] Odler, Ivan. "Hydration, setting and hardening of Portland cement." *Lea's Chemistry of Cement and Concrete* 4 (1998): 241-297.
- [3] Zayed, A., Ahmadreza Sedaghat, and Paul Sandberg. "Measurement and prediction of heat of hydration of portland cement using isothermal conduction calorimetry." *Journal of Testing and Evaluation* 41.6 (2013): 1-8.
- [4] Azenha, Miguel, and Rui Faria. "Temperatures and stresses due to cement hydration on the R/C foundation of a wind tower-A case study." *Engineering Structures* 30.9 (2008): 2392-2400.
- [5] Schindler, Anton Karel. "Concrete hydration, temperature development, and setting at early-ages." (2011).
- [6] Alkhateb, Hunain, et al. "Materials genome for graphene-cement nanocomposites." *Journal of Nanomechanics and Micromechanics* 3.3 (2013): 67-77.
- [7] Makar, J. M., J. C. Margeson, and Jeanne Luh. "Carbon nanotube/cement composites-early results and potential applications." (2005): 1-10.
- [8] Vandamme, Matthieu, and Franz-Josef Ulm. "Nanogranular origin of concrete creep." *Proceedings of the National Academy of Sciences* 106.26 (2009): 10552-10557.
- [9] Ulm, Franz-Josef. "Green concrete." (2007): 27-27.
- [10] Cardenas, Henry E. *Nanomaterials in concrete: advances in protection, repair, and upgrade*. Destech Publications, Inc, (2012).
- [11] Peyvandi, Amirpasha, et al. "Surface-modified graphite nanomaterials for improved reinforcement efficiency in cementitious paste." *Carbon* 63 (2013): 175-186.
- [12] Lv, Shenghua, et al. "Effect of graphene oxide nanosheets of microstructure and mechanical properties of cement composites." *Construction and Building Materials* 49 (2013): 121-127.
- [13] Diamanti, Maria Vittoria, Marco Ormellese, and MariaPia Pedferri. "Characterization of photocatalytic and superhydrophilic properties of mortars containing titanium dioxide." *Cement and Concrete Research* 38.11 (2008): 1349-1353.
- [14] Chung, D. D. L. "Comparison of submicron-diameter carbon filaments and conventional carbon fibers as fillers in composite materials." *Carbon* 39.8 (2001): 1119-1125.

- [15] Morsy, M. S., S. H. Alsayed, and M. Aqel. "Hybrid effect of carbon nanotube and nano-clay on physico-mechanical properties of cement mortar." *Construction and Building Materials* 25.1 (2011): 145-149.
- [16] Musso, Simone, et al. "Influence of carbon nanotubes structure on the mechanical behavior of cement composites." *Composites Science and Technology* 69.11 (2009): 1985-1990.
- [17] Campillo, Igor, et al. "Improvement of initial mechanical strength by nanoalumina in belite cements." *Materials Letters* 61.8 (2007): 1889-1892.
- [18] Li, Zhenhua, et al. "Investigations on the preparation and mechanical properties of the nano-alumina reinforced cement composite." *Materials Letters* 60.3 (2006): 356-359.
- [19] Li, Hui, Mao-hua Zhang, and Jin-ping Ou. "Abrasion resistance of concrete containing nano-particles for pavement." *Wear* 260.11 (2006): 1262-1266.
- [20] Li, Hui, Mao-hua Zhang, and Jin-ping Ou. "Flexural fatigue performance of concrete containing nano-particles for pavement." *International Journal of Fatigue* 29.7 (2007): 1292-1301.
- [21] Qing, Ye, et al. "Influence of nano-SiO₂ addition on properties of hardened cement paste as compared with silica fume." *Construction and Building Materials* 21.3 (2007): 539-545.
- [22] Vera-Agullo, J., et al. "Mortar and concrete reinforced with nanomaterials." *Nanotechnology in Construction* 3. Springer Berlin Heidelberg, (2009). 383-388.
- [23] Wei, Weili, and Xiaogang Qu. "Extraordinary physical properties of functionalized graphene." *Small* 8.14 (2012): 2138-2151.
- [24] Shahil, Khan MF, and Alexander A. Balandin. "Thermal properties of graphene and multilayer graphene: Applications in thermal interface materials." *Solid State Communications* 152.15 (2012): 1331-1340.
- [25] Eletskaa, Aleksandr Valentinovich, et al. "Graphene: fabrication methods and thermophysical properties." *Physics-Uspekhi* 54.3 (2011): 227-258.
- [26] Basnayaka, Punya A., et al. "Supercapacitors based on graphene–polyaniline derivative nanocomposite electrode materials." *Electrochimica Acta* 92 (2013): 376-382.
- [27] Gómez, Humberto, et al. "Graphene-conducting polymer nanocomposite as novel electrode for supercapacitors." *Journal of Power Sources* 196.8 (2011): 4102-4108.
- [28] Alvi, Farah, et al. "Graphene–polyethylenedioxythiophene conducting polymer nanocomposite based supercapacitor." *Electrochimica Acta* 56.25 (2011): 9406-9412.

- [29] "Standard Test Method for Measurement of Heat of Hydration of Hydraulic Cementitious Materials Using Isothermal Conduction Calorimetry," In Construction, ASTM International, (2012), Vol. 4.01, C1702-09a.
- [30] Gaal, P. S., M-A. Thermitus, and Daniela E. Stroe. "Thermal conductivity measurements using the flash method." *Journal of Thermal Analysis and Calorimetry* 78.1 (2004): 185-189.
- [31] ASTM C150. "Standard specification for Portland Cement." (2009).
- [32] Brown, Wilbur K., and Kenneth H. Wohletz. "Derivation of the Weibull distribution based on physical principles and its connection to the Rosin–Rammler and lognormal distributions." *Journal of Applied Physics* 78.4 (1995): 2758-2763.

**CHAPTER 5: INVESTIGATION OF THE PHYSICAL PROPERTIES OF
GRAPHENE NANOPATELET CEMENT PASTE MATRIX IN CONCRETE
ELEMENTS SUSCEPTIBLE TO CRACKING**

5.1 Introduction

Concrete is a composite material consisting of cementitious materials (Portland cement, pozzolanic materials, nonreactive additives), water, fine and coarse aggregates in addition to chemical admixtures [1-2]. Graphene is a 2D crystal of sp^2 hybridized carbon atoms organized in 6 carbon atom rings. The long 2D π -conjugation in graphene results in very high specific area, high Young's modulus and extraordinary thermal and electrical conductivity [3]. Concrete gain strength due to the chemical interaction and hydration of its cementitious constituents. The main phases in Portland cement contributing to the hydration process are tricalcium silicate (C_3S), tricalcium aluminate (C_3A), dicalcium silicate (C_2S), and tetracalcium aluminoferrite (C_4AF) in addition to calcium sulfates [4-5].

Recent research indicates the possibility of implementing the use of nanomaterials including titanium oxide, graphene platelets, nano-alumina, nano-silica and carbon nanotube in several civil engineering applications [6]. The incorporation of nanomaterials in hydrated cement paste affect the microstructure of the resulting hydration products; specifically, the nanostructure of calcium silicate hydrate (C-S-H) which is the main network bonding component [7]. Du et al. [8] research study indicates that graphene nanoplatelets (GNP) can reduce the permeability and ionic diffusivity in cement mortars up to 70% by the addition of less than 5% graphene by weight of cement in the composite. This effect is ascribed to capillary pores refinement in the hydrated

cement network and the barrier effect of GNP resulting from tortuosity escalation against chloride ions and water penetration. The research also indicates that an increase of GNP over 5% by weight of cement may lead to agglomeration of GNP particles and as a result may compromise the impedance effects of GNP towards ionic diffusion. Sedaghat et al. [9] indicates that incorporation of 10% graphene nanoplatelets in cement paste improves the composite electrical conductivity by a factor of 10^7 and thermal diffusivity by 60% to 75% in the temperature range from 25 °C through 400 °C, respectively. It is further indicated that the noted increase in thermal diffusivity of graphene cement paste is due to the heat sink capacity of graphene which can also have another potential application of reducing temperature gradient in concrete elements in which thermal cracking is an issue. Thermal diffusivity of graphene cement composite measured using Linseis (C) XFA500 is shown in Figure 5.1 for varied graphene content (0-10%) at different temperatures [9].

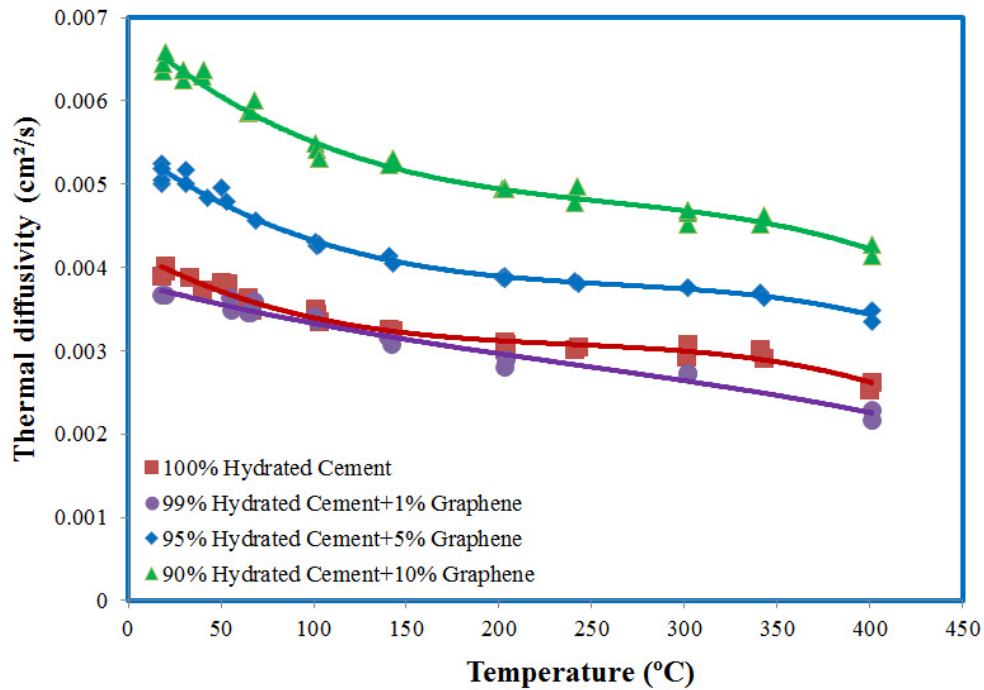


Figure 5.1 Thermal diffusivity of graphene cement composite measured using Linseis (C) XFA500

Konsta-Gdoutos et al. [10] findings on the effect of multiwalled carbon nanotubes concentration and their aspect ratio on flexural strength of cement paste indicates that incorporation of MWCNTs in the quantities of 0.025 to 0.1% as a cement replacement results in flexural strength improvement of the cement paste. It is also demonstrated that MWCNTs aspect ratio is a significant factor controlling the quantity of nanotubes required to achieve the optimum flexural strength. Shorter MWNTs earns higher degree of dispersion in the cement paste matrix; however, higher amounts are required to reduce the fiber-free area for subsequent reduction of nano-cracks [10-11]. Chaipanich et al. [12] demonstrated that fly ash-cementitious mixture reinforced with carbon nanotubes has a denser microstructure and higher strength due to the filler effect of nanotube particles within the larger pore structure of the hydrated cementitious matrix. Stronger network bonding of C-S-H/ettringite and carbon nanotubes was observed when examined by SEM and micrographs analysis. Lv et al. research study indicates that the use of graphene oxide (GO) with cement drastically affects the microstructure of hydrated cement composite and leads to the formation of flower-like hydration crystals, reduction of brittleness and enhancement of toughness. It is further indicated that incorporation of 0.03% GO at 29.5% oxygen content remarkably improves the flexural strength (60.7%), tensile strength (78.6%) and compressive strength (38.9%) relative to the plain mortar samples [13]. Gong et al. study indicates that incorporation of 0.03% of graphene oxide by weight of cement results in over 40% increase in the compressive and tensile strength and a drop of 13.5% in total porosity with more than 100% larger amount of gel pores and 27.7% lower capillary pores in graphene cement composite pastes at the age of 28 days compared to those for plain cement pastes. The effect was due to a higher degree of hydration, increase in nonevaporable water and calcium hydroxide content at different ages [14]. Le et al. indicated that incorporation of graphene nanoplatelets (GNP) up to 20% in cement

composites can be used to evaluate the structural health by monitoring the electric potential arising from the damage which is equivalent to the fractional change in elastic compliance [15].

One of the problems or critical issues with the use of graphene nanoparticles is the potential of particle agglomeration. Agglomeration of nano particles in cement paste and concrete can occur due to the existence of strong van der Waal's forces at the nano scale which can lead to less workable mixes. Incorporation of nano materials in cement paste matrix reduces the workability of concrete. Workability, however, can be improved by using mechanical techniques, sonication or through the additions of chemical admixtures. Chuah et al. stated that incorporation of nanomaterials in mortar and concrete severely reduces the workability of mixtures since larger surface area of nanomaterials would naturally demand more water to wet the particles of higher surface area. This shall result in reduction of the amount of water available to wet cement particles. Proper dispersion techniques can result in better workability of the cementitious system, thus leading to a better contribution of nano materials to improve the physical properties of composite. Measurement of non-evaporable water and CH content using TGA analysis indicates that GO accelerates cement rate of hydration [16].

The current study aims to evaluate the effect of incorporating graphene in cement paste on the physical and chemical properties of the mixture. In order to address this effect, work was conducted first on unblended cements of different phase compositions and fineness. The cracking potential of the unblended cements were studied first on mortar mixtures at a constant w/c ratio of 0.45. Subsequently, cements triggering higher cracking potential in mortar mixtures were selected to be further studied with different amounts of graphene as a partial replacement of cement to evaluate their physical properties including compressive strength, heat of hydration (HOH) mechanisms and modulus of elasticity. It was formerly indicated that incorporation of graphene

up 10%, as a partial replacement of cement, improves thermal diffusivity of the composite and as a result has the potential to reduce the temperature gradient and thermal cracking in concrete elements.

5.2 Material and Methods

Six industrial Portland cements (3 cements x 2 fineness levels = 6 cements) G (1) through G (6) with variable mineralogical composition and finenesses were selected. Mineralogical analysis was conducted using X-ray diffraction. The diffractometer used in this study was a PANalytical Cubix Pro and Cu K α radiation. HighScore Plus software was used for phase identification and quantification. The scans were collected at a current of 40 mA and voltage of 45 KV. The 2 θ scan range was set for 5–60° at a step size of 0.012°. X-ray scans were collected in triplicates for each cement. The averages for phase quantification of the six cements are reported in Table 5.1.

Table 5.1 Quantification of crystal phase composition of cements G (1) through G (6)

Crystal phase composition	G (1)	G (2)	G (3)	G (4)	G (5)	G (6)
Tricalcium Silicate (C ₃ S), (%)	61.4	61.7	56.9	56.8	57.3	58.8
Dicalcium Silicate (C ₂ S), (%)	13.0	14.0	16.1	19.7	12.9	13.3
Tricalcium Aluminate (C ₃ A), (%)	6.6	6.9	7.1	7.1	9.8	11.2
Tetracalcium Aluminoferrite (C ₄ AF), (%)	11.7	12.7	10.9	10.8	6.4	5.9
Arcanite (K ₂ SO ₄), (%)	1.3	1.1	0.9	0.9	2.0	1.8
Free Lime (CaO), (%)	0.1	0.2	0.3	0.2	0.0	0.0
Calcium Hydroxide (Ca (OH) ₂), (%)	0.3	0.2	0.5	0.7	0.4	0.3
Calcite (CaCO ₃), (%)	2.1	1.0	4.0	0.8	2.1	2.2
Periclase (MgO), (%)	0.1	0.2	0.3	0.1	2.0	1.8
Gypsum (C \bar{S} H ₂), (%)	1.1	2.9	2.4	2.6	3.5	6.2
Hemihydrate (C \bar{S} H($\frac{1}{2}$)), (%)	0.6	1.0	0.5	0.5	1.0	1.1
Anhydrite (C \bar{S}), (%)	0.0	0.1	0.0	0.0	0.0	0.1

The Blaine fineness was measured in accordance to ASTM C-204 [17]. A Horiba laser scattering particle size analyzer (LA-950) was used to study the particle size distribution of the as-received cements [18-19]. Prior to conducting the measurements, HORIBA instrument was set to

obtain 5000 data measurements per second with 15 iterations. Refractive index of 1.7-1.0i was selected for the diffraction measurements of cement particles based on “Certification of SRM 114q: Part II (Particle size distribution) and NIST Special Publication 260-166”. The particle size distribution measurements were conducted on dry cement powder in the automatic mode and using a small nozzle at 0.3 (MPa) air pressure. A maximum standard deviation of 0.6% (cumulative volume basis) is noted on three runs per cement indicating a strong repeatability of the measurements. The particle size distribution of the cements studied here, G (1) through G (6), are presented in Figure 5.2 and the physical properties of cements are presented in Table 5.2.

Table 5.2 Blaine fineness, measured seven day heat of hydration and particle size analysis data for cements G(1) through G(6)

Physical properties of cements	G (1)	G (2)	G (3)	G (4)	G (5)	G (6)
Blaine Fineness, (m ² /kg)	417	612	402	590	405	530
Measured 7-day HOH, J/g (cal/g), ASTM C1702 Isothermal conduction calorimetry (Internal mixing)	348 (83)	387 (93)	332 (79)	356 (85)	386 (92)	406 (97)
Measured 7-day HOH, J/g (cal/g), ASTM C186 Heat of Solution calorimetry	349 (83)	370 (88)	337 (80)	367 (88)	361 (86)	391 (93)
Mean (µm)	12.9	10.0	11.9	9.61	14.3	10.2
Median (µm)	10.4	8.23	9.85	7.65	10.7	9.08
Span	2.03	2.26	2.12	2.32	2.46	1.83
D10 (µm)	3.61	1.33	2.51	1.43	3.2	2.55
D50 (µm)	10.4	8.23	9.85	7.64	10.7	9.08
D90 (µm)	24.8	19.9	23.3	19.1	29.7	19.1

A TAMAIR isothermal conduction calorimetry (manufactured by TA instruments) was used to measure the heat of hydration (HOH) of cements, under isothermal conditions. The methodology adopted here was conforming to ASTM C-1702, method A for internal mixing, [20] at 23 °C. HOH of cements was measured immediately from the time of water addition. Further

detailed information regarding implementation of this methodology is outlined in [4]. A water to cement ratio of 0.5 was used to rule out self-desiccation [21]. HOH measurements were performed in duplicate runs to ensure repeatability and reproducibility of the collected data. It is notable that all duplicate runs have less than 1% heat deviation from the average of the two runs at seven day of hydration and the heat flow curves, generated from the first and second runs, overlap throughout the duration of the test, except within the initial 20 minutes, with a maximum deviation of 30 ($\mu\text{W/g}$). It is important to note that shape of the heat flow curve at the initial stages of hydration is influenced by the speed used by the designated admixer and that the cumulative heat curves merge, from duplicate runs, after approximately an hour from the initiation of the hydration process [5].

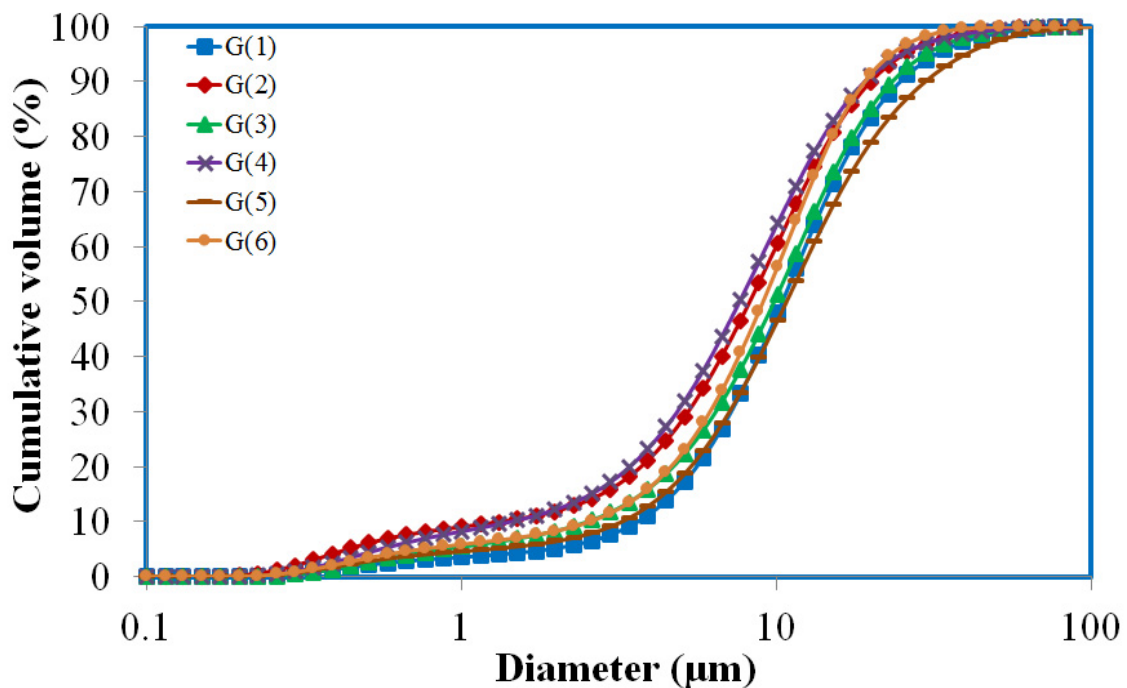


Figure 5.2 Particle size distribution of the cements studied here, G (1) through G (6)

The physical properties of cements G (1) through G (6) are outlined in Table 5.2. The cracking potential due to drying/autogenous shrinkage and HOH of the mortar specimens prepared with G (1) through G (6) cements were examined using restrained shrinkage rings conforming to

ASTM C1581-09 [22]. Each experiment includes preparation of three individual mortar rings placed around the structural steel rings as shown in Figure 5.3. The water to cement ratio was maintained constant at 0.45 to provide adequate water for the hydration of cements of variable finenesses. The curing process of the mortar specimens includes 24 hours of encapsulating and wet curing of the specimens using burlap. The mortar ring specimens were cured in a BLUE M CEO series environmental chamber (Thermal Product Solutions product) and at a constant temperature of 23 ± 2 °C and relative humidity of $50\% \pm 4\%$. In this experiment, mortar specimens will experience drying and autogenous shrinkage thus inducing compressive stresses in the structural steel ring with the progress of hydration. Due to the high modulus of elasticity of the steel rings, the mortar specimens cannot shrink freely and therefore will experience induced tensile stresses due to the restraint imposed by the steel rings. Once the induced tensile stresses in the mortar specimens exceed the tensile strength of mortar, an abrupt cracking is expected to occur in the mortar specimens. The mixture proportions are: cement: 9(lbs), Ottawa sand: 24 (lbs); deionized water: 4.05(lbs).



Figure 5.3 Restrained shrinkage ring specimens

Compressive strength of graphene cement mortar samples prepared with G (5) and G (6) cements were measured using ToniPRAX compression testing machine conforming to ASTM C109 [23] and ASTM C305 [24]. Mortar samples were prepared at two levels of graphene content, Blaine fineness and water to cement ratio (hereon referred to (w/c)). Hysitron Ti 900 Triboindenter was used to determine the modulus of elasticity and hardness of graphene cement paste composites at 0, 1%, 5%, 10% graphene content.

5.3 Results and Discussion

5.3.1 Evaluation of Cracking Potential of Mortar Specimens under Restrained Shrinkage

This section addresses the evaluation of the cracking potential of mortar specimens prepared with cements G (1) through G (6). Mineralogical phase composition and physical properties of the as-received cements are presented in Table 5.1 and 5.2. The age at cracking is considered a significant factor used to evaluate the effect of Portland cement fineness and phase composition on autogenous/drying shrinkage and thermal cracking. Restrained shrinkage results of mortar specimens are outlined in Table 5.3, while the induced strain in the steel rings are presented in Figure 5.4. From Table 5.3, the effect of fineness can be observed by comparing cements G(1) and G(3), with an average age at cracking of 6 days, versus cements G(2) and G(4) with an average age at cracking of 5 days.

Table 5.3 Restrained shrinkage results of mortar specimens for cements G (1) through G (6)

Specimen	Average age at cracking (days)	Average initial strain (micro strain)	Average maximum strain (micro strain)	Average stress rate at cracking (Mpa/day)	Average net time to cracking (days)
G(1)	6	6	-48	0.46	4.78
G(2)	5	4	-42	0.43	4.15
G(3)	6	3.8	-39	0.33	4.70
G(4)	5	1.7	-43	0.44	3.63
G(5)	3	18	-31	0.97	2.20
G(6)	3	-5	-33	0.71	1.62

Average age at cracking (days) is considered as age measured from the time of casting to the time when a sudden decrease in strain occurs.

Average initial strain (microstrain) is considered as initial strain at the age when drying is initiated (24 hours after mortar rings placement).

Average maximum strain (microstrain) is considered as strain at the age when cracking occurred or the age when the test is terminated.

Average stress rate at cracking (Mpa/day) is considered as stress rate at cracking or at the time the test is terminated calculated to the nearest 0.01 (MPa/day).

Average net time to cracking (days) is considered as time to cracking calculated as the difference between the age at cracking and the age drying was initiated.

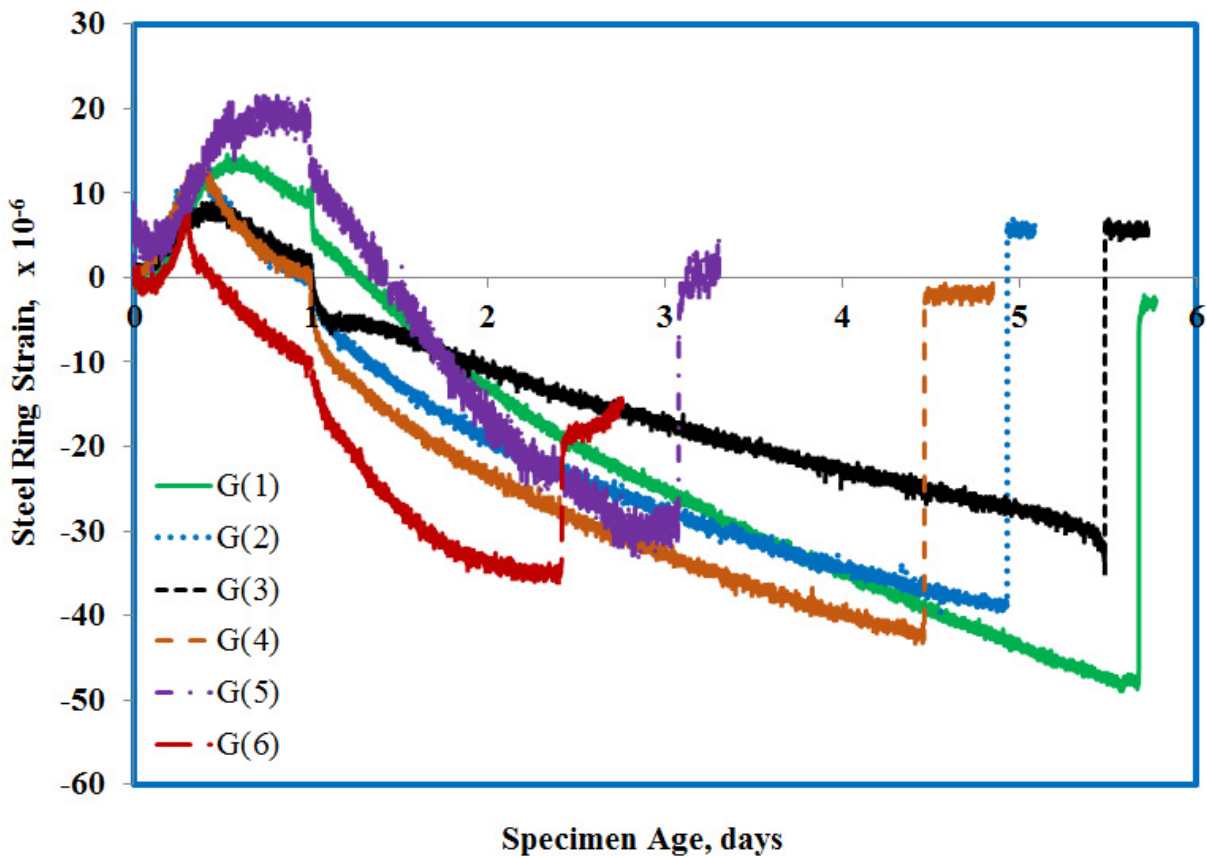


Figure 5.4 Restrained shrinkage results of mortar specimens for cements G (1) through G (6)

The effect of cement fineness on the net time to cracking is more significant for G (3) cement, 4.70 days, and G (4) cement, 3.63 days, when compared to G (1) cement, 4.78 days, and G (2) cement, 4.15 days. Cement fineness does not show any significant or justifiable effect on the average maximum strain experienced by cements G (1) through G (4). Among all 6 cements, G(5) and G(6) showed the shortest average age at cracking, three days, and the highest average stress rate at cracking of 0.97 MPa/day (for G(5)) and 0.71 MPa/day (for G(6)). These two cements contain the highest C₃A content, 9.8% and 11.2% respectively, and the lowest C₄AF content, 6.4% and 5.9%, respectively. The average net time to cracking is at 2.2 days for G (5) cement while it is 1.62 days for G (6) cement indicating that the increase in cement fineness decreases the net time to cracking for these cements. The average maximum strain was recorded as -31 μS and -33μS, respectively, for G (5) and G (6) cements, thus indicating insignificant effect of cement fineness on the average maximum strain for these cements. The experimental results indicate that increasing cement fineness, in general, may decrease the age at cracking while this effect may not be significant. On the other hand, the tricalcium aluminate content of cements appears to be more critical in affecting the cracking potential of Portland cement mixtures. Calcium sulfate in the form of gypsum, hemihydrate and anhydrite is added to Portland cement to control the quick reaction of tricalcium aluminate (C₃A) with water. The corresponding reaction results in the formation of ettringite (Ca₆Al₂(SO₄)₃(OH)₁₂.26H₂O, C₆A \hat{S} ₃H₃₂) [25]. Ettringite (AFt) is the main hydration product of the initial interaction between sulfate ions, alumina and calcium ions in solution and contributes to the initial mechanical strength of the complex cement systems [26]. The literature indicates that when the sulfuate/aluminate ratio falls below 3, ettringite becomes unstable and converts to monosulfate (AFm), (Ca₄Al₂O₆(SO₄).14H₂O,C₄A \hat{S} H₁₄), liberating sulfates which later react with C₃A to generate more monosulfates until all C₃A or sulfates are consumed [25]. If the

sulfate content is too low, the main C_3A reaction peak (AFt formation mechanism before AFm mechanism initiation) occurs before the main hydration peak, which interferes with proper hydration of C_3S and cement setting and can result in delayed C_3S peak occurrence as a consequence. It is demonstrated, that in general, sulfate ions accelerate the C_3S reaction while alumina containing hydration phases decelerates the alite reaction in the cement matrix. This effect may be cancelled out since C_3A and sulfate both react in the matrix solution to form ettringite. To clearly understand the hydration mechanism of cement and its effect on the cracking potential of mortars, heat of hydration of cements G (1) through G (6) was measured using isothermal calorimetry at water to cement ratio of 0.5. As it is demonstrated in Figure 5.5, sulfate depletion occurs after the main hydration peak for cements G (1) through G (4). This is indicative of adequate presence of sulfates to control the aluminate phase reaction. It appears that an increase in cement fineness reduces the occurrence time of the main hydration peak by approximately 2 hrs. for cements G (1) and G (3). On the other hand, the main peak for aluminate phase occurs before the silicate main peak for G (6) cement, indicating an undersulfated system. The main nucleation and growth peak (alite peak) is observed to be drastically delayed by 5 h for G (6) cement compared to G (2) and G (4) cements. It is indicated in the literature that thaumasite ($CaCO_3 \cdot CaSO_4 \cdot CaSiO_3 \cdot 15H_2O$) is formed as a result of reaction between SO_4^{2-} and C-S-H which has similar XRD pattern to that of ettringite. Thaumasite formation may be accompanied by formation of secondary gypsum and brucite which consumes C-S-H phase and degrades the structure and strength of the hydrated phase [27]. It is further indicated that an increase in gypsum content increases the amount of C-S-H while reducing the intrinsic strength of C-S-H and reducing the mechanical properties of C-S-H and hydrated cement paste [28]. When the cement sulfate content is too low, the cement hydration mechanism reacts in an undersulfated manner, meaning

that C_3A main hydration peak to form monosulfate occurs before C_3S main heat of evolution peak resulting in lower, broader and delayed main hydration peak. This effect can be the result of high concentration of aluminum ions in solution, which retards alite hydration process. Generally, sulfate ions accelerate alite reaction while it decelerates C_3A hydration. In presence of adequate supply of sulfates, ettringite forms which leads to reduction of alumina ions in solution and the acceleration of C_3S hydration. Approximately 17% of the added gypsum can be absorbed in C-S-H crystal structure (affinity of C-S-H and gypsum). After depletion of sulfates in the matrix, C_3A starts absorbing sulfate ions embedded in C-S-H structure for further ettringite formation under proper pH and temperature conditions [29].

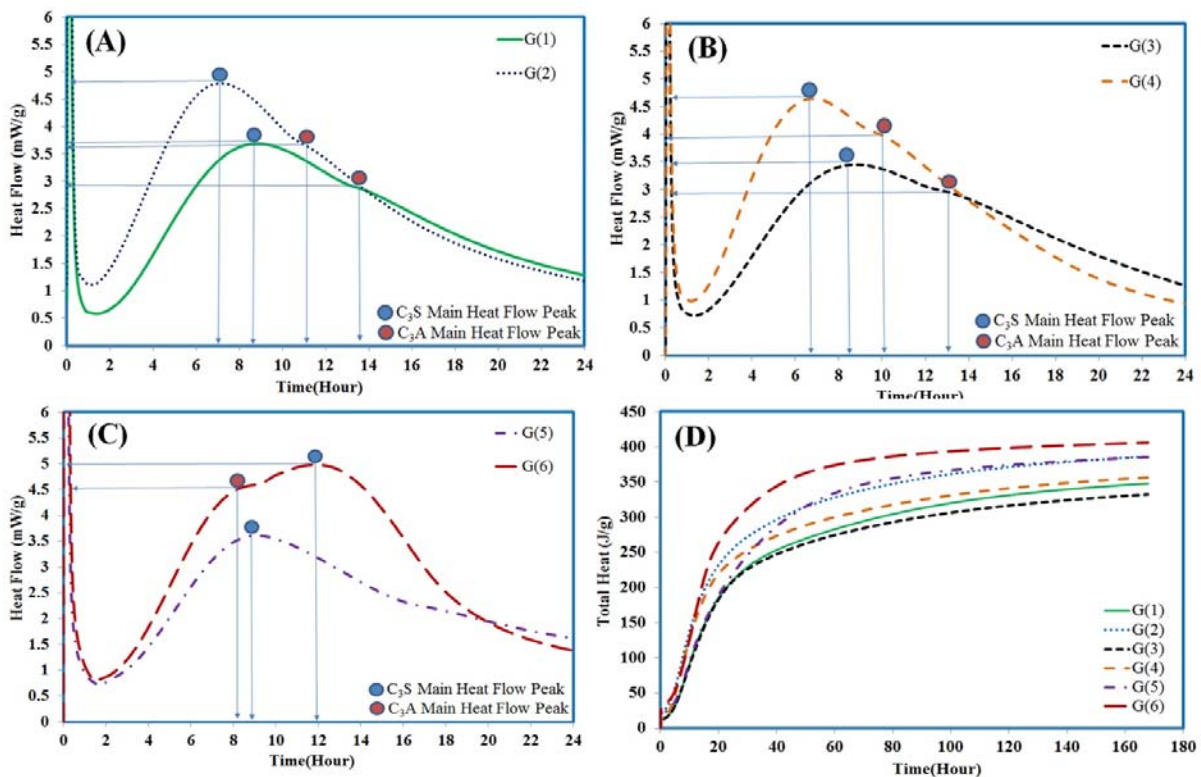
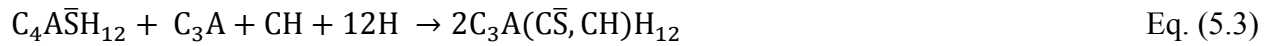


Figure 5.5 Heat and heat flow curves for cements G (1) through G (6)

Further experiments were conducted to understand the effect of C_3A and sulfate on the cracking potential of mortar samples. Calcium hydroxide (CH) content of G (1) through G (6)

hydrated paste was qualitatively measured using x-ray diffraction. In this regard, paste samples were prepared at w/c ratio of 0.5 and tested at hydration ages of 2, 4, 6, 9, 24 and 168 hours in triplicate runs. To stop the hydration, each sample (20 g) was immediately removed from the encapsulated container at the designated hydration age and was crushed for 10 min. to approx. 50-100 micron particles using mortar and pestle and then immersed in container of ethanol 200 proof 99.95% absolute for 24 hours to stop hydration. Before conducting x-ray diffraction experiments, each sample was removed from the ethanol container and was vacuum filtered with an ultrafine Durapore membrane filter (0.45 μ m mesh), and a Buchner funnel to extract the ethanol from the mix [30]. The filtered sample was then dried at 105 °C for approx. 2 hours until reaching constant mass. The dried sample was then ground using mortar and pestles for 30 min. to reach very fine particles (at least 95% less than 25 μ m for all samples). The samples were then mixed with 10% rutile (TiO₂) as an internal standard and analyzed using x-ray diffraction. The ratio of the area under the peak for CH, ($2\theta = 18^\circ$), and TiO₂, ($2\theta = 27.4^\circ$), were determined using HighScore Plus software. The (Ca (OH)₂/ TiO₂) ratio versus hydration age is plotted in Figure 5.6 for each sample. It appears that for G (1), G (3), G (5) cements, (Ca (OH)₂/TiO₂) increases with increase in hydration age without any significant change in pattern. On the other hand, (CH/TiO₂) increases for cements G (2) and G (4) in the initial 10h, then decreases until mid-20th hour followed by a gradual increase up to 7 days of hydration. This trend is a little different for G (6) cement since (CH/TiO₂) starts diminishing after 20 hours of hydration. It is speculated that the availability of sulfate ions plays critical role in the change of CH content of hydrated cement paste matrix. For cements G(1), G(3) and G(5), there is an ample supply of sulfate ions to adequately control the C₃A reaction and therefore aluminate phase hydration products mostly include ettringite and monosulfate (Please see Equations (5.1) and (5.2)). For G (2), G (4) and G (6) cements, the sulfate

ions are not readily available during the early stages of hydration. The sulfate content may be adequate in cements G (2) and G (4), since the main C₃A hydration peak occurs after alite main peak but the calcium sulfate particles may be larger than an optimized size to freely dissolve in hydration solution and supply adequate sulfate ions to react with C₃A and monosulfate in nucleation and growth stage of hydration. Cement C (6) is understood to be undersulfated since the aluminate peak occurs before the main alite peak. Lack of availability of sulfate ions or inadequate supply of sulfate ions in solution kicks another mechanism in which monosulfate and C₃A react with available CH to generate monosulfoaluminate solid solution (please see Equation (5.3)).



It is understood that an increase in cement fineness enhances the potential for cracking in concrete structural elements [31]. Also, when C₃A content of Portland cement exceeds 8%, higher sulfate content is required for proper control of C₃A hydration. Higher sulfate content in cements results in higher sulfate adsorption in the crystal structure of C-S-H (due to the affinity of C-S-H and sulfate ions [29]) and as a consequence chemically bond weakening reaction occurring in C-S-H crystal phase. In an undersulfated system, where C₃A main peak occurs before alite main peak, C₃A and monosulfate tend to react with calcium hydroxide and generate monosulfoaluminate solid solution when the sulfate source is depleted. This process additionally reduces the potential amount of ettringite that could otherwise be formed if the matrix was adequately supplied with sulfate source. Reduction of ettringite content reduces the strength that could potentially be contributed by ettringite phase during the initial stages of reaction and to the overall hydrated

cement paste strength. It is perceived that higher amount of C_3A and gypsum content play the primary role while cement fineness comes second to affect the cracking potential in structural concrete elements.

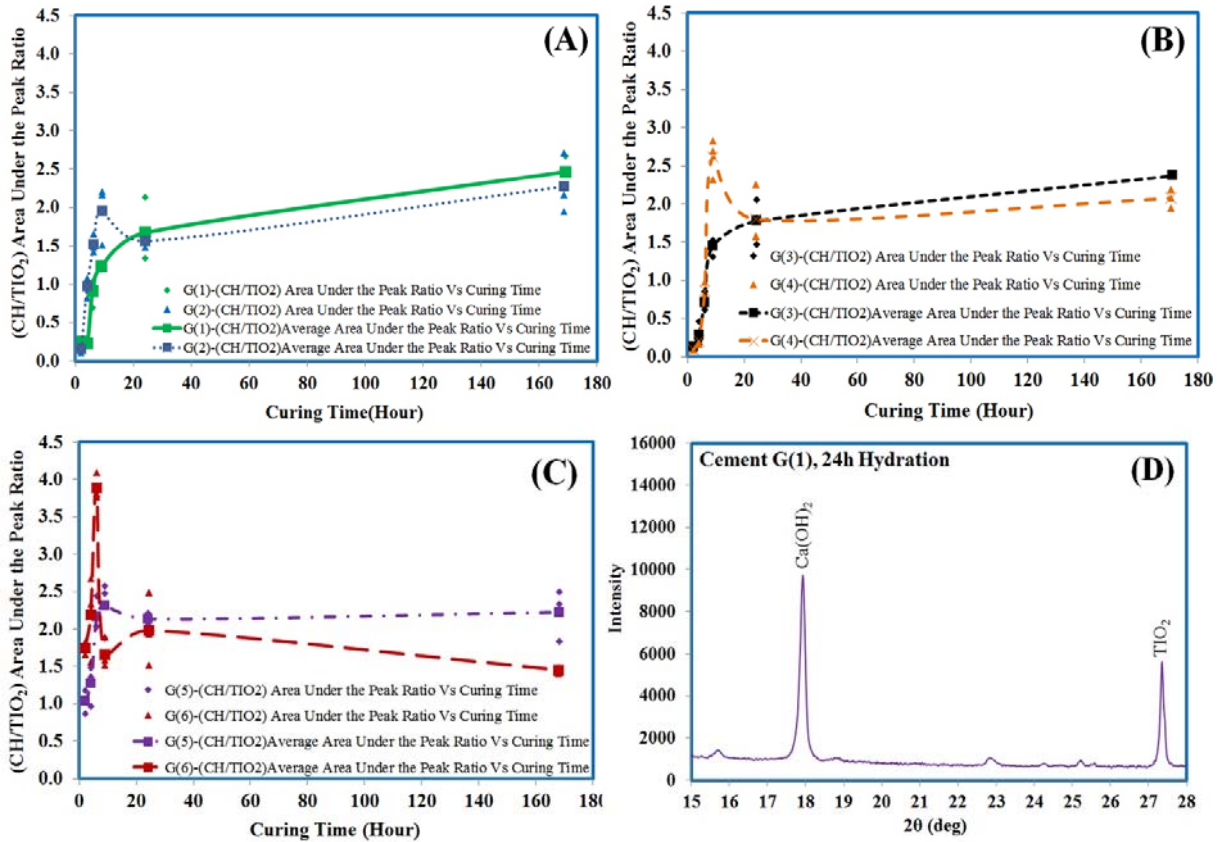


Figure 5.6 Calcium hydroxide determinations for cements G (1) through G (6)

It is understood that graphene with its extraordinary thermal conductivity can be used as a potential additive to concrete structures to reduce cracking in elements susceptible to high temperature gradients resulting from cement heat of hydration. It was well demonstrated in prior publication by the author of this paper [9] that implementation of graphene with cement improves the thermal diffusivity of the composite and as a result could potentially reduce thermal gradients in concrete elements. In the next section, the physical properties of graphene-cement composites,

including compressive strength of mortar, HOH and modulus of elasticity of paste composites will be investigated.

5.3.2 Investigation of Hydration Mechanism of Graphene Cement Paste

Graphene cement paste samples were prepared at 0, 1%, 5% and 10% graphene content as a partial replacement of cement G(6). G (6) cement was identified previously as the cement with the highest HOH and therefore with higher potential to induce thermal cracking in concrete elements. HOH of graphene cement paste samples was measured using TAMAIR isothermal conduction calorimetry at a water to binder ratio (hereon referred to (w/b)) of 0.5 and 0.6 conforming to ASTM C1702-09, internal mixing procedure [20]. The heat flow rate and the HOH curves are normalized relative to Portland cement content and are depicted in Figure 5.7.

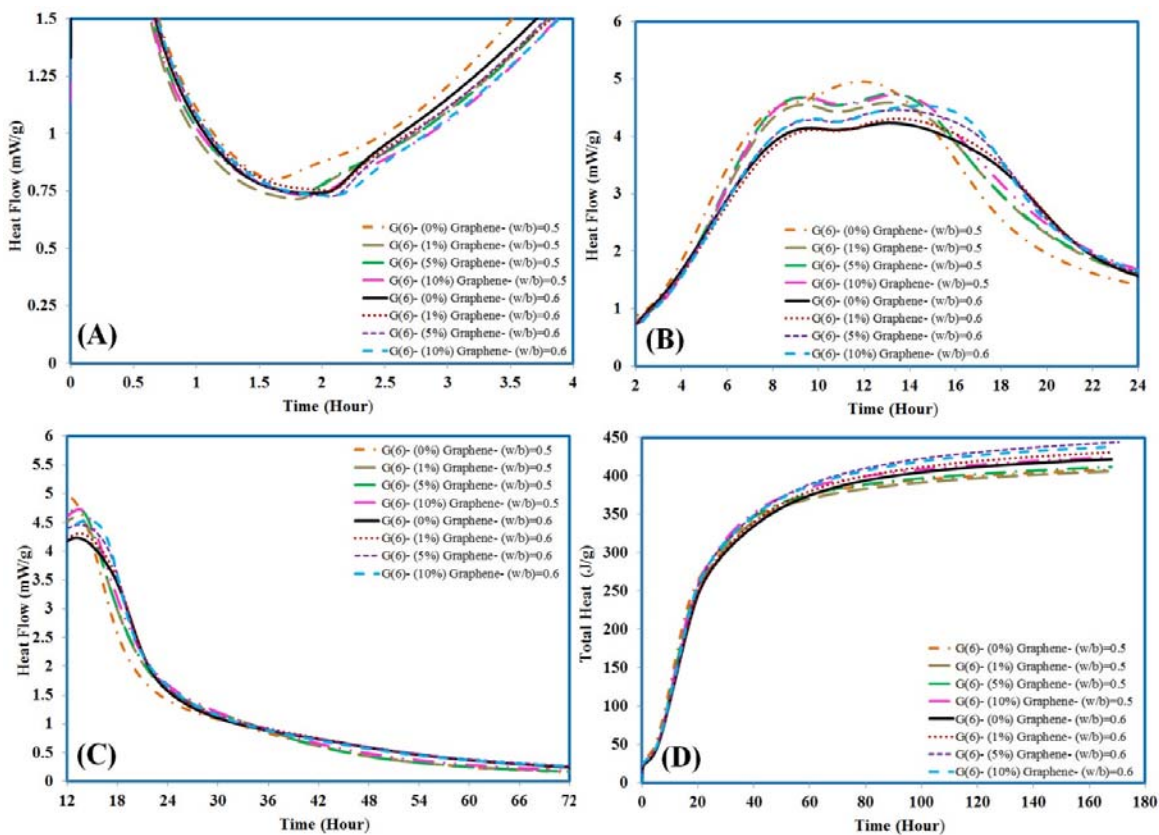


Figure 5.7 G (6) graphene cement heat flow and heat flow curves

As indicated in Figure 5.7 (A), an increase in (w/b) results in longer induction period and a longer time to achieve undersaturation state (as a result of hydration products precipitation) with respect to dissolving phases in the solution [32]. Samples without graphene at w/b =0.5 show the shortest induction period (1.5 h) while an increase in graphene content gradually increases the induction period (2.2 h for sample with 10% graphene at w/b =0.6). This phenomena can be explained by the fact that graphene nanoplatelets have much larger surface area (over 4,000 times larger than cement particles) compared to cement grains [3] and as a result may attract significant amount of water that could otherwise participate in cement hydration and faster calcium hydroxide (hereon referred to CH) saturation and C-S-H precipitation in solution. The literature indicates that for cement pastes, the concentration of calcium ions in solution increases, eventually up to 35 to 40 mmol at the end of the induction period, when precipitation of C-S-H and calcium hydroxide starts to occur [33, 34]. At w/b of 0.5 and in absence of graphene, the sample may reach the undersaturation state faster and C-S-H may precipitate in shorter period of time and as a result the acceleration period initiates earlier than the other samples. At w/b =0.6, adequate quantity of water is provided to wet the graphene nanoplatelets particles surface and at the same time regulates/balance the hydration of cement particles. Precipitation of CH until reaching the acceleration stage occurs at the same time for all the samples prepared at w/b =0.6 regardless of their graphene content. It appears that at lower w/b =0.5 an increase in graphene content increases the induction period and delays the onset of the rapid C-S-H growth while the effect is minimal at the higher w/b of 0.6.

At the end of the induction period, C-S-H and Portlandite are growing rapidly [35]. As can be seen in Figure 5.7 (B), the samples prepared at lower w/b =0.5 show higher rate of heat flow compared to pastes of higher w/b =0.6. It is perceived that at lower w/b less particle interspace is

available and therefore the solution saturates faster with respect to the reacting ions hence precipitation of more C-S-H and Portlandite occur thus promoting the formation of more active sites for the nucleation and growth of C-S-H, Portlandite and other hydration products. For the graphene-free paste at w/b =0.5, the main peak shows the highest heat flow and is approximately 15% higher than the paste prepared at a higher w/b ratio of 0.6. This finding is in agreement with Hu et al. [36]. It is noteworthy that sulfate depletion point occurs at around 9hr after initiation of hydration for all the samples regardless of their w/b or graphene content. This might be indicating that adjustments of the sulfate amount may not be necessary for samples prepared at varied quantities of graphene since graphene does not interfere with hydration mechanism of C₃A and sulfate source. Graphene nanoplatelets have large theoretical surface area (2,630 m²/g) [3] that attracts the available water to its surface and as a result hydration products/ions saturate faster in the solution triggering quicker C-S-H precipitation and shifting of the hydration mechanism toward nucleation of more C-S-H and CH [35]. Among the samples prepared at w/b =0.6, the sample with 10% graphene shows the highest magnitude for the main heat flow peak. It is speculated that fine graphene particles attract remarkable portion of water and hence the solution saturates faster and the mechanism progress toward precipitation of more C-S-H and CH and nucleation of more hydration products.

As the hydration mechanism reaches the deceleration period, (demonstrated in Figure 5.7 (C)) the samples prepared at w/b =0.6 and higher graphene contents (5% to 10% cement replacement) show higher heat flow rate relative to the others. Both graphene, as a filler substance, and a higher amount of water create more interparticle space for the formation/nucleation of hydration products after the samples reached the final set [36]. Additionally, at a higher w/b, more water is available for further progress of hydration. In the steady state stage of hydration, as

demonstrated in Figure 5.7 (C), samples prepared with 5 and 10% graphene content at w/b=0.5 show slightly lower heat flow compared to other samples. It is understood that the combination of low w/b and high graphene content may create denser composite which is more resistant to water diffusion mechanism and as a result lower heat flow can be observed in the heat flow curve.

Investigation of HOH curve (Figure 5.7 (D)) indicates that an increase in graphene content and w/b in the samples may result in an increase in the total HOH at three and seven days while all the samples show similar HOH at the first 24 hours. As indicated earlier, an increase in w/b and graphene content (as a filler) increases the interparticle spacing between cement particles which provides more space for further hydration of cement grains at later ages.

5.3.3 Investigation of Compressive Strength of Graphene Cement Mortars

The three day compressive strength of graphene-cement mortar samples, prepared with G (5) and G (6) cements was measured using ToniPRAX mortar compression tester. Each sample was prepared and tested in triplicate runs conforming to ASTM C109 [23] and ASTM C305 [24]. A total of twenty four specimens (8 samples x 3 runs) were prepared at two levels of low and high Blaine fineness (BF= 4,000 and 6,000 (cm²/g)), water to cement ratio (w/c = 0.5 and 0.6) and graphene content (0 and 10% as a partial replacement of Portland cement). Graphene content, cement Blaine finenesses and water to binder ratio are considered significant factors affecting the compressive strength of the mortar specimens [2]. The compressive strength results in addition to analysis of variance (ANOVA) using full factorial design method are outlined in Table 5.4.

Factorial design statistical method is most efficient for studies in which the effect of two or more factors are investigated. In this method, all possible combinations of different levels of the factors, in each complete replication or trial of experiments, are probed. The effect of the factor on the target is evaluated based on the change in response produced by the change in the level of

the factor. To determine the effect of the factor on the targeted response, the sum of squares of each factor and its combination in addition to the critical F distribution with 0.05 error (95% confidence limit) and the corresponding P-value are determined. P-value is defined as the smallest level of significance that would result in rejection of the null hypothesis. P-value of less than or equal to 0.05 indicates the evident effect of the corresponding factor on the targeted response. Smaller P-value indicates the more significant effect of the factor on the targeted response [37].

Table 5.4 Analysis of variance for compressive strength of graphene-cement mortars based on three factor model, full factorial design and analysis

(W/C) ratio	<u>Graphene content as partial replacement of cement (%)</u>				Yi...
	<u>0 (%)</u>		<u>10 (%)</u>		
	<u>Blaine Fineness (cm²/g)</u>		<u>Blaine Fineness (cm²/g)</u>		
	<u>G (5) = 4,000</u>	<u>G (6) = 6,000</u>	<u>G (5) = 4,000</u>	<u>G (6) = 6,000</u>	
(0.5)	4,770	6,140	4,720	3,260	<u>56,780</u>
	4,500	6,130	4,950	3,320	
	4,850	6,260	4,600	3,280	
(0.6)	4,400	4,880	3,830	4,490	<u>52,000</u>
	4,650	4,570	3,500	4,400	
	4,700	4,450	3,620	4,530	
Y.jk.	<u>27,870</u>	<u>32,410</u>	<u>25,230</u>	<u>23,270</u>	
Y.j..	60,280		48,500		

Compressive strength is rounded up to 10 (psi) Y.... = 108,780

(w/c) ratio	Yij..		Yi.k.	
	Graphene content = (0%)	Graphene content = (10%)	Fineness = 4,000 (cm ² /g)	Fineness = 6,000 (cm ² /g)
0.5	32,650	24,130	28,400	28,400
0.6	27,640	24,370	24,700	27,310

As indicated in Table 5.4, in absence of graphene, increasing w/b from (0.5) to (0.6) results in 33% reduction in the average compressive strength of samples containing G (6) cement (BF= 6,000 cm²/g) compared to 2% reduction for samples of G (5) cement (BF= 4,000 cm²/g). To justify this trend, several factors need to be brought into consideration. The compressive strength of

mortar is mainly controlled by the packing density of C-S-H, (hydration product of C_3S and C_2S), and capillary porosity. Capillary pores formation is the direct result of w/b and filler materials that do not participate in chemical reaction of cementitious materials. The degree of hydration of Portland cement is contingent upon several factors including water to cement ratio w/c, curing temperature, and cement fineness. Bullard et al. [38] indicated that at w/c = 0.4 or less, the capillary porosity in cement paste depercolates before full hydration can be achieved.

Colak [39] noted that optimum quantity of water is required to have optimum compressive strength in concrete. It is understood that in absence of graphene at w/b = 0.5 sufficient water is provided for hydration of cement particles in samples prepared with G (5) cement. Increasing w/b to 0.6 does not show any significant effect on compressive strength and as a result capillary porosity in the sample. On the other hand, in absence of graphene at w/b = 0.5, the available water for the samples prepared with G (6) cement is nearly optimized to provide hydration and adequate workability in the samples while at the same time maintaining the capillary porosity to the minimum level which results in higher C-S-H packing density and higher compressive strength (average compressive strength of 6,180 psi). Increasing w/b to 0.6 results in increase of capillary porosity and reduction of compressive strength by 33%.

For G (5) cement at w/b =0.5, 10% replacement of cement with graphene did not show any significant change in the compressive strength of mortar specimens. As it was indicated in the previous section, graphene does not show any chemical interaction with cement and water. It is anticipated that some portion of the water was consumed to wet the very fine graphene nanoplatelet particles surface. Although incorporation of graphene may reduce the quantity of cement per unit volume of the cube, there is no evidence of reduction in the compressive strength of the mortar cubes. It is speculated that at w/b =0.5, sufficient quantity of water is provided to wet the

nanoplatelet particles and at the same time hydrating cement particles while avoiding self-desiccation of mortar sample with adequate space available for the hydration products. As a result, graphene nanoplatelets may reduce the interparticle spacing between hydrating cement particles capillary pores which makes up for the compressive strength that might be diminished otherwise due to the reduction of cement per unit volume. For G (5) cement at 10% graphene content, increasing w/b from 0.5 to 0.6 results in formation of larger capillary pores and a subsequent 30% reduction in the compressive strength.

For G (6) cement at w/b =0.5, 10% replacement of cement with graphene results in 47% reduction of the average compressive strength of the mortar cubes. This phenomenon can be due to inadequacy of water to wet the nanoplatelet particles and hydration of cement grains. Deficient hydration of cement particles result in formation of less amount of C-S-H and as a consequence lower compressive strength of mortar cubes. For G (6) cement at w/b =0.6, 10% replacement of cement with graphene does not show remarkable impact on compressive strength. It is understood that for G (6) cement at w/b =0.6, sufficient quantity of water is provided to wet graphene nanoplatelet particles while properly hydrating cement particles. 10% graphene nanoplatelets may reduce the interparticle spacing which makes up for the compressive strength that might be otherwise diminished due to reduction of cement per unit volume of cubes. The same trend was observed in the compressive strength of mortar cubes prepared with G (5) cement at w/b = 0.5 when graphene nanoplatelets of up to 10% was added to the composite mortar.

In summary, ANOVA statistical analysis of the compressive strength of mortar cubes at variable cement Blaine fineness, w/c and graphene content is outlined in Table 5.5.

Based on the full factorial design results, calculated using Equations (5.4) through (5.13) and provided in Table 5.5, it appears that all the factors constituting the sources of variation have

a P-value less than 0.05 which identifies their significance on the seven day compressive strength of the composite samples. It is noteworthy that the quantity of graphene (P-value=26.19561E-12) and also the combined effect of w/c, graphene content and fineness (P-value=1E-10) with the results in the lowest P-values; they are the therefore the most significant factors affecting the seven day compressive strength of graphene-cement mortar composites. It can therefore be concluded that where graphene is used as a partial replacement of cement, w/c and fineness of cement should be carefully considered to gain optimum compressive strength.

Table 5.5 Analysis of variance for compressive strength of graphene cement mortar cubes

Source of Variation	Sum of Squares	Degrees of Freedom	Mean Square	F ₀	F _{critical}	P-value
(w/c)	948,830	1	948,830	43	4.49	71E-7
graphene	5,789,870	1	5,789,870	259	4.49	26.19561E-12
fineness	279,070	1	279,070	13	4.49	27.478E-4
((w/c), (graphene))	1,147,560	1	1,147,560	51	4.49	22E-7
((w/c), fineness)	286,890	1	286,890	13	4.49	24.766E-4
(graphene, fineness)	1,758,250	1	1,758,250	79	4.49	1E-7
((w/c), graphene, fineness)	5,181,960	1	5,181,960	232	4.49	1E-10
Error	357,160	16	22,320			
Total	15,749,610	23	684,770			

SS= Sum of Squares

SS_T = Sum of Squares of Total

[a=2; b=2; c=2; n=3]

$$SS_T = \sum_{i=1}^a \sum_{j=1}^b \sum_{k=1}^c \sum_{l=1}^n y_{ijkl}^2 - \frac{y_{...}^2}{abcn} \quad SS_T = 15,749,610 \quad \text{Eq. (5.4)}$$

$$SS_{\left(\frac{w}{c}\right)} = \frac{1}{bcn} \sum_{i=1}^a y_{i...}^2 - \frac{y_{...}^2}{abcn} \quad SS(w/c) = 948,830 \quad \text{Eq. (5.5)}$$

$$SS_{\text{(graphene)}} = \frac{1}{acn} \sum_{j=1}^b y_{.j..}^2 - \frac{y_{...}^2}{abcn} \quad SS(\text{graphene}) = 5,789,870 \quad \text{Eq. (5.6)}$$

$$SS_{\text{(fineness)}} = \frac{1}{abn} \sum_{k=1}^c y_{..k.}^2 - \frac{y_{...}^2}{abcn} \quad SS(\text{fineness}) = 279,070 \quad \text{Eq. (5.7)}$$

$$SS_{\left(\left(\frac{w}{c}\right), \text{graphene}\right)} = \frac{1}{cn} \sum_{i=1}^a \sum_{j=1}^b y_{ij..}^2 - \frac{y_{...}^2}{abcn} - SS_A - SS_B$$

$$SS((w/c), \text{graphene}) = 1,147,560 \quad \text{Eq. (5.8)}$$

$$SS\left(\left(\frac{w}{c}\right), \text{ fineness}\right) = \frac{1}{bn} \sum_{i=1}^a \sum_{k=1}^c y_{i.k}^2 - \frac{y_{\dots}^2}{abcn} - SS_A - SS_C$$

$$SS((w/c), \text{ fineness}) = 286,890 \quad \text{Eq. (5.9)}$$

$$SS_{(\text{graphene}, \text{ fineness})} = \frac{1}{an} \sum_{j=1}^b \sum_{k=1}^c y_{.jk}^2 - \frac{y_{\dots}^2}{abcn} - SS_B - SS_C$$

$$SS(\text{graphene}, \text{ fineness}): 1,758,250 \quad \text{Eq. (5.10)}$$

$$SS\left(\left(\frac{w}{c}\right), \text{ graphene}, \text{ fineness}\right) = \frac{1}{n} \sum_{i=1}^a \sum_{j=1}^b \sum_{k=1}^c y_{ijk}^2 - \frac{y_{\dots}^2}{abcn} - SS_A - SS_B - SS_C - SS_{AB} -$$

$$SS_{AC} - SS_{BC} \quad SS((w/c), \text{ graphene}, \text{ fineness}): 5,181,960 \quad \text{Eq. (5.11)}$$

$$SS_{\text{Subtotal}}\left(\left(\frac{w}{c}\right), \text{ graphene}, \text{ fineness}\right) = \frac{1}{n} \sum_{i=1}^a \sum_{j=1}^b \sum_{k=1}^c y_{ijk}^2 - \frac{y_{\dots}^2}{abcn}$$

$$SS(\text{subtotal}((w/c), \text{ graphene}, \text{ fineness})): 15,392,450 \quad \text{Eq. (5.12)}$$

$$SS_E = SS_T - SS_{\text{Subtotal}}\left(\left(\frac{w}{c}\right), \text{ graphene}, \text{ fineness}\right) \quad SS(\text{error}): 357,160 \quad \text{Eq. (5.13)}$$

5.3.4 Determination of Hardness and Young's Modulus of Graphene Cement Samples

Hardness and Young's modulus of graphene cement (G (6)) paste were determined using Hysitron Ti900 Triboindenter, based on Oliver and Pharr indentation method and using Berkovich tip with a radius of 150 nm [40]. Graphene cement paste samples were prepared at (w/c) of 0.5 and graphene content of 0, 1%, 5%, 10% hydrated for 44 hours. The hydration process was stopped by grinding the hydrated samples at 44h ±0.5h and mixing with 99.95% ethanol 200 proof. Air and tip area function calibrations for Triboindenter were performed using a standard fused quartz. Implemented indentation parameters are indicated in Izadi et al. [41]. A trapezoidal loading profile with loading, hold and unloading times of 3, 2 and 3 (s), respectively, was used to perform nanoindentation with four different peak loads of 2.5, 5, 7.5 and 10 (mN). At least 30 different indents were performed at each load for each sample. A minimum of 25 μm was maintained to prevent any kind of interaction or mutual effect between adjacent indents. Considering the

indentation size effect and collected nanoindentation results [42], it was decided to use only the data from 7.5 and 10 mN peak loads in Table 5.6 which corresponds to relatively higher penetration depths. Samples thicknesses were in the scale of few millimeters which ensures that the maximum penetration depth does not exceed the 1/10 of total thickness and will not affect the final results [43]. Surface roughness was measured using DI AFM with a scan size of $3\ \mu\text{m} \times 3\ \mu\text{m}$, which is larger than the largest indentation mark at the highest load. The scan rate was adjusted at 1 Hz with a tip velocity of $6\ \mu\text{m/s}$ covering 512 data points per line of scan. It was determined that the roughness for all the samples falls in the range of 34-44 nm as demonstrated in Figure 5.8. Considering roughness to penetration depth ratio of less than 6% for all the samples studied here, it can be assumed that smooth surfaces were used for nanoindentation measurements purposes. The average Young's modulus (E_r), hardness (H) and maximum penetration depth (h_{max}) of the indenter tip along with arithmetic surface roughness (R_a) of samples are reported in Figure 5.9. It appears that addition of 1% graphene results in 21% reduction of Young's modulus. Increasing graphene from 1% to 5% does not show significant effect on Young's modulus; however, increasing replacement levels to 10% increased the modulus by 4-5%. The same trend can be observed in the hardness of graphene cement paste samples.

5.4 Conclusions

Restrained shrinkage data indicates that mortar specimens prepared with cements of varied phase composition and finenesses indicate that interaction of C_3A and sulfate source is the prime phenomenon followed by cement fineness as the second main factor influencing concrete cracking potential. Determination of thermal diffusivity of graphene cement paste indicates that samples prepared with graphene (up to 10% by weight) as a partial replacement of cement showed more than 70% improvement in thermal diffusivity. Improved thermal diffusivity results in better heat

dissipation and therefore potentially a reduction in the temperature gradient in concrete elements with consequences of lowering the potential of thermal cracking in mass concrete elements. Measurements of HOH of graphene cement paste, at w/c=0.5, using isothermal conduction calorimetry, indicates that incorporation of graphene up to 10% by weight increases the length of the induction period while reduces the intensity of the main hydration peak due to the filler effect of graphene particles in graphene-cement paste. Furthermore, increasing w/c from 0.5 to 0.6 and graphene content up to 10% (as a partial replacement of cement) increases the seven-day HOH of portland cement by up to 50 (J/g) in isothermal condition. Isothermal conduction calorimetry heat flow curves show that incorporation of graphene up to 10% does not have significant impact on the interaction of C₃A and the sulfate source since the time of occurrence of the sulfate depletion peak did not show significant variation in the samples prepared with varied graphene contents.

Full factorial statistical analysis conducted on the compressive strength of mortar prepared at two different w/c ratios, 2 levels of cement finenesses and variable graphene content indicates that 1- quantity of graphene and 2- physical interaction of w/c, graphene and cement fineness, have the smallest P-Value among all the samples, representing the most significant factors on mortar compressive strength. It appears that in graphene-cement paste composites, addition of 1% graphene results in 21% reduction of Young's modulus. Increasing graphene content from 1% to 5% and 10% does not show significant effect on Young's modulus. Same trend can be observed in the hardness of graphene cement paste samples. A lower elastic modulus can result in lowering the cracking potential of massive concrete elements subjected to a degree of restraint during early age deformation.

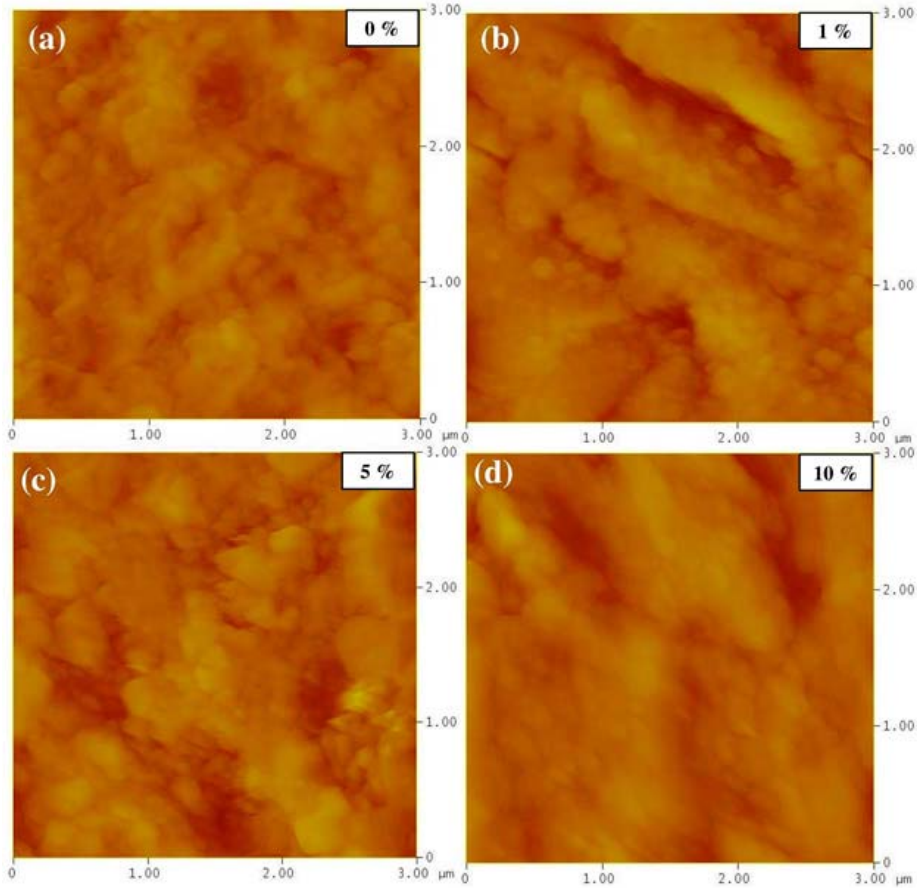


Figure 5.8 Surface roughness of G (6) graphene cement

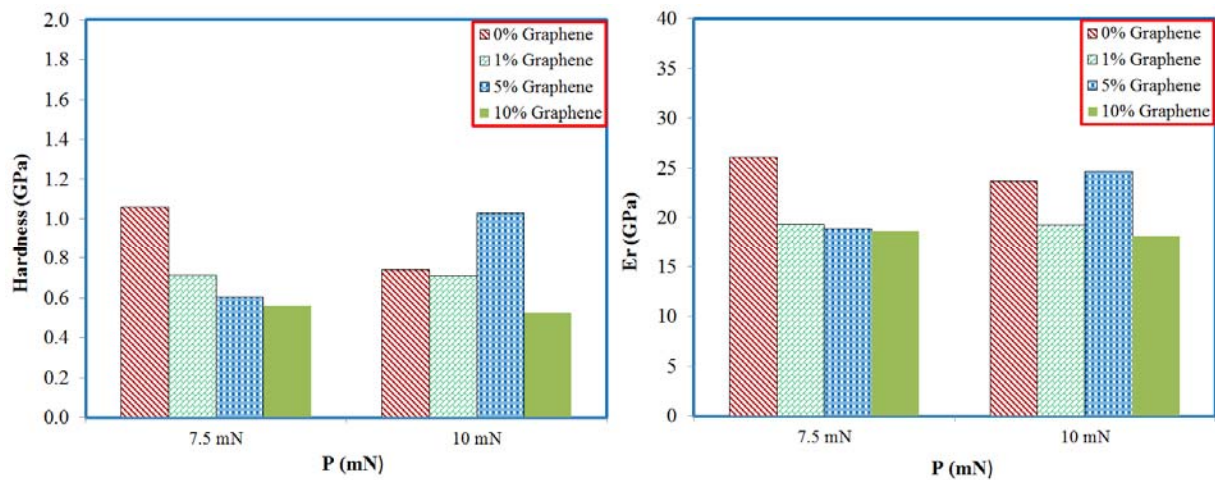


Figure 5.9 G (6) graphene-cement hardness and Young modulus for different quantities of graphene

5.5 References

- [1] Mindess, Sidney, J. Francis Young, and David Darwin. *Concrete*. (2003).
- [2] Odler, Ivan. "Hydration, setting and hardening of Portland cement." *Lea's Chemistry of Cement and Concrete* 4 (1998): 241-297.
- [3] Wei, Weili, and Xiaogang Qu. "Extraordinary physical properties of functionalized graphene." *Small* 8.14 (2012): 2138-2151.
- [4] Zayed, A., Ahmadreza Sedaghat, and Paul Sandberg. "Measurement and prediction of heat of hydration of portland cement using isothermal conduction calorimetry." *Journal of Testing and Evaluation* 41.6 (2013): 1-8.
- [5] Sedaghat, Ahmadreza, Natallia Shanahan, and A. Zayed. "Predicting One-Day, Three-Day, and Seven-Day Heat of Hydration of Portland Cement." *Journal of Materials in Civil Engineering* 27.9 (2014): 04014257.
- [6] Alkhateb, Hunain, et al. "Materials genome for graphene-cement nanocomposites." *Journal of Nanomechanics and Micromechanics* 3.3 (2013): 67-77.
- [7] Makar, J. M., J. C. Margeson, and Jeanne Luh. "Carbon nanotube/cement composites-early results and potential applications." (2005): 1-10.
- [8] Du, Hong Jian, and Sze Dai Pang. "Transport of Water and Chloride Ion in Cement Composites Modified with Graphene Nanoplatelet." *Specialized Collections*. Vol. 3. Trans Tech Publications, (2015).
- [9] Sedaghat, Ahmadreza, et al. "Investigation of physical properties of graphene-cement composite for structural applications." *Open Journal of Composite Materials* (2014).
- [10] Konsta-Gdoutos, Maria S., Zoi S. Metaxa, and Surendra P. Shah. "Multi-scale mechanical and fracture characteristics and early-age strain capacity of high performance carbon nanotube/cement nanocomposites." *Cement and Concrete Composites* 32.2 (2010): 110-115.
- [11] Siddique, Rafat, and Ankur Mehta. "Effect of carbon nanotubes on properties of cement mortars." *Construction and Building Materials* 50 (2014): 116-129.
- [12] Chaipanich, Arnon, et al. "Compressive strength and microstructure of carbon nanotubes-fly ash cement composites." *Materials Science and Engineering: A* 527.4 (2010): 1063-1067.
- [13] Lv, Shenghua, et al. "Effect of graphene oxide nanosheets of microstructure and mechanical properties of cement composites." *Construction and Building Materials* 49 (2013): 121-127.

- [14] Gong, Kai, et al. "Reinforcing effects of graphene oxide on portland cement paste." *Journal of Materials in Civil Engineering* 27.2 (2014): A4014010.
- [15] Le, Jia-Liang, Hongjian Du, and Sze Dai Pang. "Use of 2D Graphene Nanoplatelets (GNP) in cement composites for structural health evaluation." *Composites Part B: Engineering* 67 (2014): 555-563.
- [16] Chuah, Samuel, et al. "Nano reinforced cement and concrete composites and new perspective from graphene oxide." *Construction and Building Materials* 73 (2014): 113-124.
- [17] ASTM C204-07. Standard test methods for fineness of hydraulic cement by air-permeability apparatus. ASTM International, West Conshohocken, PA (2010).
- [18] Horiba Instruments Incorporated. Laser Scattering Particle Size Distribution Analyzer LA 950 Instruction Manual. <www.horibalab.com> (accessed 07/04/ 2015).
- [19] Horiba Scientific. A guidebook to particle size analysis. <http://www.horiba.com/fileadmin/uploads/Scientific/Documents/PSA/PSA_Guidebook.pdf> (accessed 07/04/ 2015).
- [20] ASTM C1702-09a. Standard test method for measurement of heat of hydration of hydraulic cementitious materials using isothermal conduction calorimetry. ASTM International, West Conshohocken, PA, USA (2010).
- [21] Mindess, Sidney, J. Francis Young, and David Darwin. *Concrete*. (2003).
- [22] ASTM C1581-09a. Standard test method for determining age at cracking and induced tensile stress characteristics of mortar and concrete under restrained shrinkage. ASTM International, West Conshohocken, PA (2012).
- [23] ASTM C109/C109M-13. Standard test method for compressive strength of hydraulic cement mortars (Using 2-in. Cube Specimens). ASTM International, West Conshohocken, PA (2013).
- [24] ASTM C305-14. Standard practice for mechanical mixing of hydraulic cement pastes and mortars of plastic consistency. ASTM International, West Conshohocken, PA (2014).
- [25] Black, Leon, et al. "Hydration of tricalcium aluminate (C_3A) in the presence and absence of gypsum-studied by Raman spectroscopy and X-ray diffraction." *Journal of Materials Chemistry* 16.13 (2006): 1263-1272.
- [26] Merlini, Marco, et al. "Tricalcium aluminate hydration in additivated systems. A crystallographic study by SR-XRPD." *Cement and Concrete Research* 38.4 (2008): 477-486.

- [27] Santhanam, Manu, Menashi D. Cohen, and Jan Olek. "Sulfate attack research-whither now?" *Cement and Concrete Research* 31.6 (2001): 845-851.
- [28] Bentur, A. "Effect of gypsum on the hydration and strength of C3S pastes." *Journal of the American Ceramic Society* 59.5-6 (1976): 210-213.
- [29] Quennoz, Alexandra, and Karen L. Scrivener. "Interactions between alite and C₃A-gypsum hydrations in model cements." *Cement and Concrete Research* 44 (2013): 46-54.
- [30] Stutzman, Paul E. *Guide for X-ray powder diffraction analysis of Portland cement and clinker*. US Department of Commerce, Technology Administration, National Institute of Standards and Technology, Office of Applied Economics, Building and Fire Research Laboratory, (1996).
- [31] Zayed, A, et al. "Effects of portland cement particle size on heat of hydration." (2014).
- [32] Juilland, Patrick, et al. "Dissolution theory applied to the induction period in alite hydration." *Cement and Concrete Research* 40.6 (2010): 831-844.
- [33] Brown, Paul Wencil, et al. "Analyses of the aqueous phase during early C₃S hydration." *Cement and Concrete Research* 14.2 (1984): 257-262.
- [34] Young, J. F., H. S. Tong, and R. L. Berger. "Compositions of solutions in contact with hydrating tricalcium silicate pastes." *Journal of the American Ceramic Society* 60.5-6 (1977): 193-198.
- [35] Scrivener, Karen L., Patrick Juilland, and Paulo JM Monteiro. "Advances in understanding hydration of Portland cement." *Cement and Concrete Research* 78 (2015): 38-56.
- [36] Hu, Jiong, Zhi Ge, and Kejin Wang. "Influence of cement fineness and water-to-cement ratio on mortar early-age heat of hydration and set times." *Construction and Building Materials* 50 (2014): 657-663.
- [37] Montgomery, Douglas C. *Design and analysis of experiments*. John Wiley & Sons, (2008).
- [38] Bullard, Jeffrey W., and Edward J. Garboczi. "A model investigation of the influence of particle shape on portland cement hydration." *Cement and Concrete Research* 36.6 (2006): 1007-1015.
- [39] Çolak, Adnan. "A new model for the estimation of compressive strength of Portland cement concrete." *Cement and Concrete Research* 36.7 (2006): 1409-1413.
- [40] Oliver, Warren Carl, and George Mathews Pharr. "An improved technique for determining hardness and elastic modulus using load and displacement sensing indentation experiments." *Journal of Materials Research* 7.06 (1992): 1564-1583.

- [41] Izadi, Sina, Hesham Mraied, and Wenjun Cai. "Tribological and mechanical behavior of nanostructured Al/Ti multilayers." *Surface and Coatings Technology* 275 (2015): 374-383.
- [42] Milman, Yu V., A. A. Golubenko, and S. N. Dub. "Indentation size effect in nanohardness." *Acta Materialia* 59.20 (2011): 7480-7487.
- [43] Saha, Ranjana, and William D. Nix. "Effects of the substrate on the determination of thin film mechanical properties by nanoindentation." *Acta Materialia* 50.1 (2002): 23-38.

CHAPTER 6: CONCLUSIONS AND RECOMMENDATIONS

A careful study on the heat of hydration of Portland cement using isothermal conduction calorimetry indicates that the total heat generated at seven days can be predicted based on heat measurements for only 84 hours and using an S-curve function, with acceptable accuracy when compared to the heat measured using isothermal conduction calorimetry (ASTM C1702). The author suggest that a wider sample matrix (larger sample size) be examined to validate the proposed function as an alternative method of predicting the HOH of Portland cement at seven days. It is also suggested that the proposed function be examined for its suitability in predicting the 28 day HOH of Portland cement.

Equations predicting one, three and seven day heat of hydration of Portland cement can be established based on the Portland cement major phases of C_3S , C_3A , C_2S , C_4AF and cement mean particle size. Heat of hydration of Portland cement at one, three and seven days of hydration is a linear function of cement mean particle size when the composition is maintained constant at constant isothermal temperature of 23 °C and water to cement ratio of 0.5. The proposed equations can be used to identify Portland cements with the potential to cause thermal cracking in mass concrete elements. Also, the equations can be used to correlate the heat of hydration with other properties of Portland cement for quality control and prediction of physical and chemical properties of manufactured Portland cement and concrete.

Incorporation of graphene nanoparticles in cement pastes result in increasing thermal diffusivity and electrical conductivity; both properties increased with increasing graphene content in the composite mixture. The increase in thermal diffusivity of the hydrated graphene cement

composite is a clear indication of the heat sink capacity of graphene. This effect is of significant importance especially during the exothermic reactions taking place during the initial stages of hydration of Portland cement.

Measurements of heat of hydration of graphene cement paste, at $w/c = 0.5$, using isothermal conduction calorimetry, indicates that incorporation of graphene up to 10% by weight increases the length of the induction period and reduces the intensity of the main hydration peak, due to filler effect of graphene particles in graphene-cement paste. Furthermore, increasing w/c from 0.5 to 0.6 and graphene content up to 10% (as a partial replacement of cement) increases the seven day heat of hydration of Portland cement by up to 50 J/g. Isothermal conduction calorimetry heat flow curves show that incorporation of graphene up to 10% does not have significant impact on interaction of C_3A and sulfate source since the time of occurrence of the sulfate depletion peak is not significantly affected in the samples prepared with varied graphene contents. Full factorial statistical design, conducted on compressive strength of mortar samples prepared at varied (w/c), cement finenesses and graphene amounts, indicates that 1- quantity of graphene and 2- physical interaction of w/c , graphene and cement fineness, have the smallest P-value among all the samples, indicating their significance on blended mortar compressive strength.

Modulus measurements on graphene-cement paste composites indicate that an addition of 1% graphene results in 21% reduction in the composite Young's modulus. Increasing graphene content from 1% to 5% and 10% does not show significant effect on Young's modulus. Similar trends can be observed in the hardness values of the graphene-cement paste samples. The findings of this study indicate that graphene is potentially a beneficial blending material that can be used in a cementitious matrix to improve the thermal conductivity and diffusivity of concrete elements. It should be further explored for use in massive elements susceptible to early- age thermal cracking.

APPENDICES

Appendix A Copyright Permissions

The following are Copyright permissions for use of materials in Chapters 2, 3, and 4, respectively.

7/23/2015

University of South Florida Mail - USF Libraries - Notification



Ahmadreza Sedaghat <asedagha@mail.usf.edu>

USF Libraries - Notification

1 message

libraries@usf.edu <libraries@usf.edu>
To: asedagha@mail.usf.edu

Wed, Jul 15, 2015 at 10:30 AM

----- REPLY ABOVE THIS LINE -----

The following response has been posted for question number #2573.

Hello,

Authors of ASTM International journals are able to use their paper in full or in part in their dissertations provided that they reference the published article and the dissertation will not be used for any financial gain. A copy of the ASTM author copyright agreement is attached and linked on our guide. <http://guides.lib.usf.edu/c.php?g=6191&p=28103>.

You should include in your dissertation 1.) the author copyright agreement in an appendix and 2.) a note to the reader at the beginning of the chapter where you use the previously published material that includes a full citation and copyright statement. In APA format it would look like this:

Note. From "Title of the article," by W. Jones and R. Smith, 2007, Journal Title, 21, p. 122. Copyright 2007 by Copyright Holder. Reprinted with permission.

Please let me know if you have any further questions.

Best,
LeEtta Schmidt
lschmidt@usf.edu
813-974-1627

Your original question:

I published a paper in ASTM Journal of Testing and Evaluation in 2013. I need to incorporate this paper in my PhD dissertation. I need to know the copywrite requirements on this journal.

Thanks

By submitting email messages to Knowledge Tracker, you agree to the [Privacy Policy and Terms of Use](#).

To check the status of your question or to view the transcript, go to https://client.knowledgetrackerlib.com/p_home.php?library=usf

----- SYSTEM INFORMATION - DO NOT DELETE -----

<https://mail.google.com/mail/u/0/?ui=2&ik=efc20fa1fo&view=pt&q=ASTM&q=ASTM&qs=true&search=query&th=14e62201da680113&siml=14e62201da680113>

1/2



Title: Predicting One-Day, Three-Day, and Seven-Day Heat of Hydration of Portland Cement

Author: Ahmadreza Sedaghat, Natallia Shanahan, A. Zayed

Publication: Journal of Materials in Civil Engineering

Publisher: American Society of Civil Engineers

Date: 12/08/2014

Copyright © 2014, ASCE. All rights reserved.

[LOGIN](#)

If you're a [copyright.com](#) user, you can login to RightsLink using your [copyright.com](#) credentials. Already a [RightsLink](#) user or want to [learn more?](#)

Permissions Request

As an ASCE author, you are permitted to reuse you own content for another ASCE or non-ASCE publication.

Please add the full credit line "With permission from ASCE" to your source citation. Please print this page for your records.

Type of use: Dissertation/Thesis

Portion: full article

Format: electronic

Use of this content will make up more than 25% of the new work: no

Author of this ASCE work or ASCE will publish the new work: yes

[BACK](#)[CLOSE WINDOW](#)



Ahmadreza Sedaghat <asedagha@mail.usf.edu>

Copyright permissions

Burke, Merilyn <msburke@usf.edu>
 To: "Sedaghat, Ahmadreza" <asedagha@mail.usf.edu>

Tue, Oct 29, 2013 at 9:28 AM

According to the webpage, your article would have been assigned a creative commons license: I think the yellow highlighted parts gives you the information you need..

supports OASPA's [Statment on open Access](#).

How Open is SCIRP on the "Open Access Spectrum"?

SCIRP supports the [Budapest Open Access Initiative](#) and shows its "openness" clearly in the standardized form on the [Open Access Spectrum](#).

Open Access embraces 6 core components related to: 1.) Reader Rights, 2.) Reuse Rights, 3.) Copyrights, 4.) Author Posting Rights, 5.) Automatic Posting, 6.) Machine Readability.

SCIRP tries to be as open as practically possible on all 6 Open Access components:

1.) SCIRP is fully open on Reader Rights.
 2.) Starting with 1st April 2013 SCIRP is fully open on Reuse Rights by granting a [Creative Commons](#) license Attribution ([CC BY](#)). As such all SCIRP journals have qualify for the [SPARC Europe Seal](#) for Open Access Journals. For authors who want to be more protective SCIRP offers only on special request the Creative Commons license Attribution-NonCommercial ([CC BY-NC](#)) as an alternative. Also this license fulfills OASPA Standards on Reuse Rights. Original copyright and reuse rights are indicated on the paper depending on the author-selected CC license as: "Copyright © 2013 by author(s) and Scientific Research Publishing

Inc." together with icon  or 

3.) SCIRP asks authors to grant SCIRP a nonexclusive copyright. In this way authors continue to hold copyright with no restrictions. This makes SCIRP a fully open publisher also in this component.

4.) Only the authors hold copyright for their manuscripts before peer-review ("preprints") and after peer-review ("postprints"). For this reason authors are allowed to post their raw manuscripts on any repository or website. SCIRP does not ask authors to waive this right. Once the manuscript is accepted for publication (after peer-review) authors grant SCIRP a nonexclusive copyright (see 3.). Based on this copyright SCIRP produces the final paper in SCIRP's layout. This version is given to the public (and hence also back to the authors) under the Creative Commons license (see 2.). For this reason authors may also publish the final paper on any repository or website with a complete citation for the paper. When linking to their paper, authors should make use of the link that SCIRP has established with

[crossref.org](#). It is a pointer to the full text of the final paper. The URL provides a persistent link which will never break.

This link has the form <http://dx.doi.org/10.4236/YourPaperNumber>.

5.) Articles are made available online directly without any delay.

6.) SCIRP strives to make articles as much Machine Readable as possible with current technology. SCIRP is providing metadata for all articles to the DOAJ, who will then make the metadata [OAI-compliant](#).

Marilyn S. Burke

Reference Librarian

Tampa Library

University of South Florida

4202 E. Fowler Ave.

Tampa, FL 33620

813-974-4561

From: Ahmadreza Sedaghat [mailto:asedagha@mail.usf.edu]

Sent: Monday, October 28, 2013 4:18 PM

[Quoted text hidden]

[Quoted text hidden]